














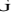




## REVIEW

## **Ocean Mesoscale and Frontal-Scale Ocean–Atmosphere Interactions and Influence on Large-Scale Climate: A Review**

HYODAE SEO<sup></sup>,<sup>a</sup> LARRY W. O'NEILL<sup></sup>,<sup>b</sup> MARK A. BOURASSA<sup></sup>,<sup>c</sup> ARNAUD CZAJA<sup></sup>,<sup>d</sup> KYLA DRUSHKA<sup></sup>,<sup>e</sup> JAMES B. EDSON<sup></sup>,<sup>a</sup> BAYLOR FOX-KEMPER<sup></sup>,<sup>f</sup> IVY FRENGER<sup></sup>,<sup>g</sup> SARAH T. GILLE<sup></sup>,<sup>h</sup> BENJAMIN P. KIRTMAN<sup></sup>,<sup>i</sup> SHOSHIRO MINOBE<sup></sup>,<sup>j</sup> ANGELINE G. PENDERGRASS<sup></sup>,<sup>k</sup> LIONEL RENAULT<sup></sup>,<sup>l</sup> MALCOLM J. ROBERTS<sup></sup>,<sup>m</sup> NIKLAS SCHNEIDER<sup></sup>,<sup>n</sup> R. JUSTIN SMALL,<sup>o</sup> AD STOFFELEN<sup></sup>,<sup>p</sup> AND QING WANG<sup>q</sup>

<sup>a</sup> Woods Hole Oceanographic Institution, Woods Hole, Massachusetts

<sup>b</sup> Oregon State University, Corvallis, Oregon

<sup>c</sup> Florida State University, Tallahassee, Florida

<sup>d</sup> Imperial College London, London, United Kingdom

<sup>e</sup> Applied Physics Laboratory, University of Washington, Seattle, Washington

<sup>f</sup> Brown University, Providence, Rhode Island

<sup>g</sup> GEOMAR Helmholtz Centre for Ocean Research, Kiel, Germany

<sup>h</sup> Scripps Institution of Oceanography, University of California San Diego, La Jolla, California

<sup>i</sup> University of Miami, Miami, Florida

<sup>j</sup> Hokkaido University, Sapporo, Japan

<sup>k</sup> Cornell University, Ithaca, New York

<sup>l</sup> LEGOS, Université de Toulouse, CNES, CNRS, IRD, UPS, Toulouse, France

<sup>m</sup> Met Office Hadley Centre, Exeter, United Kingdom

<sup>n</sup> University of Hawai'i at Mānoa, Honolulu, Hawaii

<sup>o</sup> National Center for Atmospheric Research, Boulder, Colorado


<sup>p</sup> Royal Netherlands Meteorological Institute, Utrecht, Netherlands

<sup>q</sup> Naval Postgraduate School, Monterey, California

(Manuscript received 21 December 2021, in final form 12 October 2022)

**ABSTRACT:** Two decades of high-resolution satellite observations and climate modeling studies have indicated strong ocean–atmosphere coupled feedback mediated by ocean mesoscale processes, including semipermanent and meandering SST fronts, mesoscale eddies, and filaments. The air–sea exchanges in latent heat, sensible heat, momentum, and carbon dioxide associated with this so-called mesoscale air–sea interaction are robust near the major western boundary currents, Southern Ocean fronts, and equatorial and coastal upwelling zones, but they are also ubiquitous over the global oceans wherever ocean mesoscale processes are active. Current theories, informed by rapidly advancing observational and modeling capabilities, have established the importance of mesoscale and frontal-scale air–sea interaction processes for understanding large-scale ocean circulation, biogeochemistry, and weather and climate variability. However, numerous challenges remain to accurately diagnose, observe, and simulate mesoscale air–sea interaction to quantify its impacts on large-scale processes. This article provides a comprehensive review of key aspects pertinent to mesoscale air–sea interaction, synthesizes current understanding with remaining gaps and uncertainties, and provides recommendations on theoretical, observational, and modeling strategies for future air–sea interaction research.

**SIGNIFICANCE STATEMENT:** Recent high-resolution satellite observations and climate models have shown a significant impact of coupled ocean–atmosphere interactions mediated by small-scale (mesoscale) ocean processes, including ocean eddies and fronts, on Earth's climate. Ocean mesoscale-induced spatial temperature and current variability

 Denotes content that is immediately available upon publication as open access.

Corresponding author: Hyodae Seo, hseo@whoi.edu

DOI: 10.1175/JCLI-D-21-0982.1

© 2023 American Meteorological Society. For information regarding reuse of this content and general copyright information, consult the [AMS Copyright Policy](https://www.ametsoc.org/PUBSReuseLicenses) ([www.ametsoc.org/PUBSReuseLicenses](https://www.ametsoc.org/PUBSReuseLicenses)).

modulate the air–sea exchanges in heat, momentum, and mass (e.g., gases such as water vapor and carbon dioxide), altering coupled boundary layer processes. Studies suggest that skillful simulations and predictions of ocean circulation, biogeochemistry, and weather events and climate variability depend on accurate representation of the eddy-mediated air–sea interaction. However, numerous challenges remain in accurately diagnosing, observing, and simulating mesoscale air–sea interaction to quantify its large-scale impacts. This article synthesizes the latest understanding of mesoscale air–sea interaction, identifies remaining gaps and uncertainties, and provides recommendations on strategies for future ocean–weather–climate research.

**KEYWORDS:** Atmosphere-ocean interaction; Boundary currents; Mesoscale processes; Extratropical cyclones; Ocean dynamics; Climate variability

## 1. Introduction

Decades of observational and modeling analysis have broadly identified two fundamental regimes of ocean–atmosphere coupling dependent on the spatial scale of ocean surface variability. The first regime involves the ocean response to large-scale ( $>1000$  km) internal atmospheric variability, which drives a response in sea surface temperature (SST) through the mediation of surface turbulent heat fluxes and upper-ocean turbulent mixing (e.g., Frankignoul 1985; Alexander and Scott 1997). The large-scale ocean response feeds back onto the incipient atmospheric circulation anomaly to reinforce or erode it (e.g., Bladé 1997). In this framework, the ocean is viewed as relatively passive, mainly advecting anomalies, storing heat, and integrating white noise atmospheric forcing.

The second regime, the focus of this paper, involves an atmospheric response driven by ocean mesoscale eddy-induced spatial SST and current variability. Here, the term “mesoscale eddies and fronts” broadly refers to all forms of oceanic processes with horizontal length scales smaller than the first regime of air–sea interaction ( $>1000$  km) but larger than oceanic submesoscale ( $\sim 1$ – $10$  km), although several outstanding issues regarding the submesoscale air–sea interactions will be discussed in sections 5 and 6. These processes include coherent, swirling, and transient ocean circulations with length scales near the Rossby radius of deformation (Chelton et al. 2011b), filamentary eddy structures that are widely observed in coastal upwelling systems, and semipermanent fronts and undulations near the midlatitude western boundary currents (WBCs) and their extensions, and SST fronts along the equatorial tongue in the Pacific and Atlantic Oceans.

The SST signature from these ocean mesoscale processes modifies surface turbulent heat and momentum fluxes, driving local responses in marine atmospheric boundary layer (MABL) processes (Small et al. 2008), inducing responses in winds, clouds, and rainfall (e.g., Deser et al. 1993; Tokinaga et al. 2009; Frenger et al. 2013; Miyamoto et al. 2018, 2022; Takahashi et al. 2020, 2021). The MABL responses then drive nonlocal responses in the path and activity of storm tracks in the extratropics (e.g., Czaja et al. 2019) and deep moist convection in the tropics (e.g., Li and Carbone 2012; Skillingstad et al. 2019; de Szoeke and Maloney 2020). The atmospheric response to ocean mesoscales feeds back onto eddy activity and SST, altering the large-scale ocean circulation, further

influencing these atmospheric processes (e.g., Nakamura et al. 2008; Hogg et al. 2009; Frankignoul et al. 2011; Taguchi et al. 2012). Mesoscale ocean surface currents also affect the wind stress and heat fluxes as well as the kinematic profiles in the MABL, which influence ocean circulation, including the stability and strength of the WBCs and their meanders (Renault et al. 2016b, 2019b) and the basin-scale coupled climate variability such as ENSO (e.g., Luo et al. 2005). The ocean drives the SST variability more strongly than the atmosphere at longer time scales and shorter spatial scales (Bishop et al. 2017), suggesting the need to include rectified coupled effects of ocean mesoscale eddies in high-resolution coupled climate models (Bryan et al. 2010; Kirtman et al. 2012; Roberts et al. 2016; Hewitt et al. 2020).

Aside from earlier limited observational studies showing evidence of the MABL response to mesoscale SSTs (e.g., Sweet et al. 1981), the first observational global-scale surveys of the MABL and surface wind responses based on satellite observations were provided by Chelton et al. (2004) and Xie (2004), followed by comprehensive review papers by Small et al. (2008) and Kelly et al. (2010). The number of publications that include aspects of mesoscale air–sea interaction has grown exponentially in the last decade or so (see Robinson et al. 2018, 2020), which also emphasizes a strong cross-disciplinary nature of the research subject (e.g., the AMS special collection on “Climate implications of frontal scale air–sea interaction” and the *Journal of Oceanography* special collection on “hot spots” in the climate system; Nakamura et al. 2015). Notwithstanding the existing review papers, no comprehensive synthesis papers exist that consolidate the exponential increase in scientific understanding of mesoscale air–sea interaction. This forms the key motivation of this review, which mainly focuses on a synthesis of the studies since Small et al. (2008).

The paper is organized in the following logical order. Section 2 discusses the air–sea flux responses to mesoscale SST and surface currents, along with theories and analytical studies of MABL dynamics describing the flux responses. The subsequent two sections review critical aspects of large-scale atmospheric and ocean circulation responses resulting from the atmospheric boundary layer processes. That is, section 3 discusses the tropospheric responses emphasizing the modulation of local and downstream adjustments of extratropical weather systems and their aspects related to climate change. Section 4 probes into the oceanic responses due to thermal and mechanical feedback processes. The

section emphasizes the need to develop new theories and parameterizations to account for rectified effects of eddy–atmosphere interaction. [Section 5](#) explores the emerging observational platforms critical for accurate in situ and remote sensing characterization of air–sea interaction at small spatial scales in the coming decade. [Section 6](#) provides a summary and synthesis.

The readers might find it helpful to visualize key feedback mechanisms discussed throughout the paper by referring to the schematic illustrations in [Fig. 1](#), which are organized at different characteristic length scales and by processes. The MABL response to a mesoscale SST front ([Fig. 1d](#)) corresponds to [section 2](#). The diabatic heat exchanges between the atmospheric fronts and the SST fronts ([Figs. 1b,c](#)) are elaborated in [section 3b](#), while a broader view of modulation of the midlatitude storm track by the WBCs and the subsequent downstream rainfall patterns ([Fig. 1a](#)) is discussed in detail in sections 3a–c. The discussion about the modulation of wind stress and heat fluxes by the mean and eddy currents and their feedback to oceans ([Fig. 1e](#)) jibes with [section 4a](#). The resulting fine-scale near-surface instability and turbulence ([Fig. 1d](#)) are touched upon in [sections 4b](#) and [4c](#).

It is not possible to cover all relevant aspects of mesoscale air–sea interaction with sufficient detail. There exist many review articles that might be helpful for readers interested in gaining a more in-depth understanding of specific topics. For [section 2](#), such papers include [Bourassa et al. \(2013\)](#) on challenges/needs for accurate air–sea flux measurements in high-latitude oceans; [Swart et al. \(2019\)](#) on observational strategies to improve Southern Ocean heat and gas flux estimates; [Cronin et al. \(2019\)](#) on global air–sea flux accuracy requirements; [Bourassa et al. \(2019\)](#) on satellite remote sensing of wind and winds stress; and [Deskos et al. \(2021\)](#) on sea state impacts on surface winds from a wind energy perspective. For [section 3](#), [Kushnir et al. \(2002\)](#) reviewed the atmospheric responses to extratropical SST anomalies in climate models. [Czaja et al. \(2019\)](#) updated the extratropical air–sea interaction based on high-resolution climate modeling studies, while [Kwon et al. \(2010\)](#) and [Kelly et al. \(2010\)](#) reviewed the impacts of WBC SST anomalies on seasonal to decadal climate variability. For [section 4](#), more detailed accounts of surface waves, upper ocean mixing, and submesoscale dynamics are provided by [Sullivan and McWilliams \(2010\)](#), [D’Asaro \(2014\)](#), and [McWilliams \(2016\)](#). [McGillicuddy \(2016\)](#) offers a comprehensive review of mechanisms of physical–biological–biogeochemical interactions on the oceanic mesoscale. For [section 5](#), helpful review papers include [Ardhuin et al. \(2019\)](#) on observing sea state information, [Villas Bôas et al. \(2019\)](#) on wind–wave–current interaction, [Centurioni et al. \(2019\)](#) on global ocean surface observation networks, and [Wanninkhof et al. \(2019\)](#) on global CO<sub>2</sub> flux measurements. The observational needs for data assimilation, coupled reanalyses, and short-term and extended-range predictions have been discussed by [Penny and Hamill \(2017\)](#), [Domingues et al. \(2019\)](#), and [Subramanian et al. \(2019\)](#).

## 2. Boundary layer and surface heat, momentum, and gas flux responses

Surface fluxes communicate mass and energy between the ocean and atmosphere and are thus vital processes in Earth’s

climate system. The ocean is a major reservoir of heat and carbon in the Earth system, and it is increasingly clear that exchanges with the atmosphere occurring on the oceanic mesoscale are significant in shaping Earth’s climate. Recent assessments on projected trends in surface air temperature (SAT) and SST have indicated a need to better understand surface heat fluxes to reconcile conflicting lines of evidence on the projected trends in SAT and SST (e.g., Box TS.1; [IPCC 2021](#), p. 59). The surface turbulent heat fluxes are composed of sensible and latent heat fluxes, while the surface wind stress represents the turbulent momentum flux between the atmosphere and ocean mediated by surface waves. This section discusses air–sea heat, momentum, and gas flux responses to spatially heterogeneous fields of SST, surface currents, and sea state. We also discuss the local MABL response to ocean-induced mesoscale forcing, given its strong relationship with the surface fluxes. These processes are illustrated in [Fig. 1d](#).

Spatially heterogeneous SST and surface currents generate localized anomalies in the surface heat and momentum fluxes. The atmospheric and oceanic responses to these flux anomalies are initially confined to the MABL and ocean mixed layer, but the responses to this coupling may spread to the free atmosphere above ([section 3](#)) or the ocean thermocline below ([section 4](#)). The atmospheric boundary layer and the oceanic mixed layer directly mediate responses of the large-scale oceanic and atmospheric circulation to the mesoscale and frontal-scale air–sea coupling.

[Figure 2](#) shows the strong correlation between monthly mesoscale surface fluxes and ocean mesoscale variability from the ERA5 reanalysis ([Hersbach et al. 2020](#)). Here, the turbulent heat flux is defined as positive downward (ocean warming). When the local point-by-point correlation between the turbulent fluxes and SST is strongly negative, the SST variability can be viewed as the ocean forcing the atmosphere (e.g., the warm ocean heats the atmosphere). Similarly, when the correlation between turbulent heat flux and SST *tendency* is positive, the atmosphere is considered to drive ocean variability. Over mesoscale, the wind stress and upward heat fluxes are enhanced over warm SST anomalies (SSTA) and reduced over cool SSTA. The correlations are much stronger for sensible and latent heat flux responses, while the surface stress response on this spatial scale is much more apparent in oceanic frontal boundary regions where mesoscale SST variability is most pronounced. However, it should be noted that the amplitude of correlation represents empirical estimates of the strength of covariability since the atmospheric response to an ocean anomaly modifies the turbulent fluxes and would obscure this simple rule (e.g., [Sutton and Mathieu 2002](#)). The effect of the surface flux on the ocean is discussed in [section 4](#).

### a. Turbulent heat flux response

On smaller scales encompassed by the oceanic mesoscale and on time-scales longer than synoptic time scales in the atmosphere (e.g., 2–8 days), spatial variations in the surface turbulent heat fluxes are driven primarily by spatial perturbations of SST, such that negative heat flux anomalies (i.e., atmosphere heat gain) occur over warm SST perturbations and

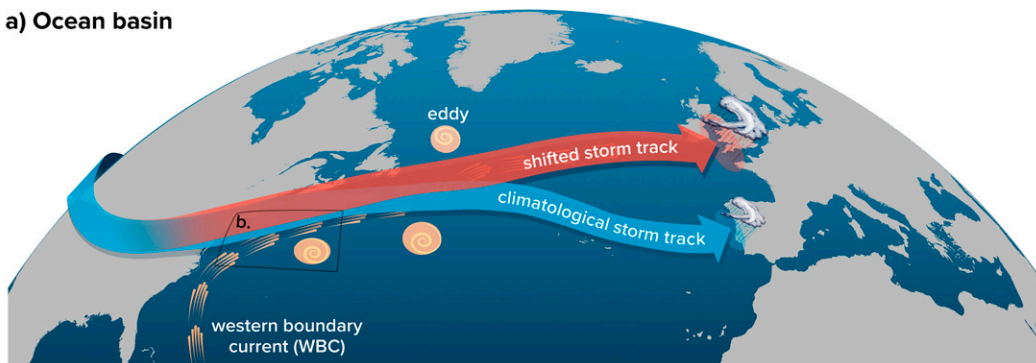
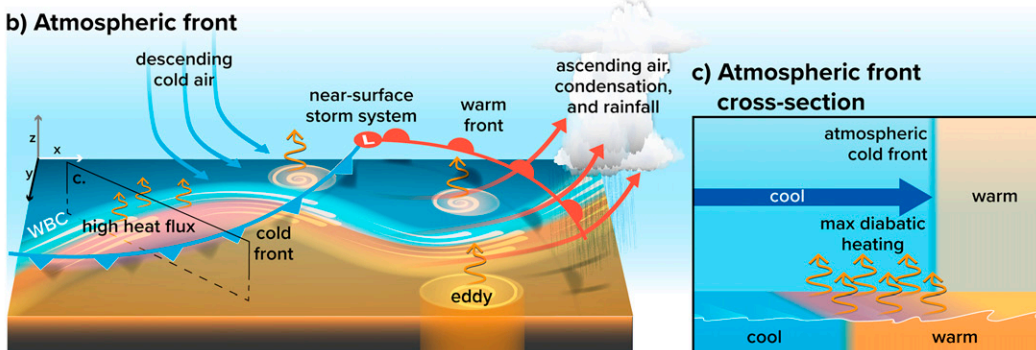
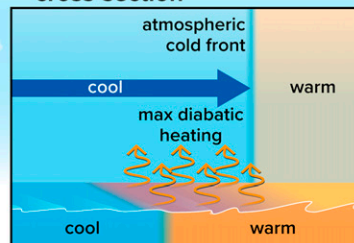
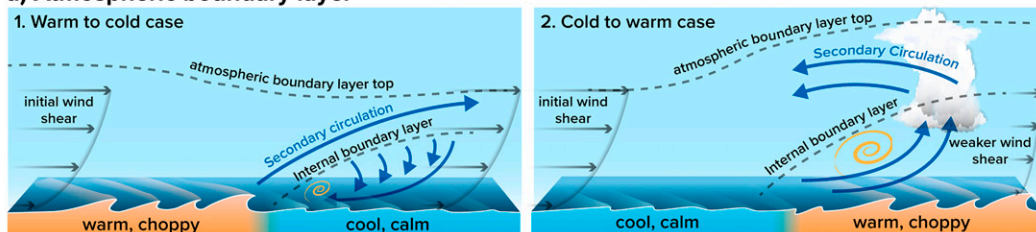
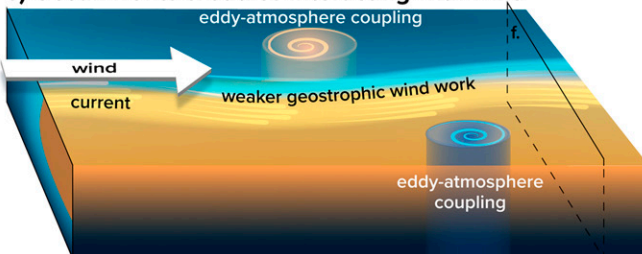
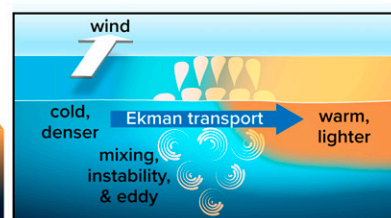
**a) Ocean basin****b) Atmospheric front****c) Atmospheric front cross-section****d) Atmospheric boundary layer****e) Ocean fronts & eddies interacting with wind****f) Stratification, instability & turbulence at fronts**

FIG. 1. Schematic illustrations of the coupled ocean–atmosphere feedback processes in the Northern Hemisphere. (a) On the basin scale, the storm track affected by the WBCs leads to anomalous rainfall patterns downstream. (b) A zoom-in view over the black box in (a) illustrates cold and warm fronts within a low pressure system traversing the semipermanent SST front. On the trailing edge of the cold front (purple), the cold/dry air mass over the warm ocean water induces large diabatic heating of the storms, strengthening the storm. A similar process might occur over the transient mesoscale eddies. The modified air mass ascends over the warm front, leading to deep cumulus clouds and heavy precipitation. (c) A 2D view of the cross section in (b), where the cold front translates eastward over the SST front. When the cold front is east of the SST front, the large air–sea temperature and humidity differences (purple) cause the maximum upward turbulent heat flux, facilitating the diabatic frontogenesis. (d) A 2D view of the MABL with the cross-frontal winds. For the warm-to-cold case, the warm air blowing over cold water downwind of the SST front leads to a stable internal boundary layer with a capping inversion and a shallow clockwise secondary circulation. Due to weaker vertical mixing, the surface wind slows down, reinforcing the initial wind shear. The weak wind over cold SST yields a reduced surface drag. For the cold-to-warm case, MABL and internal boundary layers deepen quickly, with the counterclockwise secondary circulation developing downstream. The increased turbulent mixing



positive heat flux anomalies (i.e., atmosphere heat loss) occur over cool SST perturbations (Figs. 2b,c). Over these scales, the ocean forces a response of the atmosphere driven by the surface heat exchange, which is fundamentally distinct from the response over larger spatial scales. Near-surface air temperature and specific humidity adjust slowly to spatially heterogeneous SST as air flows across SST gradients. Ocean mesoscale eddies and SST fronts near the semipermanent WBCs often generate large air–sea temperature and humidity differences (Figs. 1b,c). A dramatic example was observed during the CLIMODE experiment near the Gulf Stream during wintertime, when air–sea temperature differences exceeded 10°C over 200 km, yielding  $>1000 \text{ W m}^{-2}$  surface turbulent heat fluxes into the atmosphere (Marshall et al. 2009).

Past field experiments captured less extreme but nonetheless strong responses of turbulent heat fluxes and MABL convective turbulence to mesoscale and frontal-scale SSTs. Examples can be found from the Sargasso Sea during the FASINEX experiment (e.g., Friehe et al. 1991), as well as from the Gulf Stream (e.g., Plagge et al. 2016), the Kuroshio (e.g., Tokinaga et al. 2009), Pacific tropical instability waves (Thum et al. 2002), the Brazil–Malvinas Confluence system (e.g., Pezzi et al. 2005; Villas Bôas et al. 2015; Souza et al. 2021; Cabrera et al. 2022), the Agulhas Current (e.g., Jury and Courtney 1991; Messenger and Swart 2016), and the western Arabian Sea (e.g., Vecchi et al. 2004).

The scale dependence of turbulent flux responses to mesoscale SST variations has been quantified primarily from reanalysis-based surface flux and SST datasets (e.g., Li et al. 2017; Sun and Wu 2022). Bishop et al. (2017), in particular, showed that on time scales longer than one month, the turbulent heat fluxes on the ocean mesoscale and frontal scale are driven by SST variability associated with oceanic internal processes. On shorter time scales, the variability is driven more by synoptic-scale weather variability, particularly along the storm tracks overlying the WBCs. Based on this simple diagnostic, Kirtman et al. (2012) concluded that eddy-parameterized models grossly underestimate the ocean forcing of the atmosphere in eddy-rich regions (e.g., WBCs and the Southern Ocean) and overestimate the atmospheric forcing of the ocean throughout much of the midlatitudes compared to the ocean eddy-resolving simulations.

## b. Turbulent momentum flux and MABL wind responses

The turbulent heat flux response to SST is a crucial process that drives the responses in turbulent momentum flux to SST. The variability in ocean surface currents at mesoscales also affects the wind stress through the relative motion of the surface winds and currents. The most immediate local atmospheric response to SST and surface currents is initially confined to the MABL. The wind and wind stress responses mainly result from a dynamical adjustment of the MABL pressure and vertical turbulent stress profile distinct from simple adjustments of the surface layer logarithmic wind profile (Small et al. 2008; O'Neill 2012; Renault et al. 2016a), the relative importance of which strongly depends upon background wind condition (e.g., Schneider and Qiu 2015; Byrne et al. 2015; section 2c).

### 1) MESOSCALE SST EFFECTS

Traditionally, local atmospheric responses to the mesoscale SST have been characterized empirically by linear regressions between collocated mesoscale SSTs and surface winds and surface wind stress, all spatially high-pass filtered to isolate the coupling on scales smaller than about  $O(1000)$  km. Linear regression coefficients, also called coupling coefficients, obtained from satellite-observed wind speed and wind stress indicates ubiquitous increases in their magnitudes over warm SSTs, increases of wind divergence and wind stress divergence collocated with the downwind component of the SST gradient, and wind curl and wind stress curl that scale with crosswind components of SST gradients (Chelton et al. 2001; O'Neill et al. 2003, 2012). The SST-induced curl and divergence responses provide further constraints on spatial scales of the SST-induced MABL response. These simple but powerful diagnostic metrics have been broadly used to diagnose the simulated air–sea interaction over a range of scales in numerical models (Bellucci et al. 2021), leading to refinements in the SST resolution (Chelton 2005) and the PBL parameterizations in NWP models (Song et al. 2017). However, the coupling coefficients include contributions from broad scales represented in the high-pass filtered input fields. Hence, other than the gross separation of small scales from large scales, it is difficult to extract useful information about scale dependence from such calculations. Alternative statistical and analytical approaches exist, including cross-spectral analysis (e.g., Small et al. 2005b;

---

← accelerates the surface wind, leading to a well-mixed wind profile. The choppy surface waves on the warm side due to higher winds enhance surface drag. Wind direction also changes across the front as wind speed adjusts to local stability (not featured in this schematic). The surface currents near the ocean front (also not shown) modulate the wave slopes and surface roughness via wave–current interaction and the wind stress via current–wind interaction. (e) Meandering eastward currents and mesoscale eddies under a uniform westerly wind. On a large scale, because surface currents are oriented downwind, the relative wind leads to weaker geostrophic wind work than the absolute wind, stabilizing the large-scale circulation but stimulating submesoscale instabilities. Over the eddies, eddy–atmosphere coupling induces the diabatic dissipation of eddy potential energy (thermal feedback) and the negative geostrophic eddy wind work via current–wind interaction (mechanical feedback), weakening the eddy energy. The eddies' swirling currents manifest reversely in the wind stress, leading to current-induced wind stress curls and the up/downwelling in the ocean. (f) The cross section across the front/jet in (e). The down-front wind drives an eastward Ekman transport of cold/dense water over warm/light water, reducing stratification near the front. The unstable front leads to enhanced turbulence and submesoscale activity, with the induced secondary circulation accelerating the jet. The oceanic frontogenesis influenced by the surface waves is not featured in this schematic but illustrated in Fig. 9.

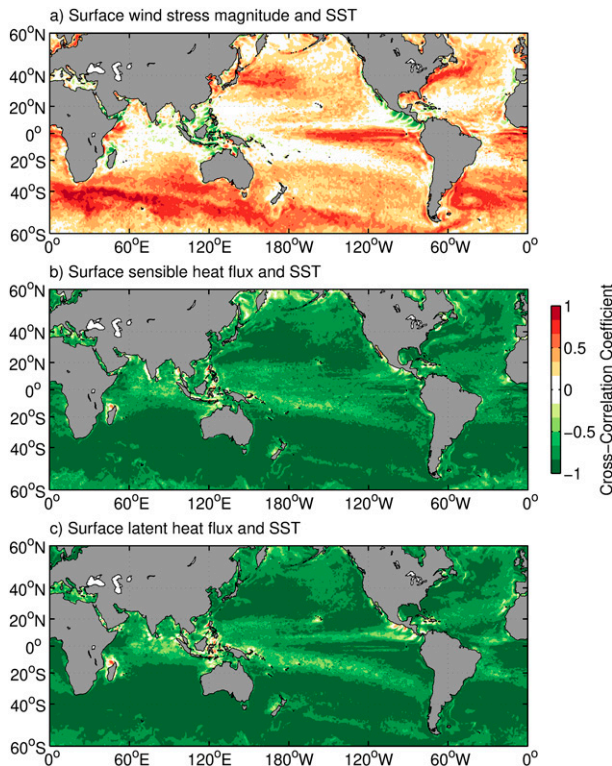


FIG. 2. Maps of the cross-correlation coefficients between ERA5 monthly spatially high-pass filtered SST and (a) wind stress magnitude, (b) surface sensible heat flux, and (c) surface latent heat flux. The spatial high-pass filter removed variability with spatial scales greater than 1000 km. These maps were averaged over the 30-yr period 1991–2020. The ERA5 reanalysis time period used here was 1991–2020. The standard sign convention for ERA5 surface fluxes is used: positive fluxes mean energy entering the ocean. The high correlations in these maps correspond to regions of strong mesoscale SST variability, such as in the WBCs and their extension regions (Kuroshio, Gulf Stream, Brazil Current, and Agulhas Current), along the Antarctic Circumpolar Current and equatorial fronts, and near the Somali Current. A similar plot to (a) can be found in Small et al. (2008) and Seo (2017).

O'Neill et al. 2012; Laurindo et al. 2019; Samelson et al. 2020), cross-covariance and correlation functions between SST (and its tendency), wind and turbulent heat fluxes (e.g., Frankignoul and Hasselmann 1977; Wu et al. 2006; Bishop et al. 2017; Small et al. 2019), and an analytical model for MABL heat and momentum budgets (Schneider and Qiu 2015; Schneider 2020). The analytical model for MABL is explored in detail in section 2c.

## 2) MESOSCALE CURRENT EFFECTS

Regions of strong SST gradients are also regions of substantial variability in ocean surface current. The current feedback (CFB) mechanism directly modifies wind stress through the relative motion of surface winds and currents, which in turn alters the low-level wind shear and wind. That is, a negative current anomaly induces a positive stress anomaly acting on the atmosphere, which causes a negative wind anomaly (Renault et al. 2016a). At the mesoscale, CFB primarily

impacts the surface wind stress curl but not its divergence due to the quasigeostrophic nature of ocean currents (Chelton et al. 2004). The wind stress and wind responses to CFB can also be diagnosed using empirical relationships based on satellite and numerical simulations. Renault et al. (2016a, 2019a) defined two coupling coefficients related to CFB:  $s_w$  is the regression slope between mesoscale surface currents and 10-m wind and  $s_\tau$  is the linear regression coefficient linking mesoscale surface current and surface stress. The coefficient  $s_\tau$  can be interpreted as a measure of the damping efficiency of CFB to ocean eddy energy, as discussed in greater detail in section 4.

The SST and current-induced stress responses are challenging to separate since mesoscale SST and current variations covary strongly near ocean fronts and eddies. Nonetheless, estimates of the contributions of the current-induced wind stress response via the linear coupling coefficients indicate that the current-induced stress anomalies exceed the SST-induced response over strong WBCs and within isolated ocean eddies (e.g., Gaube et al. 2015; Renault et al. 2019a). The current-induced stress response exists in scatterometer and direct air–sea flux observations and coupled ocean–atmosphere simulations, but it is not directly apparent in atmosphere-only simulations and reanalyses, such as the ERA5 wind stress anomalies used in Fig. 2. Including both current and SST-induced stress anomalies strongly impacts the mesoscale wind stress curl field (e.g., Renault et al. 2019a).

### c. Analytic framework for SST-induced boundary layer response

The MABL response to ocean mesoscale current must incorporate coupling between the MABL thermodynamics and dynamics to adequately represent the influence of SST and surface current on the surface wind stress and sensible and latent heat fluxes. An analytical framework for SST impacts was recently proposed, which incorporates MABL heat and momentum budgets that capture the first-order response of the MABL to SST forcing (Schneider and Qiu 2015; Schneider 2020) and includes a representation of the processes shown in the literature to be of primary importance. This framework considers an MABL capped by an inversion (Battisti et al. 1999). Within this layer, air temperature is assumed to be well mixed and vertically constant, and subject to horizontal advection and air–sea heat exchanges. The system is driven by winds with horizontal scales far larger than the ocean mesoscale that satisfy a drag law at the sea surface and experience zero vertical momentum flux at the inversion. The large-scale winds  $\mathbf{U}$  form a modified Ekman spiral (Holton 1965a,b), which is considered horizontally homogeneous on scales commensurate with the ocean mesoscale.

SST  $T$  enters the heat budget of the layer via the air–sea heat exchanges due to the air–sea temperature difference with a rate  $\gamma$ . The MABL air temperature  $\Theta$  results, to first order, from a quasi-steady balance of surface sensible heat fluxes with advection by large-scale winds (e.g., Small et al. 2005a):

$$\mathbf{U} \cdot \nabla \Theta = \gamma(T - \Theta). \quad (1)$$

The air temperatures  $\Theta$  adjust to SST  $T$  over a length scale of  $U/\gamma$ , forming a wake of elevated values of the air–sea

temperature differences in the lee of spatial SST variations. Thermal adjustment rates of the boundary layer  $\gamma$  correspond to adjustment times of a few hours to half a day (Schubert et al. 1979), yielding length scales of the response of  $O(100)$  km. The momentum equations govern the wind response to the ocean mesoscale SST-induced acceleration  $\mathbf{F}$  (Schneider and Qiu 2015) such that

$$\underbrace{\mathbf{U} \cdot \nabla \mathbf{u}}_{\text{I}} + \underbrace{\frac{w^*}{H} \partial_s \mathbf{u}}_{\text{II}} + \underbrace{f \hat{\mathbf{e}}_3 \times \mathbf{u}}_{\text{III}} - \underbrace{\frac{1}{H^2} \partial_s A \partial_s \mathbf{u}}_{\text{IV}} + \underbrace{g' \nabla h}_{\text{V}} = \mathbf{F}. \quad (2)$$

On the left-hand side of Eq. (2), term I represents the horizontal advection by large-scale winds  $\mathbf{U}$  of SST-induced winds  $\mathbf{u}$ . Term II is the vertical advection by  $w^*$  of the large-scale shear, where a sigma coordinate is used in the vertical so that  $s = 0$  is the sea surface and  $s = 1$  is the mean inversion height  $H$ . Term III indicates the Coriolis acceleration with Coriolis frequency  $f$ , where  $\hat{\mathbf{e}}_3$  denotes the unit vector in the vertical. Term IV is the divergence of vertical fluxes of horizontal momentum due to large-scale mixing with eddy coefficient  $A$ . Term V is the hydrostatic pressure gradient forces, including the so-called back pressure effect (e.g., Hashizume et al. 2002), due to ocean mesoscale-induced changes of inversion height ( $h$ ). Together with the continuity equation and boundary conditions of a drag law at the sea surface, and a material inversion with no flux of momentum, these equations provide a complete analytical solution for the wind response to ocean mesoscale SSTs.

The changes in  $\Theta$  due to ocean mesoscale SSTs impact acceleration  $\mathbf{F}$  to the horizontal momentum equation

$$\mathbf{F} = \underbrace{\frac{gH}{\Theta_0} (1-s) \nabla \Theta}_{\text{VI}} + \underbrace{\frac{1}{H^2} \partial_s (\dot{A} \partial_s \mathbf{u})}_{\text{VII}} \quad (3)$$

through the modulation of the hydrostatic pressure gradients (term VI) and the sensitivity of the vertical mixing to the fluxes at the air–sea interface (term VII). Here,  $\Theta_0$  is a reference temperature,  $g$  is Earth's gravitational acceleration, and  $\dot{A}$  is the sensitivity of vertical mixing coefficient  $A$  to SST.

The pressure effect (term VI), originally formulated by Lindzen and Nigam (1987), designates the acceleration of surface winds to the baroclinic pressure gradient imparted by air temperature gradients, which drive secondary wind circulations and updrafts and downdrafts (e.g., Wai and Stage 1989; Wenegrat and Arthur 2018; Sullivan et al. 2020; Fig. 1d). Lindzen and Nigam (1987) neglected advection and assumed that air temperature decays linearly from the SST to zero at a height of 3000 m. In contrast, we include advection in the momentum budget in Eq. (2) and assume that the SST imprint is vertically constant, consistent with a reduced gravity formulation (Battisti et al. 1999).

The vertical mixing effect (term VII) is a linearization of the “nonlinear” term envisioned by Wallace et al. (1989) and Hayes et al. (1989) that captures the modulations of the vertical mixing acting on the large-scale wind profile. The dynamics, amplitude, and vertical structure of  $\dot{A}$  determine the

character of mixing sensitivity. Mixing can intensify and change its vertical scale. The dependence of vertical mixing on the nonequilibrium air–sea temperature difference is but one possibility. Alternatively, SST induces convective adjustment of the lapse rate and permanently deepens the atmospheric boundary layer over warmer waters (Samelson et al. 2006). These diagnostic formulations for  $\dot{A}$  are endpoints of the nonequilibrium evolution of vertical mixing simulated by large-eddy simulations (LES; e.g., de Szoeke and Bretherton 2004; Skillingstad et al. 2007; Sullivan et al. 2020), which allow for changes in the vertical mixing that lag modulations of boundary layer stability (Wenegrat and Arthur 2018). As such, the coupling between surface winds and SST is sensitive to the MABL turbulence closure schemes (e.g., Song et al. 2009, 2017; Perlin et al. 2014; Samelson et al. 2020). The MABL turbulence subsequently affects the SST by altering mixing and entrainment in the ocean surface boundary layer, indicating co-dependence of the turbulent boundary layer schemes in the atmosphere and oceans (Fox-Kemper et al. 2022).

Advection by large-scale winds allows for disequilibrium in air–sea temperature and shifts responses of winds or stress as a function of the SST spatial scales and the large-scale wind direction and speed (e.g., Small et al. 2005a, 2008). Spectral transfer functions, or their corresponding physical-space impulse response functions, capture these nonlocal relationships and generalize the widely used coupling coefficients to include spatial lags. Estimates from satellite observed winds and SST of spectral transfer functions suggest scale-dependent, lagged dynamics as a function of the Rossby number determined by large-scale winds, the wavenumbers of ocean mesoscale SST, and the Coriolis frequency  $f$ , or thermal or frictional adjustment rates  $\gamma$  or  $A/H^2$  (Schneider 2020; Masunaga and Schneider 2022). For small Rossby numbers, the pressure effect dominates, while large Rossby numbers favor the vertical mixing effect, and order one Rossby numbers combine both with rotational effects, consistent with modeling studies of boundary layer responses to prototype SST fronts (Spall 2007a; Kilpatrick et al. 2014, 2016) and ocean eddy fields (Foussard et al. 2019a) in the presence of large-scale winds.

The analytical model described above considers a dry MABL without incorporating MABL moisture or latent heat fluxes. The contribution of moisture to buoyancy fluxes, latent heating/cooling, and overall MABL structure has not been investigated in as much detail within the context of the mesoscale MABL response. However, it is anticipated to have a nonnegligible impact on the MABL dynamical response to mesoscale SSTA (Skillingstad and Edson 2009). For instance, during CLIMODE, the buoyancy heat flux was approximately 20% larger than the sensible heat flux due to moisture, and the average magnitude of the latent heat flux was  $\sim 2.5$  times greater than the sensible heat flux (Marshall et al. 2009). In the tropics, the ratio of latent to sensible heat flux is even larger (e.g., de Szoeke et al. 2015), so the moisture contribution is often an order of magnitude greater than the sensible heat contribution. The impact of moist convection during a cold air outbreak over the Gulf Stream was investigated with an LES (Skillingstad and Edson 2009), showing that the latent and sensible heat fluxes are enhanced over a simulated



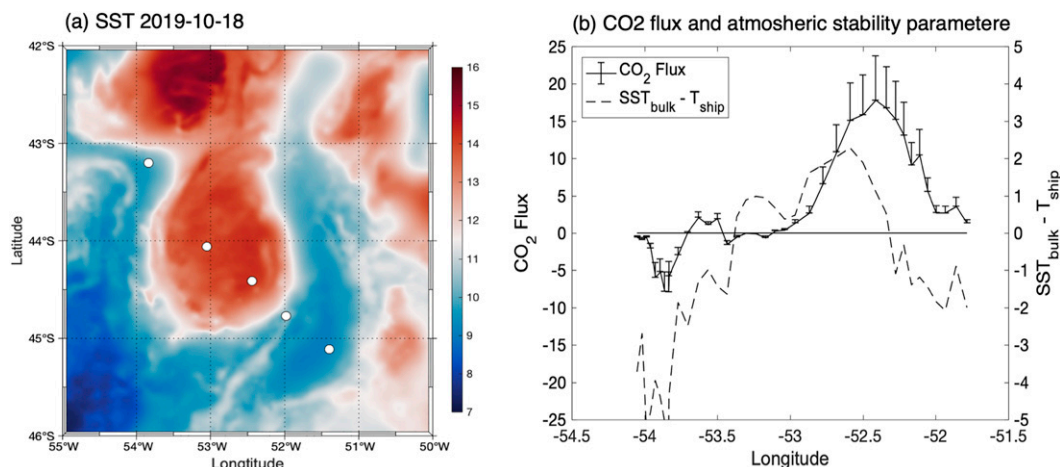


FIG. 3. (a) Observed SST ( $^{\circ}\text{C}$ ) in the southwestern Atlantic Ocean on 18 Oct 2019. The white circles denote the Po/V *Almirante Maximiliano* trajectory. (b) In situ  $\text{CO}_2$  fluxes ( $\mu\text{mol m}^{-2} \text{s}^{-1}$ ) measured by eddy covariance method (solid) and atmospheric stability parameter,  $\text{SST}_{\text{bulk}} - T_{\text{ship}}$  ( $^{\circ}\text{C}$ ) (dotted), where  $\text{SST}_{\text{bulk}}$  and  $T_{\text{ship}}$  denote the sea surface and near-surface air temperatures, respectively. The error bars denote the standard error representing a 95% confidence interval. Figures adapted from Pezzi et al. (2021). Figure reproduced with permission.

SST front resulting in stronger turbulent mixing and precipitation compared to a constant SST simulation. The simulation across the SST front shows that relatively low humidity values near the surface are maintained by the continual expansion of the boundary layer in the entrainment layer, which mixes dry air from aloft into the MABL. This maintains the large air–sea specific humidity and temperature differences necessary for strong latent and sensible heat fluxes in the surface layer. Additional simulations and measurements are required to investigate the role of moisture in response to mesoscale SST. For example, the analytical model could provide insight by using the virtual temperature at both the sea surface and aloft.

#### d. Modulation of air–sea fluxes of tracers

Air–sea gas fluxes of tracers depend on the air–sea disequilibrium and processes driving exchange, such as winds and breaking waves. From the ocean perspective, the disequilibrium can be understood as the difference of the concentrations of a gas in the seawater,  $C$ , relative to the concentration the gas would have at equilibrium with the atmosphere,  $C_{\text{eq}}$ , which, in turn, is determined by the solubility of the gas in seawater. The air–sea flux  $F_x$  of a gas  $x$  then is estimated as  $F_x = k(C - C_{\text{eq}})$ , where  $k$  is the gas transfer velocity (e.g., Woolf 1993; McGillis et al. 2001; Wanninkhof et al. 2009; Dong et al. 2021). Impacts of ocean mesoscale features on the net  $F$  may be introduced via  $k$  or  $C_{\text{eq}}$ , each of which varies nonlinearly with wind speed and depends on sea state. The mesoscale may also affect  $C$  by impacting biological sources and sinks of tracers (section 4d). Indeed, studies find local modulations of air–sea  $\text{CO}_2$  fluxes due to the effects of mesoscale eddies on solubility, productivity, or winds (Jones et al. 2015; Song et al. 2015, 2016; Olivier et al. 2022). One such study in the southwest Atlantic Ocean detected clear spatial

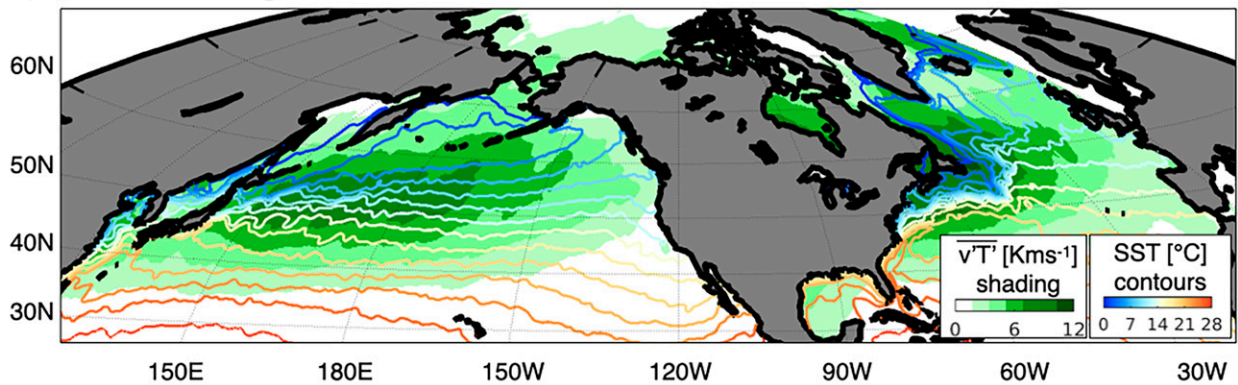
covariations of  $\text{CO}_2$  flux with the MABL stability over a warm-core eddy (Fig. 3; Pezzi et al. 2021). Yet, on the basin-to-global scales, positive and negative mesoscale anomalies of  $\text{CO}_2$  fluxes appear to essentially cancel (Wanninkhof et al. 2011; Song et al. 2015). Clear separation and quantification of the individual and rectified effects of mesoscale phenomena on  $k$ ,  $C$ , and  $C_{\text{eq}}$  from observations and models remain challenging, given the difficulty of capturing transient mesoscale variations in the ocean and atmosphere, including the concentration of tracers such as carbon.

### 3. Free-tropospheric, extratropical atmospheric circulation responses

This section investigates atmospheric response beyond the MABL (section 2) by focusing on local and nonlocal circulation responses in the extratropics to SSTA patterns observed in the WBC regions, including the semipermanent SST fronts and transient mesoscale eddies. Some aspects of deep convective response in the tropical atmosphere have also been attributed to MABL adjustments to the mesoscale SST fields (Li and Carbone 2012; Skillingstad et al. 2019; de Szoeke and Maloney 2020), although much of the studies on deep atmospheric responses published to date is based on the extratropics. We start with a summary of previous studies on the role of extratropical SSTA in quasi-equilibrium atmospheric circulation and storm tracks. We then revisit the debates about the observed near-surface wind convergence and precipitation in WBC regions diagnosed as a response to either SST variations or extratropical storms. Finally, we will consider whether these processes may be important to future climate, focusing on the difference between projections at high and low resolution in the oceans. The feedback processes examined in this section are schematically illustrated in Figs. 1a–c.



### (a) Climatological storm track over Kuroshio and Gulf Stream



### (b) Climatological “baroclinicity” over Agulhas and ACC

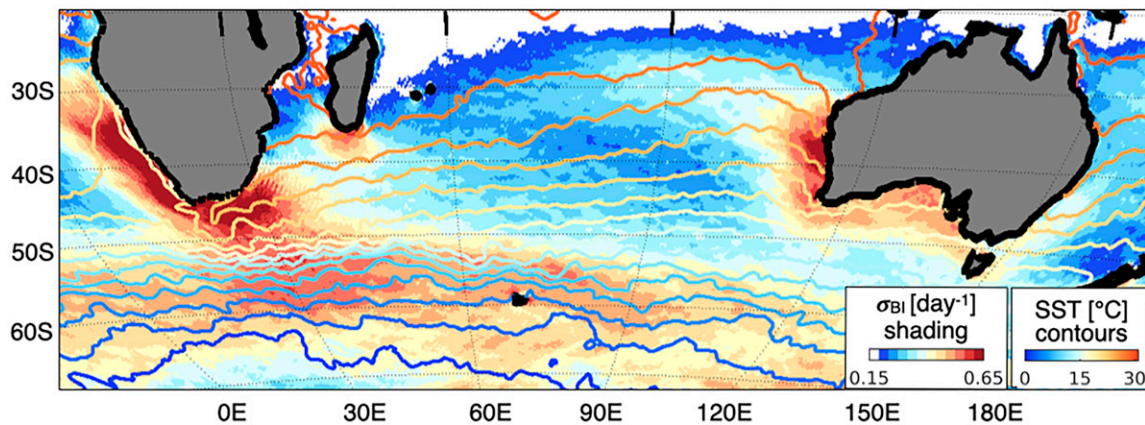


FIG. 4. The climatological relationship of the extratropical storm tracks with the SST fields in (a) Kuroshio–Oyashio Extension and Gulf Stream in the Northern Hemisphere and (b) Agulhas Current and the Antarctic Circumpolar Current systems in the south Indian Ocean. The atmospheric storm track is estimated in (a) as the time-mean meridional heat transport by atmospheric transient eddies  $\overline{v'T'}$  at 850 hPa (lower troposphere), where primes denote the 2–8-day bandpass filtered fields and the overbar indicates the time mean, and in (b) as the atmospheric maximum Eady growth rate, defined as the most unstable baroclinic mode whose growth rate is scaled as the magnitude of the baroclinicity vector,  $|\sigma_{BI}| = 0.31[g/(N\theta)] |-(\partial\theta/\partial y, \partial\theta/\partial x)|$ , at 850 hPa, where  $g$  is the gravitational acceleration,  $N$  is the buoyancy frequency, and  $\theta$  is the potential temperature. These storm track quantities are derived from ERA5. The SST climatology is obtained from the NOAA daily Optimum Interpolation dataset. The climatologies are calculated from 2010 to 2015.

#### a. Time-mean general circulation responses

The question of how the extratropical atmosphere responds to variability in ocean fronts and/or extratropical SSTA has been addressed over many decades. Early studies considered the linear response (Hoskins and Karoly 1981; Frankignoul 1985), which predicted a shallow heating response characterized by a downstream trough with a baroclinic structure. This was argued against by Palmer and Sun (1985), who found a downstream ridge, with an advection of temperature anomalies by mean flow acting against anomalous advection of mean temperature gradients. Later, Peng et al. (1997) showed that the transient eddy response was important in forming an equivalent barotropic high. More recent observational analyses find a weak low-pressure response east of warm SSTA near the Gulf Stream (Wills et al. 2016) and Kuroshio (Frankignoul et al. 2011; Wills and Thompson 2018). Deser et al. (2007) demonstrated

that the initial linear, baroclinic response is quickly (within 2 weeks) replaced with the equilibrium barotropic response with a much broader spatial extent and magnitude (Ferreira and Frankignoul 2005, 2008; Seo et al. 2014). The adjustment time is shorter near WBC regions (Smirnov et al. 2015). This literature is well summarized in existing review papers (Kushnir et al. 2002; Small et al. 2008; Kwon et al. 2010; Czaja et al. 2019).

Recent studies also indicated a strong sensitivity to the spatial resolution of the atmospheric dynamics governing the large-scale circulation response. For example, Smirnov et al. (2015) show that a low-resolution ( $1^\circ$ ) model induces a weak response resulting from shallow anomalous heating balanced by equatorward cold air advection, consistent with the results from steady linear dynamics. This contrasts with the higher resolution ( $1/4^\circ$ ) model showing that the anomalous diabatic heating is balanced by a deep vertical motion mediated by the

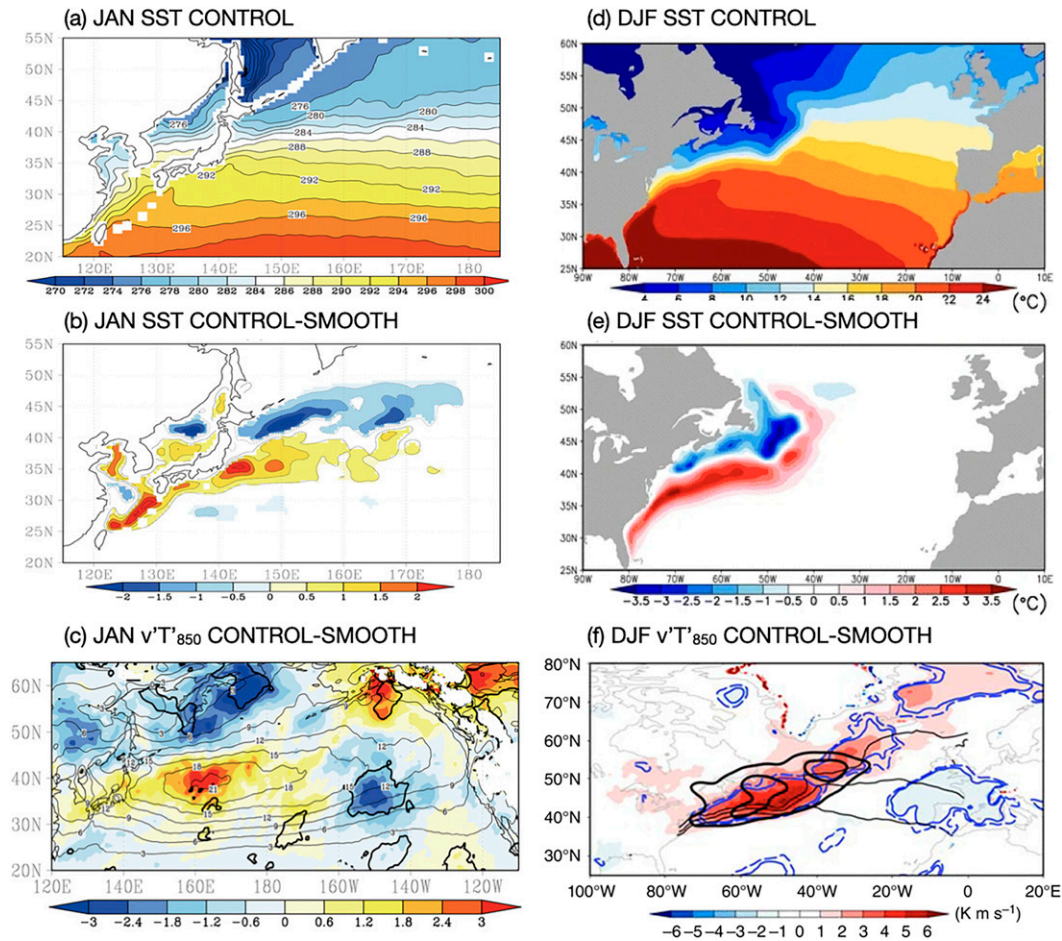


FIG. 5. (a)–(c) January observed SST, its difference (CONTROL – SMOOTH), and the difference (CONTROL – SMOOTH) in storm tracks over the North Pacific Ocean. The thin black contours show  $\overline{v'T'}$  from the CONTROL case. Thick contours denote the 95% confidence level. (d)–(f) As in (a)–(c), but for over the North Atlantic. Black contours in (f) denote atmospheric Eady growth rate at 775 hPa. The dashed and solid blue contours indicate significant differences at the 10% and 5% levels, respectively. Figures adapted from Kuwano-Yoshida and Minobe (2017) and O'Reilly et al. (2016, 2017). Figure reproduced with permission.

transient eddies (Hand et al. 2014; Wills et al. 2016; Lee et al. 2018). The anomalous diabatic heating and the induced vertical motions maintain the climatological circulation pattern over the WBCs.

#### b. Synoptic storms and storm track responses

Storm tracks typically occur in the 30°–50° latitude band coincident with the climatological SST fronts (Fig. 4) and are associated with strong and frequent precipitation, particularly via atmospheric fronts. Midlatitude storm tracks can be primarily defined in two ways (Chang et al. 2002; Hoskins and Hodges 2002): either using distributions of the tracks and intensity of synoptic cyclones (the Lagrangian view) or as regions of strong variability or covariability of winds, geopotential height, temperature, and humidity in the lower to upper troposphere (the Eulerian perspective). To better elucidate the forcing of near-surface weather by the oceans, other studies also use the surface-based storm track, defined

as the variance of near-surface meridional winds (Booth et al. 2010, 2017; O'Neill et al. 2017; Small et al. 2019). The concept of the surface storm track stems from earlier scatterometer measurements illustrating strong imprints of the free-tropospheric storm tracks in the surface wind fields over the warm WBCs (Sampe and Xie 2007; Bourassa et al. 2013). The reduced static stability and the enhanced vertical mixing within the MABL (Fig. 1d) synchronize the locations of the surface storm track with the warm currents (Fig. 4). The surface and free-tropospheric storm tracks are, thus, dynamically coupled via deep moist convection (Czaja and Blunt 2011).

One possible mechanism of midlatitude oceanic influence on the storm track was suggested by Hoskins and Valdes (1990), which found that enhanced diabatic heating by surface fluxes over WBCs supports atmospheric baroclinicity, a vital element in setting the location of the storm track (Hawcroft et al. 2012; Kaspi and Schneider 2013). Nakamura and Shimpo (2004) and Nakamura et al. (2004) further argued



that SST gradients directly influence low-level air temperature gradients via cross-frontal gradients in sensible heat flux (Nakayama et al. 2021). The baroclinicity is measured as the atmospheric maximum Eady growth rate (Charney 1947; Eady 1949; Lindzen and Farrell 1980), such that stronger low-tropospheric baroclinicity is associated with weaker static stability and a stronger meridional air temperature gradient (see the caption of Fig. 4). Both conditions are observed over WBCs. Hence, the anchoring effect by cross-frontal differential heat supply from the ocean is consistent with the formation of a storm track over the WBC SST fronts (Nonaka et al. 2009; Hotta and Nakamura 2011), while diabatic heating over the warm portion of the WBC SST fronts to the warm and cold sectors of the cyclones supports the growth of transient baroclinic waves (Booth et al. 2012; Willison et al. 2013; Hirata and Nonaka 2021; Figs. 1b,c).

A standard method to diagnose the SST forcing mechanism of the storm track is to run a pair of AGCM simulations, one using observed SSTs (CONTROL), and another using a spatially smoothed SST field with weaker gradients (SMOOTH), which also alters absolute SST (Fig. 5). Alternatively, AGCMs are forced by shifting the latitude of the SST fronts or filtering mesoscale eddy SSTs (Seo et al. 2017). Such AGCM simulations indicate a strengthening of the storm track near the Kuroshio–Oyashio Extension (KOE) (Kuwano-Yoshida and Minobe 2017) and the Gulf Stream (O'Reilly et al. 2017) in CONTROL near the climatological maximum cyclogenesis (Fig. 5). Altered storm activity over the WBC regions influences the intensity of the coastal storms, and, thereby, inland weather near the Kuroshio (Nakamura et al. 2012; Hayasaki et al. 2013; Sugimoto et al. 2021), the Gulf Stream (Infanti and Kirtman 2019; Hirata et al. 2019; Liu et al. 2020), and the Agulhas Current (Singleton and Reason 2006; Nkwinkwa Njouodo et al. 2018).

Recent studies indicate that atmospheric mesoscale phenomena within the storm tracks, such as atmospheric fronts, directly interact with the WBC fronts. Parfitt and Czaja (2016) used reanalysis data over the Gulf Stream, and Parfitt et al. (2016) used AGCM simulations over the KOE to argue that the cross-frontal sensible heat flux gradients across the SST fronts exert “thermal damping or strengthening” of atmospheric fronts depending on the space–time alignment between the SST gradients and atmospheric fronts with shared cross-frontal length scales (Figs. 1b,c). The most significant diabatic heating by surface fluxes is concentrated on the narrow space–time scales at which the cold sectors of the atmospheric front coincide with the warm sector of the SST fronts (Fig. 1c), significantly enhancing precipitation associated with the atmospheric fronts and often facilitating explosive cyclogenesis (Hirata and Nonaka 2021 and references therein).

In contrast, other studies emphasize the limited role of SST fronts on extreme cyclones. AGCM experiments by Tsopouridis et al. (2021) indicated that the direct impacts of sharp SST fronts on individual cyclones over the Gulf Stream and KOE are weak, although SST fronts induce significant indirect responses in large-scale environments in which such storms form. Using an analytic model, Reeder et al. (2021) showed that diabatic frontogenesis over the WBCs intensifies atmosphere fronts only

when strong and rapidly propagating synoptic systems are not already in the environment.

Much uncertainty remains in model simulations and observational analysis regarding the relative importance of SST gradients causing cross-atmospheric frontal sensible heat flux gradients versus absolute SST affecting the large-scale condensational heating over warm currents. Another critical issue is that since the SST contributions to the precipitation from the warm and cold sectors of extratropical cyclones differ in terms of magnitude and spatial distribution (i.e., broader for the warm sectors and more “anchored” to the SST fronts for the cold sectors; e.g., Vannière et al. 2017), the cold sector contribution might have been dominating the sensitivity of relatively high-resolution ( $\sim 50$  km) AGCM simulations to SST smoothing. It remains an open question whether even higher-resolution AGCMs might amplify a sensitivity from the dynamics of the warm sectors, including atmospheric mesoscale instabilities developing on the warm conveyor belt (Czaja and Blunt 2011; Sheldon et al. 2017).

### c. Near-surface wind convergence and vertical motion over the WBCs

A crucial part of the storm track response to SST is precipitation, which tends to cluster around the WBCs and is associated with high near-surface wind convergence (NSWC) and substantial vertical ascent. The climatological NSWC coincides with the ocean fronts and the Laplacians of SST and SLP, which indicates that the boundary layer process depicted by linear Ekman dynamics is germane to the observed NSWC and precipitation responses (Feliks et al. 2004; Minobe et al. 2008, 2010). However, the unambiguous attribution of NSWC to the steady Ekman-balanced mass adjustment mechanism remains difficult due to the coexistence of extratropical storm tracks with the WBC currents, which also induce minima in the time-mean SLP Laplacian over the SST fronts (O'Neill et al. 2017).

O'Neill et al. (2015) show from QuikSCAT observations and a regional atmospheric model that linear boundary layer dynamics cannot explain the daily time-scale occurrence of NSWC since, on rain-free days, surface divergence dominates even though the SST Laplacian would indicate convergence (Fig. 6). Using an extreme value filter, O'Neill et al. (2017) further show that NSWC and vertical motion over the Gulf Stream are highly skewed and consist of infrequent yet extreme surface convergence events and more frequent but weak, divergent events, such that the median surface flow field is weakly divergent or nearly nonconvergent (Fig. 6). Parfitt and Czaja (2016) and Parfitt and Seo (2018) argue that much of the precipitation and NSWC are associated with atmospheric fronts, given that only a weak near-surface divergence remains when the contribution from atmospheric fronts is removed (Rousseau et al. 2021). In contrast, Masunaga et al. (2020a,b) showed that storms and fronts of moderate intensity are significant contributors to the time-mean convergence observed over the Gulf Stream and KOE.

### 10-yr Mean All-Weather QuikSCAT Divergence

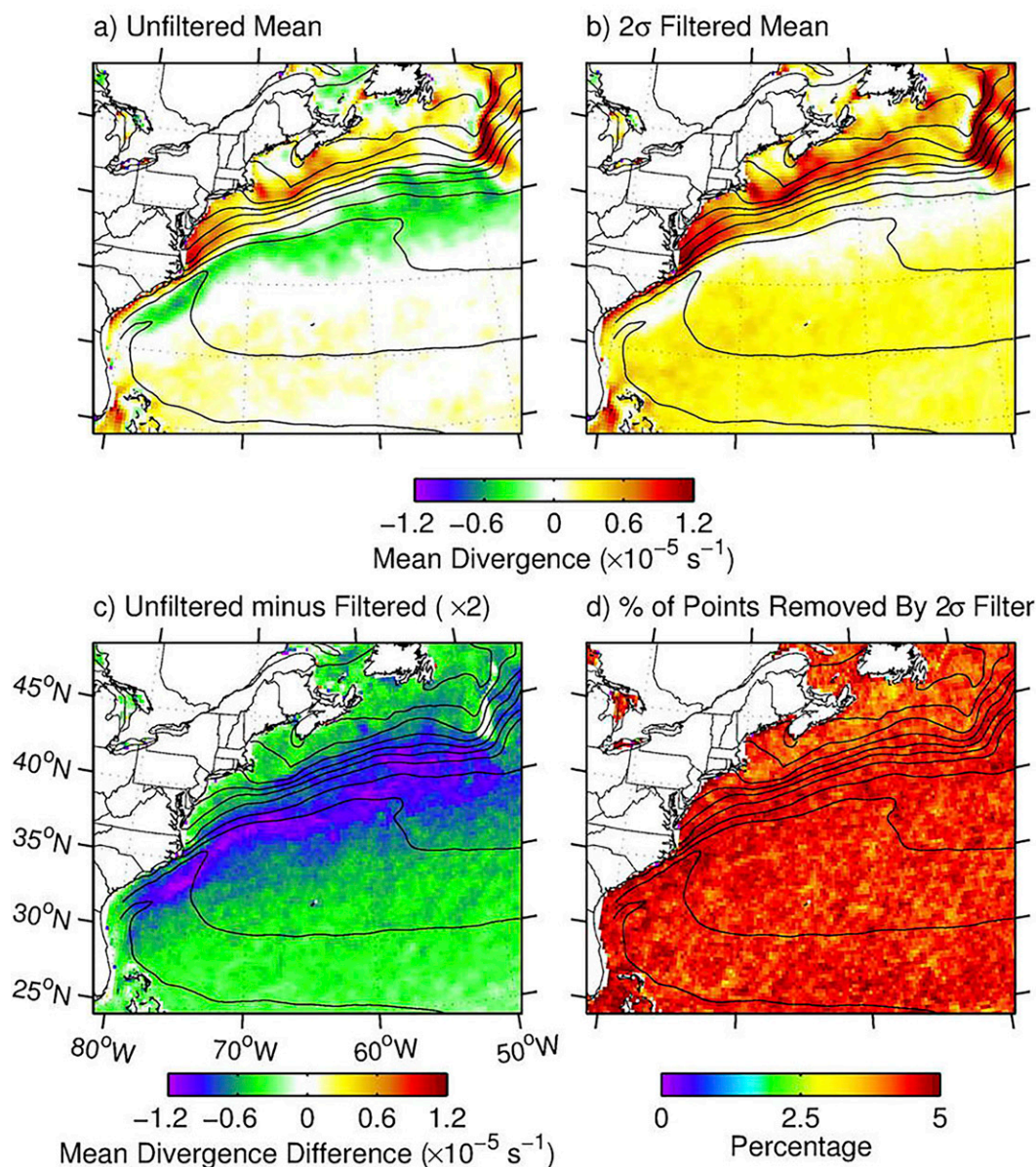


FIG. 6. Maps of the 10-yr-mean QuikSCAT all-weather divergence, (a) consisting of all points and (b) after application of the  $2\sigma$  temporal extreme-value filter, as well as (c) the difference between (a) and (b), and (d) the percentage of divergence points removed by the  $2\sigma$  extreme-value filter. The contours in each panel are of the 10-yr-mean Reynolds SST with a contour interval of  $2^\circ\text{C}$ . From O'Neill et al. (2017). Figure reproduced with permission.

Current research emphasizes identifying how and why atmospheric fronts align with and linger over ocean fronts in all major WBCs and whether there is an additional underlying, steady, small-scale boundary layer effect. There might exist a distinct temporal dependence of the NSW over WBC SSTs, where atmospheric fronts govern its day-to-day variability, while the pressure adjustment and vertical mixing mechanisms provide lower frequency modulations (e.g., Brachet et al. 2012; Small et al. 2022, manuscript submitted to *J. Climate*).

#### d. Nonlocal downstream atmospheric circulation responses

The upstream storm track variability leading to downstream development of the storm track is an essential characteristic of midlatitude baroclinic waves (Chang 1993). The altered synoptic-scale disturbances over the baroclinically unstable western basins (section 3b) radiate energy downstream, influencing the growth of a subsequent baroclinic wave toward the eastern basins (e.g., Chang and Orlanski 1993). The



downstream atmospheric circulation also results from the synoptic eddy–mean flow interactions, where low-frequency atmospheric circulation is coupled with the transient eddy activity modified over the WBCs (e.g., Haines and Marshall 1987; Nakamura and Wallace 1990). Here, downstream (or remote, or nonlocal) refer to the region immediately east of the SST forcing and the tail end of the storm track abutting the west coasts of the continents, as illustrated in Fig. 1a.

Many AGCM studies demonstrate a nonlocal, downstream response in the storm track to WBC SST forcing. Using the observational datasets, Wills et al. (2016) and Joyce et al. (2019) identified significant transient atmospheric circulation responses (storm track and atmospheric blocking) downstream that lag the SSTA in the Gulf Stream Extension by several weeks to months. The modeling studies by O'Reilly et al. (2016, 2017) showed that a strengthened storm track over the Gulf Stream leads to the northward shifted atmospheric eddy-driven jet and the increased European blocking frequency far downstream. Along a similar line, Lee et al. (2018) suggested that SST biases near the Gulf Stream trigger extended biases in the simulation of deep convection and downstream circulation via Rossby wave response.

In the North Pacific, O'Reilly and Czaja (2015) found that baroclinic eddies grow faster when the Kuroshio Extension (KE) front is in its stable regime (stronger SST gradients). The local shift in baroclinic wave activity leads to the early barotropitization of the baroclinic eddies downstream, resulting in weaker poleward eddy heat flux and increased occurrence of blocking in the eastern Pacific. An AGCM study by Kuwano-Yoshida and Minobe (2017) also suggested the enhanced storm track by the KOE SST fronts leads to a northward shifted storm track in the eastern Pacific. Ma et al. (2015, 2017) showed from AGCM simulations that the transient SSTA associated with the KOE mesoscale eddies leads to a northward shifted storm track and reduced precipitation in parts of western North America (Foussard et al. 2019b; Liu et al. 2021; Siqueira et al. 2021).

In the Southern Ocean, Reason (2001) showed that amplified cyclone activity over the warm Agulhas Current yielded an enhanced storm track in the southeast Indian Ocean. Recent aquaplanet AGCM experiments have also demonstrated the critical role of the oceanic fronts in shaping the structure of the baroclinic annular mode variability (e.g., Sampe et al. 2013; Ogawa et al. 2016; Nakayama et al. 2021), leading modes of variability of the extratropics (e.g., Thompson and Wallace 2000). Evidence exists that the oceanic frontal zones also impact the troposphere–stratosphere interactions (e.g., Hurwitz et al. 2012; Ogawa et al. 2015; Omrani et al. 2019), potentially affecting the entire hemispheric climate patterns.

#### *e. Climate change*

Climate change simulations for the twenty-first century have emphasized the critical role of ocean circulation leading to natural modes of variability such as ENSO and PDO (Seager et al. 2001), the projected weakening of the Atlantic meridional overturning circulation (AMOC; Weaver et al. 2012), and the delayed warming of the Southern Ocean

(Marshall et al. 2014). These changes are relevant to the observed and projected intensification and poleward shift of the Kuroshio and Agulhas, weakening of the Gulf Stream, and changes in the frontal systems of the Antarctic Circumpolar Current (ACC) (e.g., Wu et al. 2012; Yang et al. 2016; Sen Gupta et al. 2021).

The latest IPCC report (IPCC 2021) indicates that, during the twenty-first century, the North Pacific storm track will most likely shift poleward, the North Atlantic storm track is unlikely to have a simple poleward shift, and the Southern Hemisphere storm track will likely shift poleward. Understanding these regional differences in projected changes in midlatitude storm tracks and precipitation and their association with the predicted WBC changes has been the primary goal of high-resolution CGCM studies, especially those that contrast the CGCMs with the eddy-rich ocean (typically  $0.1^\circ$  resolution) to those with the eddy-parameterized ocean ( $0.5^\circ$ – $1^\circ$ ). These studies with increased ocean model resolution to mitigate the known biases in representing the WBC dynamics and separation show distinct responses in SSTs and storm tracks in the WBC regions to anthropogenic climate change.

In these eddy-rich simulations, the KOE front shifted equatorward, contrary to projections by the eddy-parameterized IPCC-class CGCMs, which likely reflects the large natural variability in the North Pacific (Taguchi et al. 2007; Seager and Simpson 2016). In the North Atlantic, the Gulf Stream separation tends to be too far north in lower-resolution models, an issue common to other WBCs, but is improved in eddy-rich models. This makes it possible for the separation to move northward as a response to AMOC weakening in eddy-rich models (Gervais et al. 2018; Moreno-Chamarro et al. 2021; Grist et al. 2021), leading to a significant projected ocean warming near the U.S. eastern coastline (Fig. 7; Karmalkar and Horton 2021). In the Southern Ocean, CMIP5-based climate change simulations indicate delayed warming, often attributed to stratospheric ozone depletion (McLandress et al. 2011; Polvani et al. 2011). However, the recent satellite observations and eddy-rich CGCMs simulations indicate a ubiquitous cooling trend (1961–2005) poleward of the ACC due to the effects of resolved ocean eddies (Bilgen and Kirtman 2020). Analysis of eddy-rich ocean simulations also indicates warmer and stronger Southern Hemisphere WBCs, suggesting that resolved ocean eddies play a critical role in long-term SST changes.

The reorganization of the oceanic frontal zone and its associated eddy field modulates the atmospheric low-level baroclinicity and the strength and location of the diabatic heating source for the atmosphere. It is clear from this and other studies (Woollings et al. 2012; Winton et al. 2013; Keil et al. 2020) that such features would not occur without ocean circulation changes. However, the exact pattern of large-scale SST change is highly dependent on the ocean model and its resolution (Saba et al. 2016; Menary et al. 2018; Alexander et al. 2020), which also affects the projected WBC responses to climate change (Jackson et al. 2020). Climate projections with eddy-rich oceans have typically been performed with a small number of realizations and for short durations due to high computational costs (e.g., Haarsma et al. 2016). Currently, high-resolution coupled climate modeling projects are

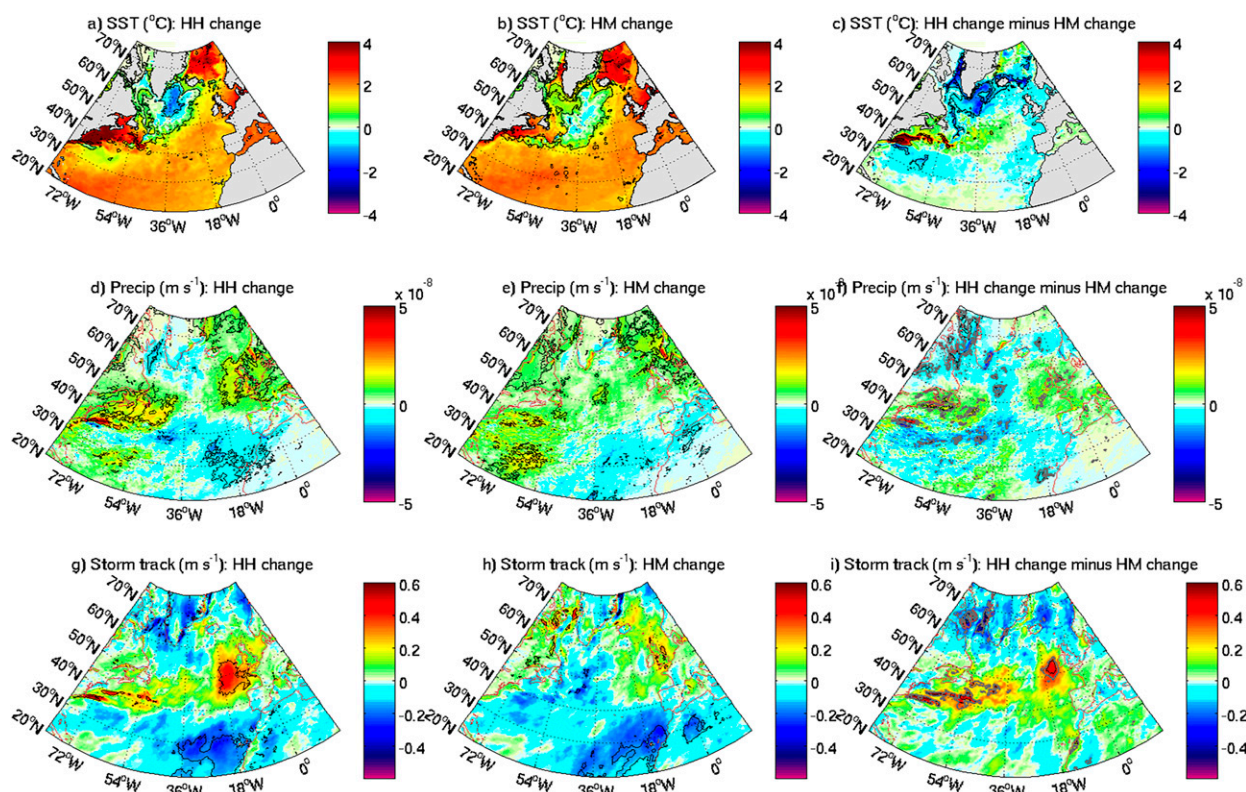


FIG. 7. 2031–50 minus 1951–70 differences simulated by the HadGEM3-GC3.1, with 25-km atmospheric resolution coupled to  $1/4^\circ$  ocean (eddy-permitting, HM) and  $1/12^\circ$  ocean (eddy-rich, HH): SST ( $^\circ\text{C}$ ) for (a) HH and (b) HM, precipitation ( $\text{m s}^{-1}$ ) for (d) HH and (e) HM, and surface storm track ( $\text{m s}^{-1}$ ) for (g) HH and (h) HM, as well as (c), (f), (i) the differences between the HH future change and the HM change. The black lines denote the 95% significance. Gray lines in (c), (f), and (i) denote the 90% significance. From Grist et al. (2021). Figure reproduced with permission.

underway with much longer integration and multiensembles (e.g., Chang et al. 2020; Wengel et al. 2021). These efforts will enable a robust assessment of the forced responses in WBC and ocean circulation from natural variability in response to projected changes in the large-scale climate.

#### 4. Feedback of atmospheric responses onto the ocean

The new insights gained from the studies discussed in section 3 have also led to improved process understanding and notable revisions of theories of ocean circulation. This section discusses current knowledge of ocean feedback mechanisms, including feedback impacts on ocean biogeochemical cycles, and theories of ocean circulation and model parameterizations to account for eddy–atmosphere interaction. The processes covered in this section correspond mainly to Figs. 1e and 1f.

##### a. Feedback on ocean circulation

For simplicity, we consider two categories of oceanic mesoscale effects on air–sea fluxes: SST impacts (thermal) described in section 2b(1) and surface current impacts (mechanical) in section 2b(2). The thermal feedback results from kinematic and thermodynamic responses in the MABL to mesoscale SSTs, modifying the wind stress and heat fluxes.

The current feedback represents the frictional processes by which the surface ocean current alters the wind stress, near-surface wind, and turbulent heat fluxes. This subsection focuses on the respective feedback impacts of the air–sea fluxes on ocean circulation.

##### 1) THERMAL FEEDBACK EFFECT

Observed near-surface wind stress responses to mesoscale processes by Chelton et al. (2004) were interpreted based mainly on the thermal feedback (TFB) effect. Vecchi et al. (2004) and Chelton et al. (2007) hypothesized that the wind stress curl responses to SST fronts exert a vital feedback mechanism driving the evolution of SST fronts via resulting anomalous Ekman pumping. Spall (2007b) considered the impacts of SST-induced Ekman pumping on baroclinic instability in the ocean in the modified linear theory by Eady (1949), showing that the SST-induced Ekman pumping adjusts the growth rate and wavelength of the most unstable waves, especially the low-latitude flows with strong stratification. Hogg et al. (2009) extended SST-induced Ekman pumping to an idealized double-gyre circulation in midlatitudes, showing that it destabilizes the eastward jet with the enhanced cross-gyre potential vorticity fluxes, stabilizing the double gyre circulation by 30%–40%.

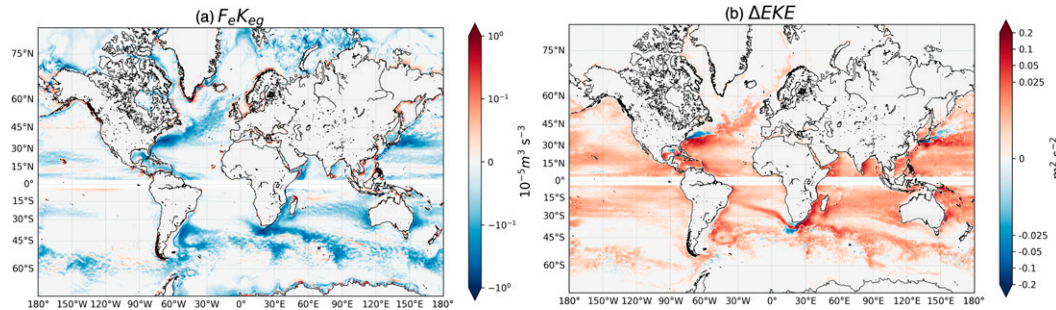


FIG. 8. (a) Geostrophic eddy wind work ( $10^{-5} \text{ m}^3 \text{ s}^{-3}$ ) estimated from the EC-Earth global coupled simulation (15 km atmosphere coupling  $1/12^\circ$  ocean) with current feedback (CFB). The negative values indicate a momentum transfer from geostrophic mesoscale currents to the atmosphere. This sink of energy is the primary driver of the damping of EKE illustrated in (b), as the difference of EKE ( $\text{m}^2 \text{ s}^{-2}$ ) between the simulations without CFB and with CFB. The positive values indicate the relative increase in EKE in the *absence* of CFB due to the transfer of the momentum to the atmosphere. The geostrophic wind work and EKE are both estimated over 30 years. Details about the coupled model and experiments can be found in [Renault et al. \(2019c\)](#).

Mesoscale SSTAs are damped by induced turbulent heat fluxes (THF), resulting in a negative SST–THF correlation at oceanic mesoscales. Over the KOE, [Ma et al. \(2016\)](#) examined this mesoscale SSTa damping in the context of the eddy potential energy (EPE) budget and the Lorenz energy cycle. Compared to the eddy-filtered coupled model simulation (using a  $1000 \text{ km} \times 1000 \text{ km}$  boxcar filter), the eddy-unfiltered simulations showed a significant increase ( $>70\%$ ) in diabatic EPE dissipation, leading to a decrease in eddy kinetic energy (EKE) by 20%–40%, most strongly at wavelengths shorter than 100 km ([Fig. 1d](#)). Other studies find that TFB has a weak impact on EKE ([Seo et al. 2016; Seo 2017](#)). It is possible that a large filter cutoff, as used in [Ma et al. \(2016\)](#), overestimates EKE damping and may also smooth large-scale meridional SST gradients, altering the large-scale wind curl and the mean circulation. [Bishop et al. \(2020\)](#) evaluated the EPE damping over the global oceans using eddy-resolving climate model simulations to find that the diabatic EPE damping was systematically stronger over warm-core eddies ([Figs. 1c,e](#)). Other studies point out that the efficacy of the negative SST–THF correlation in the maintenance of the mesoscale SSTa and their gradients depends on the distribution of the mixed-layer depth, which modulates the effective heat capacity, vertical eddy heat transport, and hence the sensitivity of the SST to the heat flux anomaly (e.g., [Tozuka et al. 2017, 2018; Jing et al. 2020](#)).

## 2) CURRENT FEEDBACK EFFECT

Although weaker than surface winds, surface currents modify surface stress directly by altering wind speed ([Bye 1986](#)). By modulating the stress, the current feedback (CFB) exerts a “bottom-up” effect on the wind, where a positive current anomaly causes a positive wind anomaly via a negative stress anomaly ([Renault et al. 2016a, 2019a](#)). The CFB effect has initially focused on impact on wind stress. Using satellite and in situ data, [Kelly et al. \(2001\)](#) showed that CFB reduces the median wind stress from 20% to 50% near the equator, and [Chelton et al. \(2004\)](#) observed a clear imprint of the Gulf Stream flow on the surface stress and the curl.

Several studies have highlighted the role of CFB as a “top drag” ([Dewar and Flierl 1987](#)), acting on the oceanic circulation over a wide range of space–time scales. At the large-scale where the currents tend to flow downwind ([Fig. 1e](#)), CFB reduces the mean energy input from the atmosphere to the ocean and slows down the mean circulation ([Pacanowski 1987](#)). By weakening net energy input to the ocean, CFB triggers a host of changes in eddy–mean flow interactions and the inverse cascade of energy, weakening baroclinic and barotropic instabilities and mesoscale activity ([Renault et al. 2017b, 2019a; Fig. 8](#)). When the wind and current are in the opposite sense, the CFB serves as a conduit of energy from the ocean to the atmosphere, which can be seen from satellite data as negative mean and eddy wind work ([Fig. 8a; Scott and Xu 2009; Renault et al. 2016a,b, 2017a](#)). Numerous studies have demonstrated a strong EKE damping effect of  $\sim 30\%$  [see references in [Jullien et al. \(2020\); Fig. 8b](#)]. CFB also induces additional Ekman pumping that weakens an eddy ([Gaube et al. 2015](#)) and influences the upper-ocean stratification and SST ([Seo et al. 2019; Song et al. 2020](#)).

Recent studies also have emphasized the CFB impact on near-surface winds ([Renault et al. 2016a, 2017a, 2019a](#)). Over the shelf oceans where the current speed at tidal frequencies well exceeds the wind speed, tidal currents induce tidal winds, with an amplitude of about one-third of the underlying tidal currents ([Renault and Marchesiello 2022](#)). Since the wind curl is more strongly impacted by current gradients ([Shi and Bourassa 2019](#)), the consideration of wind–current coupling at tidal frequency might be necessary for the simulation and prediction of surface winds and the MABL momentum EKE balances in the offshore environments.

There are several open questions. First, little is known about CFB at the submesoscale. For the U.S. West Coast, [Renault et al. \(2018\)](#) highlighted a submesoscale dual effect of CFB: it damps submesoscale eddies but also catalyzes submesoscale current generation by affecting mixing, stratification, and eddy variability. Second, CFB modulates biogeochemical variability ([McGillicuddy et al. 2007](#)), yet the detailed mechanisms behind the biogeochemical impacts are not fully understood, although the impact depends highly on background stratification (e.g.,



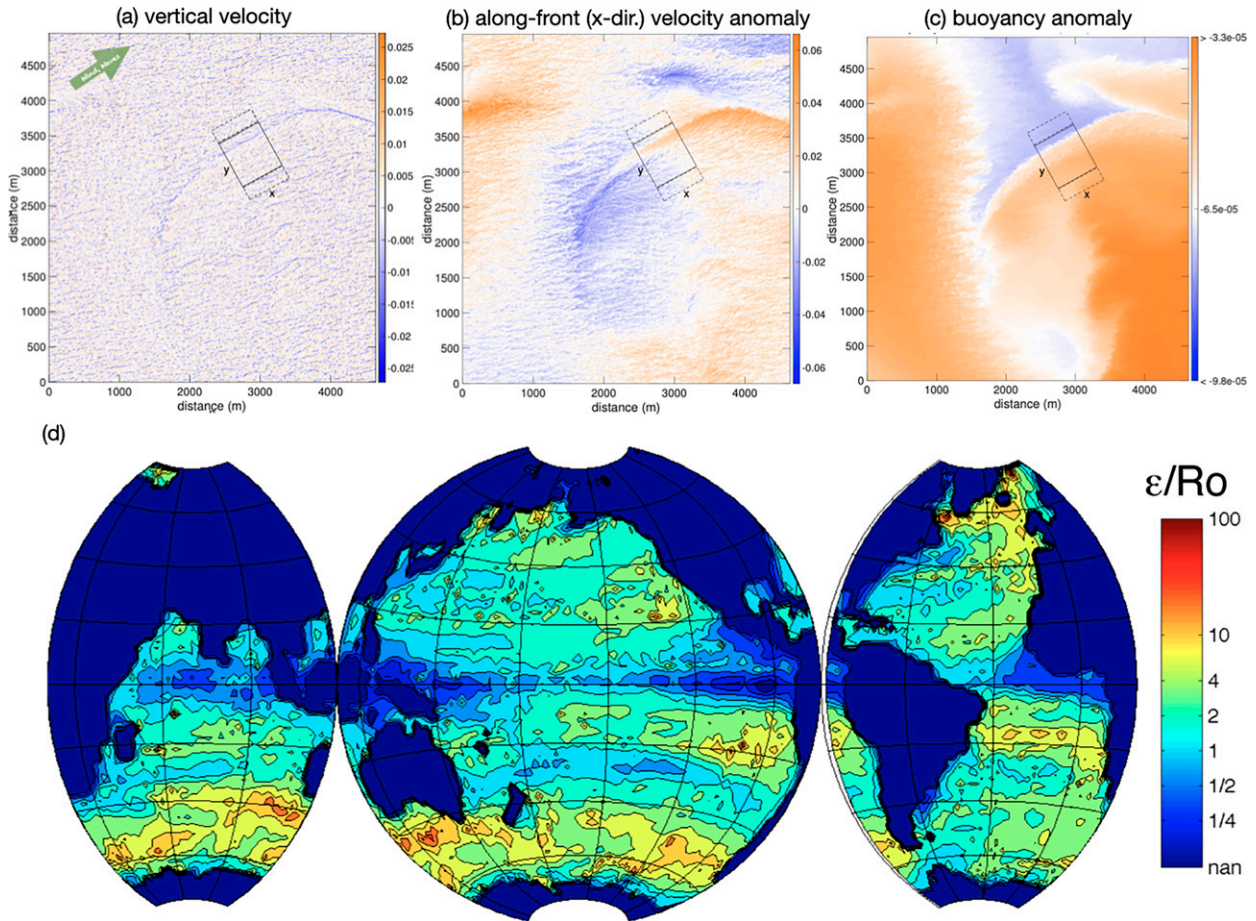


FIG. 9. (top) Examples of a front interacting with Langmuir turbulence (box centered on this feature), which is aligned in the downwind and down-Stokes direction. (a) Vertical velocity ( $\text{m s}^{-1}$ ) at  $z = -11.25$  m shows ubiquitous Langmuir cells, but also a long, coherent (downwelling) overturning circulation along the front due to frontogenesis and accelerated by the Stokes shear force. (b) Along-front ( $x$ -direction) velocity anomaly (with respect to the horizontal mean;  $\text{m s}^{-1}$ ) at  $z = -11.25$  m shows the frontal flow. (c) Buoyancy anomaly (with respect to the horizontal mean;  $\text{m s}^{-2}$ ) at  $z = -11.25$  shows the front characterized by a sharp transition in buoyancy (or temperature). Adapted from Suzuki et al. (2016). (d) Estimated ratio of  $\varepsilon$  (strength of Stokes drift-induced vertical acceleration versus buoyancy, an indicator of wave contributions added to the traditional hydrostatic balance) to Rossby number (indicating geostrophic balance). This ratio implies the deviation from the hydrostatic balance due to waves compared to the geostrophic balance due to advection. This estimate is based on the de Boyer Montégut et al. (2004) mixed layer depth climatology ( $h$ ) and a global simulation of WaveWatch3 and AVISO geostrophic velocity. Figures redrawn from McWilliams and Fox-Kemper (2013).

Kwak et al. 2021). Finally, since CFB and TFB coexist where mesoscale currents are strong (Song et al. 2006; Seo et al. 2007; Takatama and Schneider 2017; Renault et al. 2019b; Shi and Bourassa 2019), CFB likely influences large-scale boundary layer moisture, clouds, precipitation, and atmospheric circulation via rectified effects. However, this downstream influence is only beginning to be explored (e.g., Seo et al. 2021).

#### b. Wave–current interactions near ocean fronts

While sea state is a salient aspect of air–sea fluxes (Fairall et al. 1996; Cavaleri et al. 2012; Edson et al. 2013), there are other aspects related to surface wave interactions with (sub)-mesoscale currents potentially important for small-scale air–sea interaction (section 6c). For example, it has long been

known that sheared currents affect the propagation of surface wave rays (Villas Bôas and Young 2020). In the open ocean, the spatial gradients in mesoscale surface currents dominate the variability of significant wave height, leading to the refraction of waves near steep vorticity gradients (Ardhuin et al. 2017; Villas Bôas et al. 2020). Similarly, the underpinnings of the Craik–Leibovich theory of Langmuir turbulence specify that rectification of wave–vorticity interactions in the upper ocean leads to Stokes forces, which can cause substantial wave effects on currents (Leibovich 1983; Lane et al. 2007). The LES models that include vortex forces and regional models that include the wave refraction by currents (Romero et al. 2020) illustrate the frontal adjustment and frontogenesis triggered or enhanced by surface wave interactions (McWilliams and Fox-Kemper 2013;



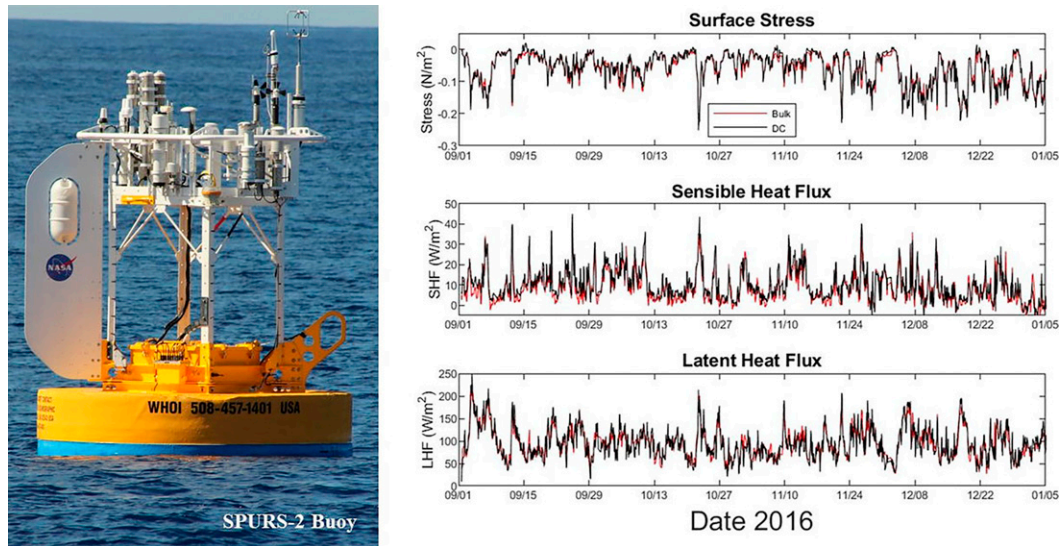


FIG. 10. (left) The SPURS-2 central mooring with instrumentation at the upper right includes a sonic anemometer, infrared hygrometer, and sensors to remove buoy motion. The sensor package can directly measure the surface stress, sensible heat, and latent heat fluxes [see [Clayson et al. \(2019\)](#) for more details on instrumentations]. (right) Time series of these fluxes showing bulk estimates in red and direct covariance (DC) fluxes in black. A good qualitative agreement is seen between the bulk and DC estimates, with the most significant discrepancies visible in the sensible heat flux ([Bigorre et al. 2013](#)). The coincident measurements of direct flux and bulk meteorology from SPURS-2 and prior field campaigns (e.g., CBLAST, DYNAMO, CLIMODE, etc.) are being used for improving the bulk flux algorithm for turbulent heat flux transfer coefficients. Photo by James B. Edson (WHOI).

[Suzuki et al. 2016](#); [Sullivan and McWilliams 2019](#)). Examples are provided in [Fig. 9](#) (upper panel), where a submesoscale density front in the downwind and down-Stokes direction interacts with Langmuir turbulence. Strong overturning circulation (downwelling) sharpens the front and strengthens the along-front jet. Classic balances are altered by waves to yield the wavy Ekman balance ([McWilliams et al. 2012](#)), the wavy geostrophic balance ([McWilliams and Fox-Kemper 2013](#); [Fig. 9](#), lower panel), and the baroclinic and symmetric instabilities affected by waves ([Haney et al. 2015](#)).

#### c. Physics of ocean mesoscale processes and air–sea interaction

Traditionally, mesoscale and submesoscale eddy parameterizations have been deterministic and focused only on effects on the mean and variance of tracers ([Gent and McWilliams 1990](#); [Fox-Kemper et al. 2011](#)), while neglecting rectified effects on air–sea coupling. However, in simulations where some eddies are resolved, deterministic closures do not stimulate a resolved eddying response or backscatter (e.g., [Bachman et al. 2020](#)). In response, there is a growing desire to implement stochastic parameterizations of the eddy transport into non-eddy-resolving models, for example, via uncertainty in location ([Mémín 2014](#)), transport ([Drivas et al. 2020](#)), closure ([Nadiga 2008](#); [Jansen and Held 2014](#); [Zanna et al. 2017](#); [Bachman et al. 2020](#)), or equation of state ([Brankart 2013](#)). These efforts should include stochastic parameterizations of the eddy-driven air–sea coupling ([Ma et al. 2016](#); [Bishop et al. 2020](#); [Jing et al. 2020](#)). As stratification and rotation parameters vary globally,

building scale awareness into parameterizations is also crucial ([Hallberg 2013](#); [Dong et al. 2020, 2021](#)). Changing the relative orientation of atmospheric winds and oceanic fronts leads to qualitatively different results (e.g., enhancement vs. suppression of submesoscales; [Fig. 1f](#)), implying that directional subgrid information will be necessary to consider (e.g., [D’Asaro et al. 2011](#); [Suzuki et al. 2016](#); [McWilliams 2016](#)). Observed air–sea fluxes are highly variable, indicating a response to high spatio-temporal variability ([Yu 2019](#)), scale dependence ([Bishop et al. 2017, 2020](#)), and sea state dependence ([Kudryavtsev et al. 2014](#)), thus offering the potential for stochastic implementation. While idealized studies have begun to develop a process-level understanding ([Sullivan et al. 2020, 2021](#)), no realistic model implementation of stochastic air–sea fluxes seems to have been evaluated carefully.

#### d. Impacts on primary productivity

Mesoscale air–sea interaction can also influence biogeochemical environments and primary productivity (e.g., [McGillicuddy 2016](#)). Satellite observations show that the wind stress responses to mesoscale SST and currents introduce perturbation Ekman upwelling and downwelling (e.g., [Gaube et al. 2015](#)), leading to dramatic midocean mesoscale plankton blooms, such as those observed in the nutrient-replete subtropics (e.g., [McGillicuddy et al. 2007](#)). Additionally, eddy-induced modifications of wind stress impact vertical mixing in the upper oceans. Eddy effects on mixed-layer depths are asymmetric between anticyclones and cyclones (e.g., [Dufois et al. 2017](#); [Hausmann et al. 2017](#)). However, to what extent

this asymmetry stems from the mesoscale modulations of surface wind stress has yet to be determined. Considering the prevalence and persistence of nonlinear mesoscale eddies in the global oceans (Chelton et al. 2011a,b), the relevance of mesoscale eddy impacts on primary productivity via eddy–wind interaction needs robust quantification.

## 5. State of observational capabilities

Observing mesoscale air–sea interaction processes is challenging since multiple oceanic and atmospheric parameters must be measured with high accuracy and spatiotemporal resolution. The past decade has seen the emergence of many novel in situ and remote sensing platforms that increasingly better capture mesoscale and smaller processes with high accuracy and resolution (e.g., Kessler et al. 2019, ch. 9). These novel observational technologies are expected to provide opportunities for multiplatform, coordinated measurements for air–sea interaction studies (e.g., Bony et al. 2017; Wang et al. 2018).

### a. In situ observations

Oceanographic moorings can be equipped with meteorological instruments, including direct covariance flux systems and bulk meteorological sensors, to provide directly measured and bulk-estimated air–sea fluxes, respectively. An example system is shown in Fig. 10 from the second Salinity Processes in the Upper-ocean Regional Study (SPURS-2) experiment, which computed and telemetered in near-real-time the motion-corrected surface wind stress and sensible and latent heat fluxes from a surface mooring for the first time (Clayson et al. 2019). There is overall a good qualitative agreement between the measured and estimated air–sea fluxes (Bigorre et al. 2013). However, the bulk formula method underestimates the momentum flux and overestimates the buoyancy flux under high wind conditions. These biases are categorically related to deficiencies in formulations for the drag and heat transfer coefficients. Edson et al. (2013) revised the formulations for drag coefficient in COARE 3.5 to alleviate the low drag coefficient bias and proposed a new formula for heat transfer coefficients. Ayt and Chapron (2022) reviewed potential wave–atmospheric turbulence coupling mechanisms that allow for further refinements. Recently, buoy arrays have been deployed as part of the Ocean Observatories Initiative (OOI; Trowbridge et al. 2019) and operated for years on both coasts. These in situ data and the simultaneous measurements of surface meteorology and wave conditions are crucial to reducing the uncertainty in air–sea flux estimates in modern bulk formulas (Edson et al. 2013; Cronin et al. 2019; Villas-Bôas et al. 2019).

Autonomous surface vehicles (ASVs) are piloted wave- or wind-propelled surface platforms that can be instrumented with ocean, atmospheric, and biogeochemical sensors. Widely used ASVs include Saildrones (Meinig et al. 2019) and Wave Gliders (Thomson and Garton 2017), which have long-endurance (~6 months) and can sample in remote locations and be piloted across fronts. Using numerous instruments can mitigate issues with cross-frontal sampling and thus capture mesoscale

and smaller variations in air–sea interaction (Quinn et al. 2021; Stevens et al. 2021).

Drifting platforms can be instrumented with various sensors that capture air–sea interaction. The Global Drifter Program, a global network of surface drifters that typically measure currents, SST, and barometric pressure, has contributed to understanding global mesoscale circulation (Laurindo et al. 2017; Centurioni et al. 2019). Drifting spar buoys (Graber et al. 2000; Edson et al. 2013) have been measuring surface fluxes in situ for decades. In recent years, sophisticated low-profile Lagrangian platforms have been developed, such as SWIFTs (Surface Wave Instrument Floats with Tracking; Thomson 2012), to measure surface currents, waves, and near-surface ocean turbulence over various wave conditions. Benefits of drifters include relatively low cost and Lagrangian sampling. However, they tend to converge at fronts; therefore, multiple drifters are necessary to characterize cross-frontal structure (D’Asaro et al. 2018).

Recent advancements in biologging technology may help facilitate autonomous measurements and real-time monitoring of essential ocean variables that may be important for air–sea interaction studies (Harcourt et al. 2019). As the biologging data can track mesoscale eddies and fronts in greater detail (Charrassin et al. 2008; Miyazawa et al. 2019) and can be assimilated into operational models (Yoda et al. 2014; Miyazawa et al. 2016), the application of animal-borne sensors has the potential to advance predictive capabilities of extratropical cyclones that strongly interact with the oceans (section 3b).

Aircraft measurements are crucial for air–sea interaction studies. The platform’s mobility is advantageous because of its ability to obtain in situ measurements of the horizontal and vertical variability in and above the MABL in a short time. With carefully designed flight patterns, it can also derive mesoscale forcing to the boundary layer using the velocity field measured at flight level (Lenschow et al. 1999; Stevens et al. 2003). In the past 20 years, air-deployable sensor packages such as GPS dropsondes, AXBT, AXCTD, and instrumented floats have further expanded the sampling capability to depict the entire column of the atmosphere and the upper ocean, particularly when low-level flights are not feasible (Doyle et al. 2017). In recent years, airborne measurements have been extended to 10 m above the sea surface using a controlled towed vehicle (Wang et al. 2018). This new capability is significant to air–sea interaction studies, particularly surface flux parameterization.

### b. Remote sensing

Emerging remote sensing platforms, including satellite, ground-based, or airborne measurements, present promising means to estimate air–sea fluxes at ocean mesoscale and smaller. Scatterometer and microwave measurements provide collocated global views of ocean vector winds and SST under all wind conditions at daily scales. However, considerable uncertainty exists under extreme conditions due to inconsistent in situ reference wind speeds from dropsondes and moored buoys to calibrate satellite winds (e.g., Polverari et al. 2021). This also implies uncertainties in modeling ocean drag and air–sea interaction. The virtual constellation of scatterometers

(Stoffelen et al. 2019) provides good temporal coverage of the extremes, with now seven scatterometers in space with revisits globally within 30 min or a few hours (Gade and Stoffelen 2019). Future satellite observations will need to resolve synoptic variability under strong wind and rain and increase the resolution of the vertical profiles within the MABL to better estimate the relationship between the surface flux and flux profiles.

For momentum fluxes, key variables are surface winds, currents, and waves. In coastal regions, high-frequency radar systems provide surface currents at  $O(1)$  km resolution (Kim 2010; Paduan and Washburn 2013; Kirincich et al. 2019), which can be used to infer surface wave conditions and wind stress (e.g., Saviano et al. 2021). The airborne DopplerScatt system simultaneously captures surface wind stress, waves, and currents (Wineteer et al. 2020) and is central to the Submesoscale Ocean Dynamics Experiment (S-MODE; Farrar et al. 2020). Similar concepts for new satellite observations have been proposed (see Villas Bôas et al. 2019) and are currently in various development stages (e.g., Bourassa et al. 2016; López-Dekker et al. 2019; Gommenginger et al. 2019; Wineteer et al. 2020). Surface waves are crucial for accurate estimates of momentum flux; new satellite missions such as CFOSAT (Chinese-French Oceanography Satellite) simultaneously measuring waves and winds (Ardhuin et al. 2019) are expected to improve the accuracy of the wind speed and wave-based formulations in the advanced bulk formula for air–sea flux. Satellite surface measurements of stress-equivalent winds more closely respond to stress than wind (e.g., de Kloe et al. 2017). Given the persistent large-scale and mesoscale errors in NWP reanalyses (Belmonte Rivas and Stoffelen 2019; Trindade et al. 2020), these new satellite observations collocated with in situ measurements of surface stress will be valuable for understanding stress-related air–sea coupling and improving ocean modeling and marine forecasting (Bourassa et al. 2019).

In contrast to momentum flux, a critical gap remains in the current satellite remote sensing capability to provide accurate global estimates of turbulent heat and moisture fluxes. Current satellite remote sensing systems rely on bulk parameterizations to estimate net heat and gas fluxes (Cronin et al. 2019). Mesoscale air–sea interaction studies will benefit significantly from a satellite mission that measures collocated, small-scale state variables, including near-surface atmospheric temperature and humidity, SST, and wind speed, that allow accurate estimates of the turbulent heat fluxes (e.g., Gentemann et al. 2020). This will also help validate the numerical models to lower the uncertainty in air–sea heat flux and improve related predictions.

## 6. Discussion and synthesis

Since the first global-scale surveys of the mesoscale air–sea interactions by Chelton et al. (2004) and Xie (2004), our theoretical understanding and observational and modeling capabilities in the past two decades have advanced significantly, leading to a substantial body of literature related to ocean mesoscale air–sea interaction. Our current scientific understanding indicates that mesoscale eddies perturb the MABL via

surface flux anomalies, leading to dynamic and thermodynamic adjustments (section 2; Fig. 1d). The MABL response is communicated to the free troposphere, especially over WBCs (Figs. 1b,c), influencing downstream development of weather and short-term climate events (section 3; Figs. 1a,b). The MABL response feeds back to the ocean circulation, modifying WBC dynamics, air–sea gas exchanges, and nutrient distribution (section 4; Figs. 1e,f). This new knowledge has transformed our classical understanding of physical processes, leading to notable revisions of oceanic and atmospheric circulation theories that incorporate the coupled effects of ocean mesoscale processes, wave, and biogeochemical processes (section 4). Our observing capability has advanced rapidly to characterize mesoscale air–sea interaction (section 5). However, numerous challenges and open questions remain. The remainder of the chapter will focus on physical and biological aspects of modeling, observational, and diagnostic approaches that require further research in the coming years.

### a. Attribution of near-surface wind convergence

While the WBC SST impact on the MABL dynamics is increasingly better understood, there are some critical remaining questions regarding the essential role of WBC SST forcing on the time-mean atmospheric state. The ongoing debates about the origin of the near-surface wind convergence (NSWC) and the maximum precipitation over WBCs are particularly relevant as they entail important implications pertinent to various aspects of the topics discussed in this article. That is, assessing whether the steady linear boundary layer dynamics account for the time-mean NSWC and vertical motion requires a detailed understanding of the modulation of boundary layer ageostrophic circulation by SST (section 2; Fig. 1d). On the other hand, the demonstrated impacts of storms and atmospheric fronts on the NSWC require a careful examination of extratropical cyclogenesis modulated by the diabatic forcing over the ocean fronts (section 3; Figs. 1b,c). Overall, any approach to quantifying the nature of the relationships between NSWC and SST will need to robustly separate the small-magnitude convergence predicted by linear boundary layer theory from the large anomalous convergence induced by storm systems that are several orders of magnitude greater.

### b. Robust diagnostic framework

The debate about the role of SST fronts in the NSWC arises partly due to the lack of a robust process-based diagnostics and analytic framework to interpret the observed convergence patterns. The existing analytical model of Schneider and Qiu (2015) discussed in section 2c offers a complete account of the role of boundary layer dynamics over the SST fronts, providing the two limiting cases of wind response to SST dependent on background wind speed. The model also suggests an extension of the diagnostic framework from the widely used coupling coefficients to lagged regression, impulse response, or corresponding spectral transfer functions. Yet, the model assumes a quasi-steady state and does not



account for the stochastic and moist processes associated with the storm tracks and their synoptic-scale influence on NSW. A critical path forward is to incorporate the time-dependent and moist processes related to extratropical storms along SST frontal zones and the local SST-induced boundary layer response in a single analytical framework. Given the coexistence of the SST and current feedback effects along the frontal zones, any future development of diagnostic frameworks will also have to consider the mechanical coupling effects simultaneously along with the thermal effects (e.g., Takatama and Schneider 2017; Seo 2017; Renault et al. 2019a).

### c. Large-scale impacts in climate models

Numerous studies have demonstrated WBC impacts on downstream atmospheric circulation (Fig. 1e). Some studies argue that the sharpness of WBC fronts shifts the storm track and jet stream, influencing the blocking frequency in Europe and the northeastern Pacific (e.g., Kuwano-Yoshida and Minobe 2017; O'Reilly et al. 2016, 2017; Piazza et al. 2016). Other studies find that meridional shifts of WBC fronts alter the atmospheric transient eddy heat flux downstream (e.g., Frankignoul et al. 2011; Kwon and Joyce 2013; Seo et al. 2017; Joyce et al. 2019). Warm-core eddies near the KOE act as significant oceanic sources of moisture and heat for large-scale circulation, altering downstream precipitation patterns (Ma et al. 2015, 2016; Liu et al. 2021). The importance of the seasonal background state in the atmosphere has also been recognized as it shapes the atmospheric response to SSTA (e.g., Taguchi et al. 2009; Huang et al. 2020).

However, some aspects of the far-field circulation response and its statistical significance remain elusive (Kushnir et al. 2002; Kwon et al. 2010; Czaja et al. 2019). Deriving a robust conclusion on downstream influences is particularly challenging difficult because the studies adopt different methods to define WBC SST impacts, leading to distinct amplitudes/patterns of SST perturbations and atmospheric responses. This uncertainty is in addition to differences in model climatologies. To date, the relative impacts of sharpness of SST gradient, its meridional shift, and activity of warm or cold-core eddies remain unquantified (Parfitt and Seo 2018). The importance of the coordinated modeling and diagnostic approaches regarding this specific point is emphasized in section 6d.

### d. Coordinated climate modeling and improved physical parameterizations

Significant progress can be made in understanding results and uncertainties in climate models of different complexity and resolutions via coordinated modeling experiments with resolutions at or beyond the ocean mesoscale and shared sets of diagnostics. The CMIP6 HighResMIP protocol (Haarsma et al. 2016) and PRIMAVERA project (Bellucci et al. 2021) well represent the community's interests in this direction. Analyses from a subset of these models reveal significant model resolution sensitivity (especially in the oceans) of the simulated air–sea interaction and climate regimes in the extratropics (e.g., Jullien et al. 2020; Moreton et al. 2021). Further

advances in model resolution, for example, DYAMOND (Stevens et al. 2019) and the planned HighResMIP2, together with programs such as OASIS (Observing Air–Sea Interaction Strategy; <https://airseaobs.org>; Cronin et al. 2022) that aims to bring observations and models closer together, will build on these previous efforts and provide further insights into the fidelity of modeled mesoscale air–sea interactions. Furthermore, in the ocean and coupled models where the ocean eddies are not fully or only partially resolved, their rectified effects on the air–sea heat, momentum, and tracer fluxes are not currently parameterized. Various stochastic representations of eddy transports are being tested and implemented (section 4c), which can potentially address this issue of low-frequency rectification effects by eddies on large-scale climate via air–sea interaction. (e.g., Siqueira and Kirtman 2016).

### e. Air–sea interaction mediated by ocean submesoscale and sea state

The ocean submesoscale processes with length scales smaller than  $\sim 10$  km are essential for the ocean energy cycle (Lorenz 1960), global heat balance (Su et al. 2018), and marine biogeochemistry and ecosystems (Omand et al. 2015; Lévy et al. 2018). While the dynamics of the submesoscale ocean instabilities are becoming better understood (e.g., Fox-Kemper et al. 2008; D'Asaro et al. 2011), their direct impact on the MABL and heat and carbon uptake by the oceans (e.g., Johnson et al. 2016; Bachman et al. 2017; du Plessis et al. 2019) remain poorly understood. Thus far, only a few satellite-based studies provide direct observational evidence of relative wind stress response to submesoscale SST fronts (e.g., Beal et al. 1997; Xie et al. 2010; Gaube et al. 2019; Ayet et al. 2021), although prior in situ observational studies have long documented such interactions in localized regions (e.g., Sweet et al. 1981; Friehe et al. 1991; Mahrt et al. 2004). While results from high-resolution numerical simulations (e.g., LES) indicate submesoscale SST-driven MABL dynamics (Skylvingstad et al. 2007; Lambaerts et al. 2013; Wenegrat and Arthur 2018; Lac et al. 2018; Sullivan et al. 2020, 2021), they also recognize the importance of advection and convective organization in characterizing the nonlinear MABL dynamics that co-occur at the submesoscale. As for the oceanic impact, the ocean current feedback dominates the wind stress response at the submesoscale, influencing the kinetic energy cascade (Renault et al. 2018). Spatial variability in sea state and surface roughness is enhanced at the submesoscale, and hence wave–current interactions (e.g., Villas Bôas and Pizzo 2021) and wave–wind interactions (e.g., Deskos et al. 2021) are expected to be critical in determining wind stress, heat flux, and MABL variations (Ayet et al. 2021; section 4b), yet such processes remain poorly observed, understood, and parameterized. Emerging in situ and satellite observations for near-surface processes (section 5), combined with dedicated atmospheric and oceanic LES and high-resolution modeling studies, will help improve the physical understanding of air–sea interactions at the submesoscale.



*f. Air–sea gas flux exchange and ocean biogeochemistry processes*

Estimates of air–sea gas exchange do not fully consider the effects of ocean mesoscale eddies and fronts. One issue is that the gas transfer velocity typically does not consider wind variations introduced by mesoscale air–sea interactions. The transfer velocity is also often based on wind speed (e.g., Wanninkhof 1992). Hence, it only implicitly accounts for the sea state variations. Studies with parameterizations that consider bubble-mediated gas exchanges due to breaking waves (e.g., Frew et al. 2007; Deike and Melville 2018) reveal their significant contribution to regionally integrated CO<sub>2</sub> flux, especially under midlatitude storm tracks (e.g., Reichl and Deike 2020). To accurately represent the sea state influence modulated by mesoscale processes in the transfer velocity-based flux parameterization (e.g., Fairall et al. 2011; Edson et al. 2011), it is imperative to increase direct measurements of CO<sub>2</sub> flux (e.g., McGillis et al. 2001) along with the coincident observations of wind, waves, solubility, and air–sea partial CO<sub>2</sub> pressure differences.

Further, mesoscale air–sea interaction feeds back to ocean primary productivity (Lévy 2008; McGillicuddy 2016) and tracer concentrations, such as carbon. Since the physical properties of mesoscale eddies and their relationships with biogeochemical variables vary widely by region (e.g., Chelton et al. 2011a; Gaube et al. 2013, 2014; Frenger et al. 2018), future work should aim to identify the specific aspects of this regional variability that are due to mesoscale air–sea interaction and subsequent impacts on upwelling and vertical mixing. Eddy-rich climate model simulations are one avenue to gain quantitative insight into the relevance of the complex coupling of ocean mesoscale features, biogeochemistry, and the atmosphere. Few such simulations exist due to their computational expense (e.g., Harrison et al. 2018), but we expect this to change in the coming years. Dedicated field experiments combined with eddy-resolving coupled physical–biogeochemical models are critical to determining what aspects of mesoscale air–sea interactions need to be considered and represented in non-eddy-resolving models.

*g. Final remarks*

Prospects for significant advances in mesoscale air–sea interaction in the coming years are incredibly bright. Strong community efforts and enthusiasm exist for building sustained observational networks to characterize detailed physical and biogeochemical processes across the air–sea coupled boundary layers (e.g., OceanObs'19 White Papers; OASIS; U.S. CLIVAR's air–sea interaction research initiatives). New satellite missions with advanced instrument technology and retrieval algorithms will continue to improve our capability to monitor state variables pertinent to air–sea interactions at fine scales and with increased accuracy. These new observations will lead to updated physical parameterizations that are becoming increasingly more scale-aware and that can be potentially built with stochastic schemes that account for rectified effects of eddy transports on air–sea flux and large scales. More field experiments are being coordinated via close

integration with process-oriented and data assimilative modeling to help not only develop the sampling plans but also improve the parameterizations and skills in prediction models (e.g., Cronin et al. 2009; Cravatte et al. 2016; Kessler et al. 2019; Sprintall et al. 2020; Shroyer et al. 2021; Shinoda et al. 2021; Newman et al. 2022). The climate modeling community is developing and refining high-resolution Earth system model simulations with advanced physical parameterizations. International partnership and coordination are becoming increasingly solid, enabling the design of multimodel, multi-ensemble, high-resolution coupled modeling protocols and diagnostic frameworks. The identified common biases in mesoscale air–sea interaction in such climate models, in turn, guide the sampling strategy of observing systems and process studies. Ensemble data assimilation systems are rapidly advancing, yielding more accurate observationally constrained ocean, atmosphere, and biogeochemical state estimates critical for subseasonal to decadal predictions (e.g., Penny and Hamill 2017; Verdy and Mazloff 2017). Overall, the successful coordination across observations, modeling, and theories has been critical, and these coordinated efforts will and should continue to enhance Earth system prediction skills across scales from weather forecasts to climate projection scales.

*Acknowledgments.* The authors of the paper are the scientists participating in the U.S. CLIVAR Working Group on Mesoscale and Frontal-Scale Ocean–Atmosphere Interactions and Influence on Large-Scale Climate (<https://usclivar.org/working-groups/air-sea-interactions-working-group>). The authors thank Mike Patterson, Jennie Zhu, and Sam Coakley at U.S. CLIVAR for sponsoring and supporting the Working Group activities. The authors thank Dr. Kuwano-Yoshida and two anonymous reviewers for their constructive comments. We also thank Natalie Renier at the WHOI Creative Studio for her assistance with scientific illustrations. The authors acknowledge many national and international funding agencies that have supported the in situ and satellite observations, modeling, and analysis efforts that are the subject of this paper. In this work, HS acknowledges support from the NSF (OCE-2022846, OCE-2148120), NOAA (NA19OAR4310376, NA22OAR4310598), NASA (80NSSC21K1524), ONR (N00014-17-1-2398), DOE (DE-EE0009424), and WHOI (Francis E. Fowler IV Center for Ocean and Climate). MAB acknowledges support from NASA via the JPL (1419699), NOAA/GOMO (100007298), and Northern Gulf of Mexico Institute (21-NGI4-04). AC is supported by NSF-NERC grants (NE/V014897/1 and NE/W004836/1). KD was supported by NASA (80NSSC18K1330). JBE thanks support from NASA NSF (OCE-1829957). BFK acknowledges support from ONR (N00014-17-1-2963), the Schmidt Futures Foundation, NSF (2148945), and NOAA (NA19OAR4310366). STG is grateful for support from NASA (80NSSC19K0059, 80NSSC21K1822, and 80NSSC20K1136). SM is supported by the Japan Society for the Promotion of Science (JSPS) KAKENHI Grant 19H05704. AGP acknowledges support from U.S. DOE BER EESM RGMA Award DE-SC0022070 and NSF IA 1947282, and NCAR, which is sponsored by NSF under CA 1852977. LR appreciates support from the CNES (Projects CARAMBA and I\_CASCADE), the ANR JPI-CLIMATE EUREC4A-OA, the

NOAA project ATOMIC, the GENCI resources project 7298 and 13051, the HPC-Europa3 program application HPC17IUTPN and HPC17MM0RX, and the Horizon 2020 project PRIMAVERA (GA 641727). MJR acknowledges support from EU PRIMAVERA and the Met Office Hadley Centre Climate Programme funded by BEIS and Defra (GA01101). NS was supported by NASA (80NSSC19K0058) and JAMSTEC IPRC Collaborative Research (JICoRe). RJS acknowledges support from NOAA (NA22OAR4310615). AS acknowledges support from EUMETSAT (OSI SAF). QW acknowledges the funding support from ONR CASPER under Multidisciplinary University Research Initiative (MURI) program (N00014-21-1-2126 and N0001420WX01066).

**Data availability statement.** Datasets used in the figures are based on ERA5 (Hersbach et al. 2020), NOAA OI SST (Reynolds et al. 2007), climate model simulations from the HighResMIP (Haarsma et al. 2016), or already published papers as cited in the figure captions.

## REFERENCES

- Alexander, M. A., and J. D. Scott, 1997: Surface flux variability over the North Pacific and North Atlantic Oceans. *J. Climate*, **10**, 2963–2978, [https://doi.org/10.1175/1520-0442\(1997\)010<2963:SFVOTN>2.0.CO;2](https://doi.org/10.1175/1520-0442(1997)010<2963:SFVOTN>2.0.CO;2).
- , S. Shin, J. D. Scott, E. Curchitser, and C. Stock, 2020: The response of the northwest Atlantic Ocean to climate change. *J. Climate*, **33**, 405–428, <https://doi.org/10.1175/JCLI-D-19-0117.1>.
- Ardhuin, F., S. T. Gille, D. Menemenlis, C. B. Rocha, N. Raschle, B. Chapron, J. Gula, and J. Molemaker, 2017: Small-scale open ocean currents have large effects on wind wave heights. *J. Geophys. Res. Oceans*, **122**, 4500–4517, <https://doi.org/10.1002/2016JC012413>.
- , and Coauthors, 2019: Observing sea states. *Front. Mar. Sci.*, **6**, 124, <https://doi.org/10.3389/fmars.2019.00124>.
- Ayet, A., and B. Chapron, 2022: The dynamical coupling of wind-waves and atmospheric turbulence: A review of theoretical and phenomenological models. *Bound.-Layer Meteor.*, **183** (1), 1–33, <https://doi.org/10.1007/s10546-021-00666-6>.
- , N. Raschle, B. Chapron, F. Couvreur, and L. Terray, 2021: Uncovering air–sea interaction in oceanic submesoscale frontal regions using high-resolution satellite observations. *U.S. CLIVAR Variations*, Vol. 19, U.S. CLIVAR Project Office, Washington, DC, 10–17, <https://usclivar.org/newsletters>.
- Bachman, S. D., J. R. Taylor, K. A. Adams, and P. J. Hosegood, 2017: Mesoscale and submesoscale effects on mixed layer depth in the southern ocean. *J. Phys. Oceanogr.*, **47**, 2173–2188, <https://doi.org/10.1175/JPO-D-17-0034.1>.
- , B. Fox-Kemper, and F. O. Bryan, 2020: A diagnosis of anisotropic eddy diffusion from a high-resolution global ocean model. *J. Adv. Model. Earth Syst.*, **12**, e2019MS001904, <https://doi.org/10.1029/2019MS001904>.
- Battisti, D. S., E. S. Sarachik, and A. C. Hirst, 1999: A consistent model for the large-scale steady surface atmospheric circulation in the tropics. *J. Climate*, **12**, 2956–2964, [https://doi.org/10.1175/1520-0442\(1999\)012<2956:ACMFTL>2.0.CO;2](https://doi.org/10.1175/1520-0442(1999)012<2956:ACMFTL>2.0.CO;2).
- Beal, R. C., V. N. Kudryavtsev, D. R. Thompson, S. A. Grodsky, D. G. Trilley, V. A. Dulov, and H. C. Graber, 1997: The influence of the marine atmospheric boundary layer on ERS 1 synthetic aperture radar imagery of the Gulf Stream. *J. Geophys. Res.*, **102**, 5799–5814, <https://doi.org/10.1029/96JC03109>.
- Bellucci, A., and Coauthors, 2021: Air–sea interaction over the Gulf Stream in an ensemble of HighResMIP present climate simulations. *Climate Dyn.*, **56**, 2093–2111, <https://doi.org/10.1007/s00382-020-05573-z>.
- Belmonte Rivas, M., and A. Stoffelen, 2019: Characterizing ERA-Interim and ERA5 surface wind biases using ASCAT. *Ocean Sci.*, **15**, 831–852, <https://doi.org/10.5194/os-15-831-2019>.
- Bigorre, S. P., R. A. Weller, J. B. Edson, and J. D. Ware, 2013: A surface mooring for air–sea interaction research in the Gulf Stream. Part II: Analysis of the observations and their accuracies. *J. Atmos. Oceanic Technol.*, **30**, 450–469, <https://doi.org/10.1175/JTECH-D-12-00078.1>.
- Bilgen, S. I., and B. P. Kirtman, 2020: Impact of ocean model resolution on understanding the delayed warming of the Southern Ocean. *Environ. Res. Lett.*, **15**, 114012, <https://doi.org/10.1088/1748-9326/abc3e>.
- Bishop, S. P., R. J. Small, F. O. Bryan, and R. A. Tomas, 2017: Scale dependence of midlatitude air–sea interaction. *J. Climate*, **30**, 8207–8221, <https://doi.org/10.1175/JCLI-D-17-0159.1>.
- , —, and —, 2020: The global sink of available potential energy by mesoscale air–sea interaction. *J. Adv. Model. Earth Syst.*, **12**, e2020MS002118, <https://doi.org/10.1029/2020MS002118>.
- Bladé, I., 1997: The influence of midlatitude ocean–atmosphere coupling on the low-frequency variability of a GCM. Part I: No tropical SST forcing. *J. Climate*, **10**, 2087–2106, [https://doi.org/10.1175/1520-0442\(1997\)010<2087:TIOMOA>2.0.CO;2](https://doi.org/10.1175/1520-0442(1997)010<2087:TIOMOA>2.0.CO;2).
- Bony, S., and Coauthors, 2017: EUREC<sup>4</sup>A: A field campaign to elucidate the couplings between clouds, convection and circulation. *Surv. Geophys.*, **38**, 1529–1568, <https://doi.org/10.1007/s10712-017-9428-0>.
- Booth, J. F., L. A. Thompson, J. Patoux, K. A. Kelly, and S. Dickinson, 2010: The signature of midlatitude tropospheric storm tracks in the surface winds. *J. Climate*, **23**, 1160–1174, <https://doi.org/10.1175/2009JCLI3064.1>.
- , —, —, and —, 2012: Sensitivity of midlatitude storm intensification to perturbations in the sea surface temperature near the Gulf Stream. *Mon. Wea. Rev.*, **140**, 1241–1256, <https://doi.org/10.1175/MWR-D-11-00195.1>.
- , Y.-O. Kwon, S. Ko, R. J. Small, and R. Msadek, 2017: Spatial patterns and intensity of the surface storm tracks in CMIP5 models. *J. Climate*, **30**, 4965–4981, <https://doi.org/10.1175/JCLI-D-16-0228.1>.
- Bourassa, M. A., and Coauthors, 2013: High-latitude ocean and sea ice surface fluxes: Requirements and challenges for climate research. *Bull. Amer. Meteor. Soc.*, **94**, 403–423, <https://doi.org/10.1175/BAMS-D-11-00244.1>.
- , E. Rodríguez, and D. Chelton, 2016: Winds and Currents Mission: Ability to observe mesoscale AIR/SEA coupling. *2016 IEEE Int. Geoscience and Remote Sensing Symp. (IGARSS)*, Beijing, China, Institute of Electrical and Electronics Engineers, 7392–7395, <https://doi.org/10.1109/IGARSS.2016.7730928>.
- , and Coauthors, 2019: Remotely sensed winds and wind stresses for marine forecasting and ocean modeling. *Front. Mar. Sci.*, **6**, 443, <https://doi.org/10.3389/fmars.2019.00443>.
- Brachet, S., F. Codron, Y. Feliks, M. Ghil, H. Le Treut, and E. Simonnet, 2012: Atmospheric circulations induced by a midlatitude SST front: A GCM study. *J. Climate*, **25**, 1847–1853, <https://doi.org/10.1175/JCLI-D-11-00329.1>.
- Brankart, J.-M., 2013: Impact of uncertainties in the horizontal density gradient upon low resolution global ocean modelling.

- Ocean Modell.*, **66**, 64–76, <https://doi.org/10.1016/j.ocemod.2013.02.004>.
- Bryan, F. O., R. Tomas, J. M. Dennis, D. B. Chelton, N. G. Loeb, and J. L. McClean, 2010: Frontal scale air–sea interaction in high-resolution coupled climate models. *J. Climate*, **23**, 6277–6291, <https://doi.org/10.1175/2010JCLI3665.1>.
- Bye, J. A. T., 1986: Momentum exchange at the sea surface by wind stress and understress. *Quart. J. Roy. Meteor. Soc.*, **112**, 501–510, <https://doi.org/10.1002/qj.49711247212>.
- Byrne, D., L. Papritz, I. Frenger, M. Münnich, and N. Gruber, 2015: Atmospheric response to mesoscale sea surface temperature anomalies: Assessment of mechanisms and coupling strength in a high-resolution coupled model over the South Atlantic. *J. Atmos. Sci.*, **72**, 1872–1890, <https://doi.org/10.1175/JAS-D-14-0195.1>.
- Cabrera, M., M. Santini, L. Lima, J. Carvalho, E. Rosa, C. Rodrigues, and L. Pezzi, 2022: The southwestern Atlantic Ocean mesoscale eddies: A review of their role in the air–sea interaction processes. *J. Mar. Syst.*, **235**, 103785, <https://doi.org/10.1016/j.jmarsys.2022.103785>.
- Cavaleri, L., B. Fox-Kemper, and M. Hemer, 2012: Wind waves in the coupled climate system. *Bull. Amer. Meteor. Soc.*, **93**, 1651–1661, <https://doi.org/10.1175/BAMS-D-11-00170.1>.
- Centurioni, L. R., and Coauthors, 2019: Global in situ observations of essential climate and ocean variables at the air–sea interface. *Front. Mar. Sci.*, **6**, 419, <https://doi.org/10.3389/fmars.2019.00419>.
- Chang, E. K. M., 1993: Downstream development of baroclinic waves as inferred from regression analysis. *J. Atmos. Sci.*, **50**, 2038–2053, [https://doi.org/10.1175/1520-0469\(1993\)050<2038:DDOBWA>2.0.CO;2](https://doi.org/10.1175/1520-0469(1993)050<2038:DDOBWA>2.0.CO;2).
- , and I. Orlanski, 1993: On the dynamics of a storm track. *J. Atmos. Sci.*, **50**, 999–1015, [https://doi.org/10.1175/1520-0469\(1993\)050<0999:OTDOAS>2.0.CO;2](https://doi.org/10.1175/1520-0469(1993)050<0999:OTDOAS>2.0.CO;2).
- , S. Lee, and K. L. Swanson, 2002: Storm track dynamics. *J. Climate*, **15**, 2163–2183, [https://doi.org/10.1175/1520-0442\(2002\)015<0216:STD>2.0.CO;2](https://doi.org/10.1175/1520-0442(2002)015<0216:STD>2.0.CO;2).
- Chang, P., and Coauthors, 2020: An unprecedented set of high-resolution Earth system simulations for understanding multi-scale interactions in climate variability and change. *J. Adv. Model. Earth Syst.*, **12**, e2020MS002298, <https://doi.org/10.1029/2020MS002298>.
- Charney, J. G., 1947: The dynamics of long waves in a baroclinic westerly current. *J. Atmos. Sci.*, **4**, 136–162, [https://doi.org/10.1175/1520-0469\(1947\)004<0136:TDOLWI>2.0.CO;2](https://doi.org/10.1175/1520-0469(1947)004<0136:TDOLWI>2.0.CO;2).
- Charrassin, J.-B., and Coauthors, 2008: Southern Ocean frontal structure and sea-ice formation rates revealed by elephant seals. *Proc. Natl. Acad. Sci. USA*, **105**, 11 634–11 639, <https://doi.org/10.1073/pnas.0800790105>.
- Chelton, D. B., 2005: The impact of SST specification on ECMWF surface wind stress fields in the eastern tropical Pacific. *J. Climate*, **18**, 530–550, <https://doi.org/10.1175/JCLI-3275.1>.
- , and Coauthors, 2001: Observations of coupling between surface wind stress and sea surface temperature in the eastern tropical Pacific. *J. Climate*, **14**, 1479–1498, [https://doi.org/10.1175/1520-0442\(2001\)014<1479:OOCBSW>2.0.CO;2](https://doi.org/10.1175/1520-0442(2001)014<1479:OOCBSW>2.0.CO;2).
- , M. G. Schlax, M. H. Freilich, and R. F. Milliff, 2004: Satellite measurements reveal persistent small-scale features in ocean winds. *Science*, **303**, 978–983, <https://doi.org/10.1126/science.1091901>.
- , —, and R. M. Samelson, 2007: Summertime coupling between sea surface temperature and wind stress in the California Current System. *J. Phys. Oceanogr.*, **37**, 495–517, <https://doi.org/10.1175/JPO3025.1>.
- , P. Gaube, M. G. Schlax, J. J. Early, and R. M. Samelson, 2011a: The influence of nonlinear mesoscale eddies on near-surface oceanic chlorophyll. *Science*, **334**, 328–332, <https://doi.org/10.1126/science.1208897>.
- , M. G. Schlax, and R. M. Samelson, 2011b: Global observations of nonlinear mesoscale eddies. *Prog. Oceanogr.*, **91**, 167–216, <https://doi.org/10.1016/j.pcean.2011.01.002>.
- Clayson, C. A., J. B. Edson, A. Paget, R. Graham, and B. Greenwood, 2019: The effects of rainfall on the atmosphere and the ocean during SPURS-2. *Oceanography*, **32**, 86–97, <https://doi.org/10.5670/oceanog.2019.216>.
- Cravatte, S., and Coauthors, 2016: First report of TPOS 2020. Tech. Rep. GOOS-215, 200 pp., <http://tpos2020.org/first-report/>.
- Cronin, M. F., S. Legg, and P. Zuidema, 2009: Climate research: Best practices for process studies. *Bull. Amer. Meteor. Soc.*, **90**, 917–918, <https://doi.org/10.1175/2009BAMS2622.1>.
- , and Coauthors, 2019: Air–sea fluxes with a focus on heat and momentum. *Front. Mar. Sci.*, **6**, 430, <https://doi.org/10.3389/fmars.2019.00430>.
- , and Coauthors, 2022: Developing an Observing Air–Sea Interactions Strategy (OASIS) for the global ocean. *ICES J. Mar. Sci.*, **2022**, fsac149, <https://doi.org/10.1093/icesjms/fsac149>.
- Czaja, A., and N. Blunt, 2011: A new mechanism for ocean–atmosphere coupling in midlatitudes. *Quart. J. Roy. Meteor. Soc.*, **137**, 1095–1101, <https://doi.org/10.1002/qj.814>.
- , C. Frankignoul, S. Minobe, and B. Vannière, 2019: Simulating the midlatitude atmospheric circulation: What might we gain from high-resolution modeling of air–sea interactions? *Curr. Climate Change Rep.*, **5**, 390–406, <https://doi.org/10.1007/s40641-019-00148-5>.
- D’Asaro, E. A., 2014: Turbulence in the upper-ocean mixed layer. *Annu. Rev. Mar. Sci.*, **6**, 101–115, <https://doi.org/10.1146/annurev-marine-010213-135138>.
- , C. Lee, L. Rainville, R. Harcourt, and L. Thomas, 2011: Enhanced turbulence and energy dissipation at ocean fronts. *Science*, **332**, 318–322, <https://doi.org/10.1126/science.1201515>.
- , and Coauthors, 2018: Ocean convergence and dispersion of flotsam. *Proc. Natl. Acad. Sci. USA*, **115**, 1162–1167, <https://doi.org/10.1073/pnas.1718453115>.
- de Boyer Montégut, C., G. Madec, A. S. Fischer, A. Lazar, and D. Iudicone, 2004: Mixed layer depth over the global ocean: An examination of profile data and a profile-based climatology. *J. Geophys. Res.*, **109**, C12003, <https://doi.org/10.1029/2004JC002378>.
- Deike, L., and W. K. Melville, 2018: Gas transfer by breaking waves. *Geophys. Res. Lett.*, **45**, 10 482–10 492, <https://doi.org/10.1029/2018GL078758>.
- de Kloe, J., A. Stoffelen, and A. Verhoef, 2017: Improved use of scatterometer measurements by using stress-equivalent reference winds. *IEEE J. Sel. Top. Appl. Earth Obs. Remote Sens.*, **10**, 2340–2347, <https://doi.org/10.1109/JSTARS.2017.2685242>.
- Deser, C., S. Wahl, and J. J. Bates, 1993: The influence of sea surface temperature gradients on stratiform cloudiness along the equatorial front in the Pacific Ocean. *J. Climate*, **6**, 1172–1180, [https://doi.org/10.1175/1520-0442\(1993\)006<1172:TIOSSST>2.0.CO;2](https://doi.org/10.1175/1520-0442(1993)006<1172:TIOSSST>2.0.CO;2).
- , R. A. Tomas, and S. Peng, 2007: The transient atmospheric circulation response to North Atlantic SST and sea ice anomalies. *J. Climate*, **20**, 4751–4767, <https://doi.org/10.1175/JCLI4278.1>.



- Deskos, G., J. C. Y. Lee, C. Draxl, and M. A. Sprague, 2021: Review of wind-wave coupling models for large-eddy simulation of the marine atmospheric boundary layer. *J. Atmos. Sci.*, **78**, 3025–3045, <https://doi.org/10.1175/JAS-D-21-0003.1>.
- de Szoeke, S. P., and C. S. Bretherton, 2004: Quasi-Lagrangian large eddy simulations of cross-equatorial flow in the east Pacific atmospheric boundary layer. *J. Atmos. Sci.*, **61**, 1837–1858, [https://doi.org/10.1175/1520-0469\(2004\)061<1837:QLESOC>2.0.CO;2](https://doi.org/10.1175/1520-0469(2004)061<1837:QLESOC>2.0.CO;2).
- , and E. D. Maloney, 2020: Atmospheric mixed layer convergence from observed MJO sea surface temperature anomalies. *J. Climate*, **33**, 547–558, <https://doi.org/10.1175/JCLI-D-19-0351.1>.
- , J. B. Edson, J. R. Marion, C. W. Fairall, and L. Bariteau, 2015: The MJO and air–sea interaction in TOGA COARE and DYNAMO. *J. Climate*, **28**, 597–622, <https://doi.org/10.1175/JCLI-D-14-00477.1>.
- Dewar, W. K., and G. R. Flierl, 1987: Some effects of the wind on rings. *J. Phys. Oceanogr.*, **17**, 1653–1667, [https://doi.org/10.1175/1520-0485\(1987\)017<1653:SEOTWO>2.0.CO;2](https://doi.org/10.1175/1520-0485(1987)017<1653:SEOTWO>2.0.CO;2).
- Domingues, R., and Coauthors, 2019: Ocean observations in support of studies and forecasts of tropical and extratropical cyclones. *Front. Mar. Sci.*, **6**, 446, <https://doi.org/10.3389/fmars.2019.00446>.
- Dong, J., B. Fox-Kemper, H. Zhang, and C. Dong, 2020: The scale of submesoscale baroclinic instability globally. *J. Phys. Oceanogr.*, **50**, 2649–2667, <https://doi.org/10.1175/JPO-D-20-0043.1>.
- , —, —, and —, 2021: The scale and activity of symmetric instability estimated from a global submesoscale-permitting ocean model. *J. Phys. Oceanogr.*, **51**, 1655–1670, <https://doi.org/10.1175/JPO-D-20-0159.1>.
- Doyle, J. D., and Coauthors, 2017: A view of tropical cyclones from above: The Tropical Cyclone Intensity Experiment. *Bull. Amer. Meteor. Soc.*, **98**, 2113–2134, <https://doi.org/10.1175/BAMS-D-16-0055.1>.
- Drivas, T. D., D. D. Holm, and J.-M. Leahy, 2020: Lagrangian averaged stochastic advection by Lie transport for fluids. *J. Stat. Phys.*, **179**, 1304–1342, <https://doi.org/10.1007/s10955-020-02493-4>.
- Dufois, F., and Coauthors, 2017: Observational insights into chlorophyll distributions of subtropical South Indian Ocean eddies. *Geophys. Res. Lett.*, **44**, 3255–3264, <https://doi.org/10.1002/2016GL072371>.
- du Plessis, M., S. Swart, I. J. Anson, A. Mahadevan, and A. F. Thompson, 2019: Southern ocean seasonal restratification delayed by submesoscale wind–front interactions. *J. Phys. Oceanogr.*, **49**, 1035–1053, <https://doi.org/10.1175/JPO-D-18-0136.1>.
- Eady, E. T., 1949: Long waves and cyclone waves. *Tellus*, **1**, 33–52, <https://doi.org/10.3402/tellusa.v1i3.8507>.
- Edson, J. B., and Coauthors, 2011: Direct-covariance measurement of CO<sub>2</sub> gas transfer velocity during the 2008 Southern Ocean Gas Exchange experiment. *J. Geophys. Res.*, **116**, C00F10, <https://doi.org/10.1029/2011JC007022>.
- , and Coauthors, 2013: On the exchange of momentum over the open ocean. *J. Phys. Oceanogr.*, **43**, 1589–1610, <https://doi.org/10.1175/JPO-D-12-0173.1>.
- Fairall, C. W., E. F. Bradley, D. P. Rogers, J. B. Edson, and G. S. Young, 1996: Bulk parameterization of air–sea fluxes for Tropical Ocean Global Atmosphere Coupled Ocean–Atmosphere Response Experiment. *J. Geophys. Res.*, **101**, 3747–3764, <https://doi.org/10.1029/95JC03205>.
- , and Coauthors, 2011: Implementation of the Coupled Ocean–Atmosphere Response Experiment flux algorithm with CO<sub>2</sub>, dimethyl sulfide, and O<sub>3</sub>. *J. Geophys. Res.*, **116**, C00F09, <https://doi.org/10.1029/2010JC006884>.
- Farrar, J. T., and Coauthors, 2020: S-MODE: The sub-mesoscale ocean dynamics experiment. *IGARSS 2020–2020 IEEE Int. Geoscience and Remote Sensing Symp.*, Waikoloa, HI, Institute of Electrical and Electronics Engineers, 3533–3536, <https://doi.org/10.1109/IGARSS39084.2020.9323112>.
- Feliks, Y., M. Ghil, and E. Simonnet, 2004: Low-frequency variability in the midlatitude atmosphere induced by an oceanic thermal front. *J. Atmos. Sci.*, **61**, 961–981, [https://doi.org/10.1175/1520-0469\(2004\)061<0961:LVTMA>2.0.CO;2](https://doi.org/10.1175/1520-0469(2004)061<0961:LVTMA>2.0.CO;2).
- Ferreira, D., and C. Frankignoul, 2005: The transient atmospheric response to midlatitude SST anomalies. *J. Climate*, **18**, 1049–1067, <https://doi.org/10.1175/JCLI-3313.1>.
- , and —, 2008: Transient atmospheric response to interactive SST anomalies. *J. Climate*, **21**, 576–583, <https://doi.org/10.1175/2007JCLI1704.1>.
- Foussard, A., G. Lapeyre, and R. Plougonven, 2019a: Response of surface wind divergence to mesoscale SST anomalies under different wind conditions. *J. Atmos. Sci.*, **76**, 2065–2082, <https://doi.org/10.1175/JAS-D-18-0204.1>.
- , —, and —, 2019b: Storm track response to oceanic eddies in idealized atmospheric simulations. *J. Climate*, **32**, 445–463, <https://doi.org/10.1175/JCLI-D-18-0415.1>.
- Fox-Kemper, B., R. Ferrari, and R. Hallberg, 2008: Parameterization of mixed layer eddies. I: Theory and diagnosis. *J. Phys. Oceanogr.*, **38**, 1145–1165, <https://doi.org/10.1175/2007JPO3792.1>.
- , and Coauthors, 2011: Parameterization of mixed layer eddies. III: Implementation and impact in global ocean climate simulations. *Ocean Modell.*, **39**, 61–78, <https://doi.org/10.1016/j.oceomod.2010.09.002>.
- , L. Johnson, and F. Qiao, 2022: Ocean near-surface layers. *Ocean Mixing*, M. Meredith and A. N. Garabato, Eds., Elsevier, 65–94, <https://doi.org/10.1016/B978-0-12-821512-8.00011-6>.
- Frankignoul, C., 1985: Sea surface temperature anomalies, planetary waves, and air–sea feedback in midlatitudes. *Rev. Geophys.*, **23**, 357–390, <https://doi.org/10.1029/RG023i004p00357>.
- , and K. Hasselmann, 1977: Stochastic climate models, Part II application to sea-surface temperature anomalies and thermocline variability. *Tellus*, **29**, 289–305, <https://doi.org/10.3402/tellusa.v29i4.11362>.
- , N. Sennechael, Y.-O. Kwon, and M. A. Alexander, 2011: Influence of the meridional shifts of the Kuroshio and the Oyashio Extensions on the atmospheric circulation. *J. Climate*, **24**, 762–777, <https://doi.org/10.1175/2010JCLI3731.1>.
- Frenger, I., N. Gruber, R. Knutti, and M. Münnich, 2013: Imprint of Southern Ocean eddies on winds, clouds and rainfall. *Nat. Geosci.*, **6**, 608–612, <https://doi.org/10.1038/ngeo1863>.
- , M. Münnich, and N. Gruber, 2018: Imprint of Southern Ocean mesoscale eddies on chlorophyll. *Beigeosciences*, **15**, 4781–4798, <https://doi.org/10.5194/bg-15-4781-2018>.
- Frew, N. M., D. M. Glover, E. J. Bock, and S. J. McCue, 2007: A new approach to estimation of global air–sea gas transfer velocity fields using dual-frequency altimeter backscatter. *J. Geophys. Res.*, **112**, C11003, <https://doi.org/10.1029/2006JC003819>.
- Friehe, C. A., and Coauthors, 1991: Air–sea fluxes and surface layer turbulence around a sea surface temperature front. *J. Geophys. Res.*, **96**, 8593–8609, <https://doi.org/10.1029/90JC02062>.
- Gade, M., and A. Stoffelen, 2019: An introduction to microwave remote sensing of the Asian seas. *Remote Sensing of the Asian Seas*, V. Barale and M. Gade, Eds., Springer, 81–101, [https://doi.org/10.1007/978-3-319-94067-0\\_4](https://doi.org/10.1007/978-3-319-94067-0_4).



- Gaube, P., D. B. Chelton, P. G. Strutton, and M. J. Behrenfeld, 2013: Satellite observations of chlorophyll, phytoplankton biomass, and Ekman pumping in nonlinear mesoscale eddies. *J. Geophys. Res. Oceans*, **118**, 6349–6370, <https://doi.org/10.1002/2013JC009027>.
- , D. J. McGillicuddy, D. B. Chelton, M. J. Behrenfeld, and P. G. Strutton, 2014: Regional variations in the influence of mesoscale eddies on near-surface chlorophyll. *J. Geophys. Res. Oceans*, **119**, 8195–8220, <https://doi.org/10.1002/2014JC010111>.
- , D. B. Chelton, R. M. Samelson, M. G. Schlax, and L. W. O'Neill, 2015: Satellite observations of mesoscale eddy-induced Ekman pumping. *J. Phys. Oceanogr.*, **45**, 104–132, <https://doi.org/10.1175/JPO-D-14-0032.1>.
- , C. C. Chickadel, R. Branch, and A. Jessup, 2019: Satellite observations of SST-induced wind speed perturbation at the oceanic submesoscale. *Geophys. Res. Lett.*, **46**, 2690–2695, <https://doi.org/10.1029/2018GL080807>.
- Gent, P. R., and J. C. McWilliams, 1990: Isopycnal mixing in ocean circulation models. *J. Phys. Oceanogr.*, **20**, 150–155, [https://doi.org/10.1175/1520-0485\(1990\)020<0150:IMIOCM>2.0.CO;2](https://doi.org/10.1175/1520-0485(1990)020<0150:IMIOCM>2.0.CO;2).
- Gentemann, C. L., and Coauthors, 2020: FluxSat: Measuring the ocean-atmosphere turbulent exchange of heat and moisture from space. *Remote Sens.*, **12**, 1796, <https://doi.org/10.3390/rs12111796>.
- Gervais, M., J. Shaman, and Y. Kushnir, 2018: Mechanisms governing the development of the North Atlantic warming hole in the CESM-LE future climate simulations. *J. Climate*, **31**, 5927–5946, <https://doi.org/10.1175/JCLI-D-17-0635.1>.
- Gommenginger, C., and Coauthors, 2019: SEASTAR: A mission to study ocean submesoscale dynamics and small-scale atmosphere–ocean processes in coastal, shelf and polar seas. *Front. Mar. Sci.*, **6**, 457, <https://doi.org/10.3389/fmars.2019.00457>.
- Graber, H. C., E. A. Terray, M. A. Donelan, W. M. Drennan, J. C. Van Leer, and D. B. Peters, 2000: ASIS—A new air–sea interaction spar buoy: Design and performance at sea. *J. Atmos. Oceanic Technol.*, **17**, 708–720, [https://doi.org/10.1175/1520-0426\(2000\)017<0708:AANASI>2.0.CO;2](https://doi.org/10.1175/1520-0426(2000)017<0708:AANASI>2.0.CO;2).
- Grist, J. P., S. A. Josey, B. Sinha, J. L. Catto, M. J. Roberts, and A. C. Coward, 2021: Future evolution of an eddy rich ocean associated with enhanced east Atlantic storminess in a coupled model projection. *Geophys. Res. Lett.*, **48**, e2021GL092719, <https://doi.org/10.1029/2021GL092719>.
- Haarsma, R. J., and Coauthors, 2016: High Resolution Model Intercomparison Project (HighResMIP). *Geosci. Model Dev.*, **9**, 4185–4208, <https://doi.org/10.5194/gmd-9-4185-2016>.
- Haines, K., and J. Marshall, 1987: Eddy-forced coherent structures as a prototype of atmospheric blocking. *Quart. J. Roy. Meteor. Soc.*, **113**, 681–704, <https://doi.org/10.1002/qj.49711347613>.
- Hallberg, R., 2013: Using a resolution function to regulate parameterizations of oceanic mesoscale eddy effects. *Ocean Modell.*, **72**, 92–103, <https://doi.org/10.1016/j.ocemod.2013.08.007>.
- Hand, R., N. Keenlyside, N.-E. Omrani, and M. Latif, 2014: Simulated response to inter-annual SST variations in the Gulf Stream region. *Climate Dyn.*, **42**, 715–731, <https://doi.org/10.1007/s00382-013-1715-y>.
- Haney, S., B. Fox-Kemper, K. Julien, and A. Webb, 2015: Symmetric and geostrophic instabilities in the wave-forced ocean mixed layer. *J. Phys. Oceanogr.*, **45**, 3033–3056, <https://doi.org/10.1175/JPO-D-15-0044.1>.
- Harcourt, R., and Coauthors, 2019: Animal-borne telemetry: An integral component of the ocean observing toolkit. *Front. Mar. Sci.*, **6**, 326, <https://doi.org/10.3389/fmars.2019.00326>.
- Harrison, C. S., M. C. Long, N. S. Lovenduski, and J. K. Moore, 2018: Mesoscale effects on carbon export: A global perspective. *Global Biogeochem. Cycles*, **32**, 680–703, <https://doi.org/10.1002/2017GB005751>.
- Hashizume, H., S.-P. Xie, M. Fujiwara, M. Shiotani, T. Watanabe, Y. Tanimoto, W. T. Liu, and K. Takeuchi, 2002: Direct observations of atmospheric boundary layer response to SST variations associated with tropical instability waves over the eastern equatorial Pacific. *J. Climate*, **15**, 3379–3393, [https://doi.org/10.1175/1520-0442\(2002\)015<3379:DOOABL>2.0.CO;2](https://doi.org/10.1175/1520-0442(2002)015<3379:DOOABL>2.0.CO;2).
- Hausmann, U., D. J. McGillicuddy, and J. Marshall, 2017: Observed mesoscale eddy signatures in southern ocean surface mixed-layer depth. *J. Geophys. Res. Oceans*, **122**, 617–635, <https://doi.org/10.1002/2016JC012225>.
- Hawcroft, M. K., L. C. Shaffrey, K. I. Hodges, and H. F. Dacre, 2012: How much Northern Hemisphere precipitation is associated with extratropical cyclones? *Geophys. Res. Lett.*, **39**, L24809, <https://doi.org/10.1029/2012GL053866>.
- Hayasaki, M., R. Kawamura, M. Mori, and M. Watanabe, 2013: Response of extratropical cyclone activity to the Kuroshio large meander in northern winter. *Geophys. Res. Lett.*, **40**, 2851–2855, <https://doi.org/10.1002/grl.50546>.
- Hayes, S. P., M. J. McPhaden, and J. M. Wallace, 1989: The influence of sea surface temperature on surface wind in the eastern equatorial Pacific: Weekly to monthly variability. *J. Climate*, **2**, 1500–1506, [https://doi.org/10.1175/1520-0442\(1989\)002<1500:TIOST>2.0.CO;2](https://doi.org/10.1175/1520-0442(1989)002<1500:TIOST>2.0.CO;2).
- Hersbach, H., and Coauthors, 2020: The ERA5 global reanalysis. *Quart. J. Roy. Meteor. Soc.*, **146**, 1999–2049, <https://doi.org/10.1002/qj.3803>.
- Hewitt, H. T., and Coauthors, 2020: Resolving and parameterising the ocean mesoscale in Earth system models. *Curr. Climate Change Rep.*, **6**, 137–152, <https://doi.org/10.1007/s40641-020-00164-w>.
- Hirata, H., and M. Nonaka, 2021: Impacts of strong warm ocean currents on development of extratropical cyclones through the warm and cold conveyor belts: A review. *Tropical and Extratropical Air–Sea Interactions: Modes of Climate Variations*, S. K. Behera, Ed., Elsevier, 267–293, <https://doi.org/10.1016/B978-0-12-818156-0.00014-9>.
- , R. Kawamura, M. Nonaka, and K. Tsuboki, 2019: Significant impact of heat supply from the Gulf Stream on a “superbomb” cyclone in January 2018. *Geophys. Res. Lett.*, **46**, 7718–7725, <https://doi.org/10.1029/2019GL082995>.
- Hogg, A. C., W. K. Dewar, P. Berloff, S. Kravtsov, and D. K. Hutchinson, 2009: The effects of mesoscale ocean–atmosphere coupling on the large-scale ocean circulation. *J. Climate*, **22**, 4066–4082, <https://doi.org/10.1175/2009JCLI2629.1>.
- Holton, J. R., 1965a: The influence of viscous boundary layers on transient motions in a stratified rotating fluid. Part I. *J. Atmos. Sci.*, **22**, 402–411, [https://doi.org/10.1175/1520-0469\(1965\)022<0402:TIOVBL>2.0.CO;2](https://doi.org/10.1175/1520-0469(1965)022<0402:TIOVBL>2.0.CO;2).
- , 1965b: The influence of viscous boundary layers on transient motions in a stratified rotating fluid. Part II. *J. Atmos. Sci.*, **22**, 535–540, [https://doi.org/10.1175/1520-0469\(1965\)022<0535:TIOVBL>2.0.CO;2](https://doi.org/10.1175/1520-0469(1965)022<0535:TIOVBL>2.0.CO;2).
- Hoskins, B. J., and D. J. Karoly, 1981: The steady linear response of a spherical atmosphere to thermal and orographic forcing. *J. Atmos. Sci.*, **38**, 1179–1196, [https://doi.org/10.1175/1520-0469\(1981\)038<1179:TSLROA>2.0.CO;2](https://doi.org/10.1175/1520-0469(1981)038<1179:TSLROA>2.0.CO;2).
- , and P. J. Valdes, 1990: On the existence of storm tracks. *J. Atmos. Sci.*, **47**, 1854–1864, [https://doi.org/10.1175/1520-0469\(1990\)047<1854:OTEOST>2.0.CO;2](https://doi.org/10.1175/1520-0469(1990)047<1854:OTEOST>2.0.CO;2).

- , and K. I. Hodges, 2002: New perspectives on the Northern Hemisphere winter storm tracks. *J. Atmos. Sci.*, **59**, 1041–1061, [https://doi.org/10.1175/1520-0469\(2002\)059<1041:NPOTNH>2.0.CO;2](https://doi.org/10.1175/1520-0469(2002)059<1041:NPOTNH>2.0.CO;2).
- Hotta, D., and H. Nakamura, 2011: On the significance of sensible heat supply from the ocean in the maintenance of mean baroclinicity along storm tracks. *J. Climate*, **24**, 3377–3401, <https://doi.org/10.1175/2010JCLI3910.1>.
- Huang, J., Y. Zhang, X.-Q. Yang, X. Ren, and H. Hu, 2020: Impacts of North Pacific subtropical and subarctic oceanic frontal zones on the wintertime atmospheric large-scale circulations. *J. Climate*, **33**, 1897–1914, <https://doi.org/10.1175/JCLI-D-19-0308.1>.
- Hurwitz, M. M., P. A. Newman, and C. I. Garfinkel, 2012: On the influence of North Pacific sea surface temperature on the Arctic winter climate. *J. Geophys. Res.*, **117**, D19110, <https://doi.org/10.1029/2012JD017819>.
- Infanti, J. M., and B. P. Kirtman, 2019: A comparison of CCSM<sub>4</sub> high-resolution and low-resolution predictions for south Florida and southeast United States drought. *Climate Dyn.*, **52**, 6877–6892, <https://doi.org/10.1007/s00382-018-4553-0>.
- IPCC, 2021: *Climate Change 2021: The Physical Science Basis*. Cambridge University Press, 2391 pp., <https://doi.org/10.1017/9781009157896>.
- Jackson, L. C., and Coauthors, 2020: Impact of ocean resolution and mean state on the rate of AMOC weakening. *Climate Dyn.*, **55**, 1711–1732, <https://doi.org/10.1007/s00382-020-05345-9>.
- Jansen, M. F., and I. M. Held, 2014: Parameterizing subgrid-scale eddy effects using energetically consistent backscatter. *Ocean Modell.*, **80**, 36–48, <https://doi.org/10.1016/j.ocemod.2014.06.002>.
- Jing, Z., and Coauthors, 2020: Maintenance of mid-latitude oceanic fronts by mesoscale eddies. *Sci. Adv.*, **6**, eaba7880, <https://doi.org/10.1126/sciadv.aba7880>.
- Johnson, L., C. M. Lee, and E. A. D'Asaro, 2016: Global estimates of lateral springtime restratification. *J. Phys. Oceanogr.*, **46**, 1555–1573, <https://doi.org/10.1175/JPO-D-15-0163.1>.
- Jones, D. G., and Coauthors, 2015: Developments since 2005 in understanding potential environmental impacts of CO<sub>2</sub> leakage from geological storage. *Int. J. Greenhouse Gas Control*, **40**, 350–377, <https://doi.org/10.1016/j.ijggc.2015.05.032>.
- Joyce, T. M., Y.-O. Kwon, H. Seo, and C. C. Ummenhofer, 2019: Meridional Gulf Stream shifts can influence wintertime variability in the North Atlantic storm track and Greenland blocking. *Geophys. Res. Lett.*, **46**, 1702–1708, <https://doi.org/10.1029/2018GL081087>.
- Jullien, S., S. Masson, V. Oerder, G. Samson, F. Colas, and L. Renault, 2020: Impact of ocean–atmosphere current feedback on the ocean mesoscale activity: Regional variations, and sensitivity to model resolution. *J. Climate*, **33**, 2585–2602, <https://doi.org/10.1175/JCLI-D-19-0484.1>.
- Jury, M. R., and S. Courtney, 1991: A transition in weather over the Agulhas Current. *S. Afr. J. Mar. Sci.*, **10**, 159–171, <https://doi.org/10.2989/02577619109504629>.
- Karmalkar, A. V., and R. M. Horton, 2021: Drivers of exceptional coastal warming in the northeastern United States. *Nat. Climate Change*, **11**, 854–860, <https://doi.org/10.1038/s41558-021-01159-7>.
- Kaspi, Y., and T. Schneider, 2013: The role of stationary eddies in shaping midlatitude storm tracks. *J. Atmos. Sci.*, **70**, 2596–2613, <https://doi.org/10.1175/JAS-D-12-082.1>.
- Keil, P., T. Mauritsen, J. Jungclaus, C. Hedemann, D. Olonscheck, and R. Ghosh, 2020: Multiple drivers of the North Atlantic warming hole. *Nat. Climate Change*, **10**, 667–671, <https://doi.org/10.1038/s41558-020-0819-8>.
- Kelly, K. A., S. Dickinson, M. J. McPhaden, and G. C. Johnson, 2001: Ocean currents evident in satellite wind data. *Geophys. Res. Lett.*, **28**, 2469–2472, <https://doi.org/10.1029/2000GL012610>.
- , R. J. Small, R. M. Samelson, B. Qiu, T. M. Joyce, Y.-O. Kwon, and M. F. Cronin, 2010: Western boundary currents and frontal air–sea interaction: Gulf Stream and Kuroshio Extension. *J. Climate*, **23**, 5644–5667, <https://doi.org/10.1175/2010JCLI3346.1>.
- Kessler, W. S., and Coauthors, 2019: Second report of TPOS 2020. Tech. Rep. GOOS-234, 265 pp., <http://tpos2020.org/second-report/>.
- Kilpatrick, T., N. Schneider, and B. Qiu, 2014: Boundary layer convergence induced by strong winds across a midlatitude SST front. *J. Climate*, **27**, 1698–1718, <https://doi.org/10.1175/JCLI-D-13-00101.1>.
- , —, and —, 2016: Atmospheric response to a midlatitude SST front: Alongfront winds. *J. Atmos. Sci.*, **73**, 3489–3509, <https://doi.org/10.1175/JAS-D-15-0312.1>.
- Kim, S. Y., 2010: Observations of submesoscale eddies using high-frequency radar-derived kinematic and dynamic quantities. *Cont. Shelf Res.*, **30**, 1639–1655, <https://doi.org/10.1016/j.csr.2010.06.011>.
- Kirincich, A., B. Emery, L. Washburn, and P. Flament, 2019: Improving surface current resolution using direction finding algorithms for multiantenna high-frequency radars. *J. Atmos. Oceanic Technol.*, **36**, 1997–2014, <https://doi.org/10.1175/JTECH-D-19-0029.1>.
- Kirtman, B. P., and Coauthors, 2012: Impact of ocean model resolution on CCSM climate simulations. *Climate Dyn.*, **39**, 1303–1328, <https://doi.org/10.1007/s00382-012-1500-3>.
- Kudryavtsev, V., B. Chapron, and V. Makin, 2014: Impact of wind waves on the air–sea fluxes: A coupled model. *J. Geophys. Res. Oceans*, **119**, 1217–1236, <https://doi.org/10.1002/2013JC009412>.
- Kushnir, Y., W. A. Robinson, I. Bladé, N. M. J. Hall, S. Peng, and R. Sutton, 2002: Atmospheric GCM response to extratropical SST anomalies: Synthesis and evaluation. *J. Climate*, **15**, 2233–2256, [https://doi.org/10.1175/1520-0442\(2002\)015<2233:AGRTES>2.0.CO;2](https://doi.org/10.1175/1520-0442(2002)015<2233:AGRTES>2.0.CO;2).
- Kuwano-Yoshida, A., and S. Minobe, 2017: Storm track response to SST fronts in the northwestern Pacific region in an AGCM. *J. Climate*, **30**, 1081–1102, <https://doi.org/10.1175/JCLI-D-16-0331.1>.
- Kwak, K., H. Song, J. Marshall, H. Seo, and D. McGillicuddy Jr., 2021: Suppressed pCO<sub>2</sub> in the Southern Ocean due to the interaction between current and wind. *J. Geophys. Res. Oceans*, **126**, e2021JC017884, <https://doi.org/10.1029/2021JC017884>.
- Kwon, Y.-O., and T. M. Joyce, 2013: Northern Hemisphere winter atmospheric transient eddy heat fluxes and the Gulf Stream and Kuroshio-Oyashio Extension variability. *J. Climate*, **26**, 9839–9859, <https://doi.org/10.1175/JCLI-D-12-00647.1>.
- , M. A. Alexander, N. A. Bond, C. Frankignoul, H. Nakamura, B. Qiu, and L. A. Thompson, 2010: Role of the Gulf Stream and Kuroshio-Oyashio systems in large-scale atmosphere–ocean interaction: A review. *J. Climate*, **23**, 3249–3281, <https://doi.org/10.1175/2010JCLI3343.1>.
- Lac, C., and Coauthors, 2018: Overview of the Meso-NH model version 5.4 and its applications. *Geosci. Model Dev.*, **11**, 1929–1969, <https://doi.org/10.5194/gmd-11-1929-2018>.
- Lambaerts, J., G. Lapeyre, R. Plougonven, and P. Klein, 2013: Atmospheric response to sea surface temperature mesoscale structures. *J. Geophys. Res. Atmos.*, **118**, 9611–9621, <https://doi.org/10.1002/jgrd.50769>.

- Lane, E. M., J. M. Restrepo, and J. C. McWilliams, 2007: Wave–current interaction: A comparison of radiation-stress and vortex-force representations. *J. Phys. Oceanogr.*, **37**, 1122–1141, <https://doi.org/10.1175/JPO3043.1>.
- Laurindo, L. C., A. J. Mariano, and R. Lumpkin, 2017: An improved surface velocity climatology for the global ocean from drifter observations. *Deep-Sea Res.*, **124**, 73–92, <https://doi.org/10.1016/j.dsr.2017.04.009>.
- , L. Siqueira, A. J. Mariano, and B. P. Kirtman, 2019: Cross-spectral analysis of the SST/10-m wind speed coupling resolved by satellite products and climate model simulations. *Climate Dyn.*, **52**, 5071–5098, <https://doi.org/10.1007/s00382-018-4434-6>.
- Lee, R. W., T. J. Woollings, B. J. Hoskins, K. D. Williams, C. H. O'Reilly, and G. Masato, 2018: Impact of Gulf Stream SST biases on the global atmospheric circulation. *Climate Dyn.*, **51**, 3369–3387, <https://doi.org/10.1007/s00382-018-4083-9>.
- Leibovich, S., 1983: The form and dynamics of Langmuir circulations. *Annu. Rev. Fluid Mech.*, **15**, 391–427, <https://doi.org/10.1146/annurev.fl.15.010183.002135>.
- Lenschow, D. H., P. B. Krummel, and S. T. Siems, 1999: Measuring entrainment, divergence, and vorticity on the mesoscale from aircraft. *J. Atmos. Oceanic Technol.*, **16**, 1384–1400, [https://doi.org/10.1175/1520-0426\(1999\)016<1384:MEDAVO>2.0.CO;2](https://doi.org/10.1175/1520-0426(1999)016<1384:MEDAVO>2.0.CO;2).
- Lévy, M., 2008: The modulation of biological production by oceanic mesoscale turbulence. *Transport and Mixing in Geophysical Flows*, J. Weiss and A. Provenzale, Eds., Springer, 219–261.
- , P. J. S. Franks, and K. S. Smith, 2018: The role of submesoscale currents in structuring marine ecosystems. *Nat. Commun.*, **9**, 4758, <https://doi.org/10.1038/s41467-018-07059-3>.
- Li, F., H. Sang, and Z. Jing, 2017: Quantify the continuous dependence of SST–turbulent heat flux relationship on spatial scales. *Geophys. Res. Lett.*, **44**, 6326–6333, <https://doi.org/10.1002/2017GL073695>.
- Li, Y., and R. E. Carbone, 2012: Excitation of rainfall over the tropical western Pacific. *J. Atmos. Sci.*, **69**, 2983–2994, <https://doi.org/10.1175/JAS-D-11-0245.1>.
- Lindzen, R. S., and B. Farrell, 1980: A simple approximate result for the maximum growth rate of baroclinic instabilities. *J. Atmos. Sci.*, **37**, 1648–1654, [https://doi.org/10.1175/1520-0469\(1980\)037<1648:ASARFT>2.0.CO;2](https://doi.org/10.1175/1520-0469(1980)037<1648:ASARFT>2.0.CO;2).
- , and S. Nigam, 1987: On the role of sea surface temperature gradients in forcing low-level winds and convergence in the tropics. *J. Atmos. Sci.*, **44**, 2418–2436, [https://doi.org/10.1175/1520-0469\(1987\)044<2418:OTROSS>2.0.CO;2](https://doi.org/10.1175/1520-0469(1987)044<2418:OTROSS>2.0.CO;2).
- Liu, W., A. V. Fedorov, S.-P. Xie, and S. Hu, 2020: Climate impacts of a weakened Atlantic meridional overturning circulation in a warming climate. *Sci. Adv.*, **6**, eaaz4876, <https://doi.org/10.1126/sciadv.aaz4876>.
- Liu, X., and Coauthors, 2021: Ocean fronts and eddies force atmospheric rivers and heavy precipitation in western North America. *Nat. Commun.*, **12**, 1268, <https://doi.org/10.1038/s41467-021-21504-w>.
- López-Dekker, P., H. Rott, P. Prats-Iraola, B. Chapron, K. Scipal, and E. De Witte, 2019: Harmony: An Earth Explorer 10 mission candidate to observe land, ice, and ocean surface dynamics. *IGARSS 2019–2019 IEEE Int. Geoscience and Remote Sensing Symp.*, Yokohama, Japan, Institute of Electrical and Electronics Engineers, 8381–8384, <https://doi.org/10.1109/IGARSS.2019.8897983>.
- Lorenz, E., 1960: Generation of available potential energy and the intensity of the general circulation. *Dynamics of Climate*, R. L. Pfeffer, Ed., Pergamon Press, 86–92.
- Luo, J.-J., S. Masson, E. Roeckner, G. Madec, and T. Yamagata, 2005: Reducing climatology bias in an ocean–atmosphere CGCM with improved coupling physics. *J. Climate*, **18**, 2344–2360, <https://doi.org/10.1175/JCLI3404.1>.
- Ma, X., P. Chang, R. Saravanan, R. M. J.-S. Hsieh, D. Wu, X. Lin, L. Wu, and Z. Jing, 2015: Distant influence of Kuroshio eddies on North Pacific weather patterns? *Sci. Rep.*, **5**, 17785, <https://doi.org/10.1038/srep17785>.
- , and Coauthors, 2016: Western boundary currents regulated by interaction between ocean eddies and the atmosphere. *Nature*, **535**, 533–537, <https://doi.org/10.1038/nature18640>.
- , P. Chang, R. Saravanan, R. Montuoro, H. Nakamura, D. Wu, X. Lin, and L. Wu, 2017: Importance of resolving Kuroshio front and eddy influence in simulating the North Pacific storm track. *J. Climate*, **30**, 1861–1880, <https://doi.org/10.1175/JCLI-D-16-0154.1>.
- Mahrt, L., D. Vickers, and E. Moore, 2004: Flow adjustments across sea-surface temperature changes. *Bound.-Layer Meteor.*, **111**, 553–564, <https://doi.org/10.1023/B:BOUN.0000016600.63382.5f>.
- Marshall, J., and Coauthors, 2009: The CLIMODE field campaign: Observing the cycle of convection and restratification over the Gulf Stream. *Bull. Amer. Meteor. Soc.*, **90**, 1337–1350, <https://doi.org/10.1175/2009BAMS2706.1>.
- , J. R. Scott, K. Armour, J.-M. Campin, M. Kelley, and A. Romanou, 2014: The Ocean's role in the transient response of climate to abrupt greenhouse gas forcing. *Climate Dyn.*, **44**, 2287–2299, <https://doi.org/10.1007/s00382-014-2308-0>.
- Masunaga, R., and N. Schneider, 2022: Surface wind responses to mesoscale sea surface temperature over western boundary current regions assessed by spectral transfer functions. *J. Atmos. Sci.*, **79**, 1549–1573, <https://doi.org/10.1175/JAS-D-21-0125.1>.
- , H. Nakamura, B. Taguchi, and T. Miyasaka, 2020a: Processes shaping the frontal-scale time-mean surface wind convergence patterns around the Kuroshio Extension in winter. *J. Climate*, **33**, 3–25, <https://doi.org/10.1175/JCLI-D-19-0097.1>.
- , —, —, and —, 2020b: Processes shaping the frontal-scale time-mean surface wind convergence patterns around the Gulf Stream and Agulhas Return Current in winter. *J. Climate*, **33**, 9083–9101, <https://doi.org/10.1175/JCLI-D-19-0948.1>.
- McGillicuddy, D. J., Jr., 2016: Mechanisms of physical–biological–biogeochemical interaction at the oceanic mesoscale. *Annu. Rev. Mar. Sci.*, **8**, 125–159, <https://doi.org/10.1146/annurev-marine-010814-015606>.
- , and Coauthors, 2007: Eddy/wind interactions stimulate extraordinary mid-ocean plankton blooms. *Science*, **316**, 1021–1026, <https://doi.org/10.1126/science.1136256>.
- McGillis, W. R., J. B. Edson, J. E. Hare, and C. W. Fairall, 2001: Direct covariance air–sea CO<sub>2</sub> fluxes. *J. Geophys. Res.*, **106**, 16 729–16 745, <https://doi.org/10.1029/2000JC000506>.
- McLandress, C., T. G. Shepherd, J. F. Scinocca, D. A. Plummer, M. Sigmond, A. I. Jonsson, and M. C. Reader, 2011: Separating the dynamical effects of climate change and ozone depletion. Part II: Southern Hemisphere troposphere. *J. Climate*, **24**, 1850–1868, <https://doi.org/10.1175/2010JCLI3958.1>.
- McWilliams, J. C., 2016: Submesoscale currents in the ocean. *Proc. Roy. Soc.*, **472A**, 20160117, <https://doi.org/10.1098/rspa.2016.0117>.



- , and B. Fox-Kemper, 2013: Oceanic wave-balanced surface fronts and filaments. *J. Fluid Mech.*, **730**, 464–490, <https://doi.org/10.1017/jfm.2013.348>.
- , E. Huckle, J.-H. Liang, and P. P. Sullivan, 2012: The wavy Ekman layer: Langmuir circulations, breaking waves, and Reynolds stress. *J. Phys. Oceanogr.*, **42**, 1793–1816, <https://doi.org/10.1175/JPO-D-12-07.1>.
- Meinig, C., and Coauthors, 2019: Public-private partnerships to advance regional ocean-observing capabilities: A Saildrone and NOAA-PMEL case study and future considerations to expand to global scale observing. *Front. Mar. Sci.*, **6**, 448, <https://doi.org/10.3389/fmars.2019.00448>.
- Mémin, E., 2014: Fluid flow dynamics under location uncertainty. *Geophys. Astrophys. Fluid Dyn.*, **108**, 119–146, <https://doi.org/10.1080/03091929.2013.836190>.
- Menary, M. B., and Coauthors, 2018: Preindustrial control simulations with HadGEM3-GC3.1 for CMIP6. *J. Adv. Model. Earth Syst.*, **10**, 3049–3075, <https://doi.org/10.1029/2018MS001495>.
- Messenger, C., and S. Swart, 2016: Significant atmospheric boundary layer change observed above an Agulhas current warm core eddy. *Adv. Meteor.*, **2016**, 3659657, <https://doi.org/10.1155/2016/3659657>.
- Minobe, S., A. Kuwano-Yoshida, N. Komori, S.-P. Xie, and R. J. Small, 2008: Influence of the Gulf Stream on the troposphere. *Nature*, **452**, 206–209, <https://doi.org/10.1038/nature06690>.
- , M. Miyashita, A. Kuwano-Yoshida, H. Tokinaga, and S.-P. Xie, 2010: Atmospheric response to the Gulf Stream: Seasonal variations. *J. Climate*, **23**, 3699–3719, <https://doi.org/10.1175/2010JCLI3359.1>.
- Miyamoto, A., H. Nakamura, and T. Miyasaka, 2018: Influence of the subtropical high and storm track on low-cloud fraction and its seasonality over the south Indian Ocean. *J. Climate*, **31**, 4017–4039, <https://doi.org/10.1175/JCLI-D-17-0229.1>.
- , —, —, Y. Kosaka, B. Taguchi, and K. Nishii, 2022: Wintertime weakening of low-cloud impacts on the subtropical high in the south Indian Ocean. *J. Climate*, **35**, 323–334, <https://doi.org/10.1175/JCLI-D-21-0178.1>.
- Miyazawa, Y., X. Guo, S. M. Varlamov, T. Miyama, K. Yoda, K. Sato, T. Kano, and K. Sato, 2016: Assimilation of the seabird and ship drift data in the north-eastern Sea of Japan into an operational ocean nowcast/forecast system. *Sci. Rep.*, **5**, 17672, <https://doi.org/10.1038/srep17672>.
- , and Coauthors, 2019: Temperature profiling measurements by sea turtles improve ocean state estimation in the Kuroshio–Oyashio confluence region. *Ocean Dyn.*, **69**, 267–282, <https://doi.org/10.1007/s10236-018-1238-5>.
- Moreno-Chamarro, E., L.-P. Caron, P. Ortega, S. Loosveldt Tomas, and M. J. Roberts, 2021: Can we trust CMIP5/6 future projections of European winter precipitation? *Environ. Res. Lett.*, **16**, 054063, <https://doi.org/10.1088/1748-9326/abf28a>.
- Moreton, S., D. Ferreira, M. Roberts, and H. Hewitt, 2021: Air–sea turbulent heat flux feedback over mesoscale eddies. *Geophys. Res. Lett.*, **48**, e2021GL095407, <https://doi.org/10.1029/2021GL095407>.
- Nadiga, B. T., 2008: Orientation of eddy fluxes in geostrophic turbulence. *Philos. Trans. Roy. Soc.*, **A366**, 2489–2508, <https://doi.org/10.1098/rsta.2008.0058>.
- Nakamura, H., and J. M. Wallace, 1990: Observed changes in baroclinic wave activity during the life cycles of low-frequency circulation anomalies. *J. Atmos. Sci.*, **47**, 1100–1116, [https://doi.org/10.1175/1520-0469\(1990\)047<1100:OCIBWA>2.0.CO;2](https://doi.org/10.1175/1520-0469(1990)047<1100:OCIBWA>2.0.CO;2).
- , and A. Shimp, 2004: Seasonal variations in the Southern Hemisphere storm tracks and jet streams as revealed in a reanalysis dataset. *J. Climate*, **17**, 1828–1844, [https://doi.org/10.1175/1520-0442\(2004\)017<1828:SVTSH>2.0.CO;2](https://doi.org/10.1175/1520-0442(2004)017<1828:SVTSH>2.0.CO;2).
- , T. Sampe, Y. Tanimoto, and A. Shimp, 2004: Observed associations among storm tracks, jet streams and midlatitude oceanic fronts. *Earth's Climate: The Ocean–Atmosphere Interaction*, *Geophys. Monogr.*, Vol. 147, Amer. Geophys. Union, 329–346, <https://doi.org/10.1029/147GM18>.
- , —, A. Goto, W. Ohfuchi, and S.-P. Xie, 2008: On the importance of midlatitude oceanic frontal zones for the mean state and dominant variability in the tropospheric circulation. *Geophys. Res. Lett.*, **35**, L15709, <https://doi.org/10.1029/2008GL034010>.
- , A. Nishina, and S. Minobe, 2012: Response of storm tracks to bimodal Kuroshio path states south of Japan. *J. Climate*, **25**, 7772–7779, <https://doi.org/10.1175/JCLI-D-12-00326.1>.
- , A. Isobe, S. Minobe, H. Mitsudera, and M. Nonaka, 2015: “Hot spots” in the climate system—New developments in the extratropical ocean–atmosphere interaction research: A short review and an introduction. *J. Oceanogr.*, **71**, 463–467, <https://doi.org/10.1007/s10872-015-0321-5>.
- Nakayama, M., H. Nakamura, and F. Ogawa, 2021: Impacts of a midlatitude oceanic frontal zone for the baroclinic annular mode in the Southern Hemisphere. *J. Climate*, **34**, 7389–7408, <https://doi.org/10.1175/JCLI-D-20-0359.1>.
- Newman, L., and Coauthors, 2022: The Southern Ocean Observing System 2021–2025 science and implementation plan. Zenodo, 55 pp., <https://doi.org/10.5281/zenodo.6324359>.
- Nkwinkwa Njouodo, A. S., S. Koseki, N. Keenlyside, and M. Rouault, 2018: Atmospheric signature of the Agulhas Current. *Geophys. Res. Lett.*, **45**, 5185–5193, <https://doi.org/10.1029/2018GL077042>.
- Nonaka, M., H. Nakamura, B. Taguchi, N. Komori, A. Yoshida-Kuwano, and K. Takaya, 2009: Air–sea heat exchanges characteristic to a prominent midlatitude oceanic front in the South Indian Ocean as simulated in a high-resolution coupled GCM. *J. Climate*, **22**, 6515–6535, <https://doi.org/10.1175/2009JCLI2960.1>.
- Ogawa, F., N.-E. Omrani, K. Nishii, H. Nakamura, and N. Keenlyside, 2015: Ozone-induced climate change propped up by the Southern Hemisphere oceanic front. *Geophys. Res. Lett.*, **42**, 10 056–10 063, <https://doi.org/10.1002/2015GL066538>.
- , H. Nakamura, K. Nishii, T. Miyasaka, and A. Kuwano-Yoshida, 2016: Importance of midlatitude oceanic frontal zones for the annular mode variability: Interbasin differences in the southern annular mode signature. *J. Climate*, **29**, 6179–6199, <https://doi.org/10.1175/JCLI-D-15-0885.1>.
- Olivier, L., and Coauthors, 2022: Impact of North Brazil current rings on air–sea CO<sub>2</sub> flux variability in winter 2020. *Biogeosciences*, **19**, 2969–2988, <https://doi.org/10.5194/bg-19-2969-2022>.
- Omand, M. M., E. A. D’Asaro, C. M. Lee, M. J. Perry, N. Briggs, I. Cetinić, and A. Mahadevan, 2015: Eddy-driven subduction exports particulate organic carbon from the spring bloom. *Science*, **348**, 222–225, <https://doi.org/10.1126/science.1260062>.
- Omrani, N.-E., F. Ogawa, H. Nakamura, N. Keenlyside, S. W. Lubis, and K. Matthes, 2019: Key role of the ocean western boundary currents in shaping the Northern Hemisphere climate. *Sci. Rep.*, **9**, 3014, <https://doi.org/10.1038/s41598-019-39392-y>.
- O’Neill, L. W., 2012: Wind speed and stability effects on coupling between surface wind stress and SST observed from buoys and satellites. *J. Climate*, **25**, 1544–1569, <https://doi.org/10.1175/JCLI-D-11-00121.1>.



- , D. B. Chelton, and S. K. Esbensen, 2003: Observations of SST-induced perturbations of the wind stress field over the Southern Ocean on seasonal timescales. *J. Climate*, **16**, 2340–2354, <https://doi.org/10.1175/2780.1>.
- , —, and —, 2012: Covariability of surface wind and stress responses to sea surface temperature fronts. *J. Climate*, **25**, 5916–5942, <https://doi.org/10.1175/JCLI-D-11-00230.1>.
- , T. Haack, and T. Durland, 2015: Estimation of time-averaged surface divergence and vorticity from satellite ocean vector winds. *J. Climate*, **28**, 7596–7620, <https://doi.org/10.1175/JCLI-D-15-0119.1>.
- , —, D. B. Chelton, and E. Skillingstad, 2017: The Gulf Stream convergence zone in the time-mean winds. *J. Atmos. Sci.*, **74**, 2383–2412, <https://doi.org/10.1175/JAS-D-16-0213.1>.
- O'Reilly, C. H., and A. Czaja, 2015: The response of the Pacific storm track and atmospheric circulation to Kuroshio Extension variability. *Quart. J. Roy. Meteor. Soc.*, **141**, 52–66, <https://doi.org/10.1002/qj.2334>.
- , S. Minobe, and A. Kuwano-Yoshida, 2016: The influence of the Gulf Stream on wintertime European blocking. *Climate Dyn.*, **47**, 1545–1567, <https://doi.org/10.1007/s00382-015-2919-0>.
- , —, —, and T. Woollings, 2017: The Gulf Stream influence on wintertime North Atlantic jet variability. *Quart. J. Roy. Meteor. Soc.*, **143**, 173–183, <https://doi.org/10.1002/qj.2907>.
- Pacanowski, R. C., 1987: Effect of equatorial currents on surface stress. *J. Phys. Oceanogr.*, **17**, 833–838, [https://doi.org/10.1175/1520-0485\(1987\)017<0833:EOECOS>2.0.CO;2](https://doi.org/10.1175/1520-0485(1987)017<0833:EOECOS>2.0.CO;2).
- Paduan, J. D., and L. Washburn, 2013: High-frequency radar observations of ocean surface currents. *Annu. Rev. Mar. Sci.*, **5**, 115–136, <https://doi.org/10.1146/annurev-marine-121211-172315>.
- Palmer, T. N., and Z. Sun, 1985: A modeling and observational study of the relationship between sea-surface temperature in the Northwest Atlantic and the atmospheric general circulation. *Quart. J. Roy. Meteor. Soc.*, **111**, 947–975, <https://doi.org/10.1002/qj.4971147003>.
- Parfitt, R., and A. Czaja, 2016: On the contribution of synoptic transients to the mean atmospheric state in the Gulf Stream region. *Quart. J. Roy. Meteor. Soc.*, **142**, 1554–1561, <https://doi.org/10.1002/qj.2689>.
- , and H. Seo, 2018: A new framework for near-surface wind convergence over the Kuroshio Extension and Gulf Stream in wintertime: The role of atmospheric fronts. *Geophys. Res. Lett.*, **45**, 9909–9918, <https://doi.org/10.1029/2018GL080135>.
- , A. Czaja, S. Minobe, and A. Kuwano-Yoshida, 2016: The atmospheric frontal response to SST perturbations in the Gulf Stream region. *Geophys. Res. Lett.*, **43**, 2299–2306, <https://doi.org/10.1002/2016GL067723>.
- Peng, S., A. Robinson, and M. P. Hoerling, 1997: The modeled atmospheric response to midlatitude SST anomalies and its dependence on background circulation states. *J. Climate*, **10**, 971–987, [https://doi.org/10.1175/1520-0442\(1997\)010<0971:TMARTM>2.0.CO;2](https://doi.org/10.1175/1520-0442(1997)010<0971:TMARTM>2.0.CO;2).
- Penny, S. G., and T. Hamill, 2017: Coupled data assimilation for integrated Earth system analysis and prediction. *Bull. Amer. Meteor. Soc.*, **98**, ES169–ES172, <https://www.jstor.org/stable/26243775>.
- Perlin, N., S. P. de Szoeke, D. B. Chelton, R. M. Samelson, E. D. Skillingstad, and L. W. O'Neill, 2014: Modeling the atmospheric boundary layer wind response to mesoscale sea surface temperature perturbations. *Mon. Wea. Rev.*, **142**, 4284–4307, <https://doi.org/10.1175/MWR-D-13-00332.1>.
- Pezzi, L. P., R. B. Souza, M. S. Dourado, C. A. E. Garcia, M. M. Mata, and M. A. F. Silva-Dias, 2005: Ocean–atmosphere in situ observations at the Brazil–Malvinas confluence region. *Geophys. Res. Lett.*, **32**, L22603, <https://doi.org/10.1029/2005GL023866>.
- , and Coauthors, 2021: Oceanic eddy-induced modifications to air–sea heat and CO<sub>2</sub> fluxes in the Brazil–Malvinas confluence. *Sci. Rep.*, **11**, 10 648, <https://doi.org/10.1038/s41598-021-89985-9>.
- Piazza, M., L. Terray, J. Boé, E. Maisonnave, and E. Sanchez-Gomez, 2016: Influence of small-scale North Atlantic sea surface temperature patterns on the marine boundary layer and free troposphere: A study using the atmospheric ARPEGE model. *Climate Dyn.*, **46**, 1699–1717, <https://doi.org/10.1007/s00382-015-2669-z>.
- Plagge, A., J. B. Edson, and D. Vandemark, 2016: In situ and satellite evaluation of air–sea flux variation near ocean temperature gradients. *J. Climate*, **29**, 1583–1602, <https://doi.org/10.1175/JCLI-D-15-0489.1>.
- Polvani, L. M., D. W. Waugh, G. J. P. Correa, and S.-W. Sens, 2011: Stratospheric ozone depletion: The main driver of twentieth-century atmospheric circulation changes in the Southern Hemisphere. *J. Climate*, **24**, 795–812, <https://doi.org/10.1175/2010JCLI3772.1>.
- Polverari, F., M. Portabella, W. Lin, J. W. Sapp, A. Stoffelen, Z. Jelenak, and P. S. Chang, 2021: On high and extreme wind calibration using ASCAT. *IEEE Trans. Geosci. Remote Sens.*, **60**, 1–10, <https://doi.org/10.1109/TGRS.2021.3079898>.
- Quinn, P. K., and Coauthors, 2021: Measurements from the RV Ronald H. Brown and related platforms as part of the Atlantic Tradewind Ocean–Atmosphere Mesoscale Interaction Campaign (ATOMIC). *Earth Syst. Sci. Data*, **13**, 1759–1790, <https://doi.org/10.5194/essd-13-1759-2021>.
- Reason, C. J. C., 2001: Evidence for the influence of the Agulhas Current on regional atmospheric circulation patterns. *J. Climate*, **14**, 2769–2778, [https://doi.org/10.1175/1520-0442\(2001\)014<2769:EFTIOT>2.0.CO;2](https://doi.org/10.1175/1520-0442(2001)014<2769:EFTIOT>2.0.CO;2).
- Reeder, M. J., T. Spengler, and C. Spensberger, 2021: The effect of sea surface temperature fronts on atmospheric frontogenesis. *J. Atmos. Sci.*, **78**, 1753–1771, <https://doi.org/10.1175/JAS-D-20-0118.1>.
- Reichl, B. G., and Deike, L., 2020: Contribution of sea-state dependent bubbles to air–sea carbon dioxide fluxes. *Geophys. Res. Lett.*, **47**, e2020GL087267, <https://doi.org/10.1029/2020GL087267>.
- Renault, L., and P. Marchesiello, 2022: Ocean tides can drag the atmosphere and cause tidal winds over broad continental shelves. *Commun. Earth Environ.*, **3**, 70, <https://doi.org/10.1038/s43247-022-00403-y>.
- , J. C. McWilliams, A. F. Shchepetkin, F. Lemarié, D. Chelton, S. Illig, and A. Hall, 2016a: Modulation of wind work by oceanic current interaction with the atmosphere. *J. Phys. Oceanogr.*, **46**, 1685–1704, <https://doi.org/10.1175/JPO-D-15-0232.1>.
- , M. J. Molemaker, J. Gula, S. Masson, and J. C. McWilliams, 2016b: Control and stabilization of the Gulf Stream by oceanic current interaction with the atmosphere. *J. Phys. Oceanogr.*, **46**, 3439–3453, <https://doi.org/10.1175/JPO-D-16-0115.1>.
- , J. C. McWilliams, and P. Penven, 2017a: Modulation of the Agulhas Current retroflection and leakage by oceanic current interaction with the atmosphere in coupled simulations. *J. Phys. Oceanogr.*, **47**, 2077–2100, <https://doi.org/10.1175/JPO-D-16-0168.1>.

- , —, and S. Masson, 2017b: Satellite observations of imprint of oceanic current on wind stress by air–sea coupling. *Sci. Rep.*, **7**, 17747, <https://doi.org/10.1038/s41598-017-17939-1>.
- , —, and J. Gula, 2018: Dampening of submesoscale currents by air–sea stress coupling in the Californian upwelling system. *Sci. Rep.*, **8**, 13388, <https://doi.org/10.1038/s41598-018-31602-3>.
- , S. Masson, V. Oerder, S. Jullien, and F. Colas, 2019a: Disentangling the mesoscale ocean–atmosphere interactions. *J. Geophys. Res. Oceans*, **124**, 2164–2178, <https://doi.org/10.1029/2018JC014628>.
- , P. Marchesiello, S. Masson, and J. C. McWilliams, 2019b: Remarkable control of western boundary currents by eddy killing, a mechanical air–sea coupling process. *Geophys. Res. Lett.*, **46**, 2743–2751, <https://doi.org/10.1029/2018GL081211>.
- , F. Lemarié, and T. Arsouze, 2019c: On the implementation and consequences of the oceanic currents feedback in ocean–atmosphere coupled models. *Ocean Modell.*, **141**, 101423, <https://doi.org/10.1016/j.ocemod.2019.101423>.
- Reynolds, R. W., T. M. Smith, C. Liu, D. B. Chelton, K. S. Casey, and M. G. Schlax, 2007: Daily high-resolution-blended analyses for sea surface temperature. *J. Climate*, **20**, 5473–5496, <https://doi.org/10.1175/2007JCLI1824.1>.
- Roberts, M. J., H. T. Hewitt, P. Hyder, D. Ferreira, S. A. Josey, M. Mizielinski, and A. Shelly, 2016: Impact of ocean resolution on coupled air–sea fluxes and large-scale climate. *Geophys. Res. Lett.*, **43**, 10 430–10 438, <https://doi.org/10.1002/2016GL070559>.
- Robinson, W., S. Speich, and E. Chassignet, 2018: Exploring the interplay between ocean eddies and the atmosphere. *Eos*, **99**, <https://doi.org/10.1029/2018EO100609>.
- , P. Chang, E. Chassignet, and S. Speich, 2020: Ocean mesoscale eddy interactions with the atmosphere. Tech. Rep. 2020-05, U.S. CLIVAR Project Office, 22 pp., <https://doi.org/10.5065/ebjm-5q77>.
- Romero, L., D. Hypolite, and J. C. McWilliams, 2020: Submesoscale current effects on surface waves. *Ocean Modell.*, **153**, 101662, <https://doi.org/10.1016/j.ocemod.2020.101662>.
- Rousseau, V., E. Sanchez-Gomez, R. Msadek, and M.-P. Moine, 2021: Mechanisms shaping wind convergence under extreme synoptic situations over the Gulf Stream region. *J. Climate*, **34**, 9481–9500, <https://doi.org/10.1175/JCLI-D-20-0719.1>.
- Saba, V. S., and Coauthors, 2016: Enhanced warming of the north-west Atlantic Ocean under climate change. *J. Geophys. Res. Oceans*, **121**, 118–132, <https://doi.org/10.1002/2015JC011346>.
- Samelson, R. M., E. D. Skyllingstad, D. B. Chelton, S. K. Esbensen, L. W. O'Neill, and N. Thum, 2006: On the coupling of wind stress and sea surface temperature. *J. Climate*, **19**, 1557–1566, <https://doi.org/10.1175/JCLI3682.1>.
- , L. W. O'Neill, D. B. Chelton, E. D. Skyllingstad, P. L. Barbour, and S. M. Durski, 2020: Surface stress and atmospheric boundary layer response to mesoscale SST structure in coupled simulations of the northern California Current System. *Mon. Wea. Rev.*, **148**, 259–287, <https://doi.org/10.1175/MWR-D-19-0200.1>.
- Sampe, T., and S.-P. Xie, 2007: Mapping high sea winds from space: A global climatology. *Bull. Amer. Meteor. Soc.*, **88**, 1965–1978, <https://doi.org/10.1175/BAMS-88-12-1965>.
- , H. Nakamura, and A. Goto, 2013: Potential influence of a midlatitude oceanic frontal zone on the annular variability in the extratropical atmosphere as revealed by aqua-planet experiments. *J. Meteor. Soc. Japan*, **91A**, 243–267, <https://doi.org/10.2151/jmsj.2013-A09>.
- Saviano, S., and Coauthors, 2021: Wind direction data from a coastal HF radar system in the Gulf of Naples (central Mediterranean Sea). *Remote Sens.*, **13**, 1333, <https://doi.org/10.3390/rs13071333>.
- Schneider, N., 2020: Scale and Rossby number dependence of observed wind responses to ocean-mesoscale sea surface temperatures. *J. Atmos. Sci.*, **77**, 3171–3192, <https://doi.org/10.1175/JAS-D-20-0154.1>.
- , and B. Qiu, 2015: The atmospheric response to weak sea surface temperature fronts. *J. Atmos. Sci.*, **72**, 3356–3377, <https://doi.org/10.1175/JAS-D-14-0212.1>.
- Schubert, W. H., J. S. Wakefield, E. J. Steiner, and S. K. Cox, 1979: Marine stratocumulus convection. Part II: Horizontally inhomogeneous solutions. *J. Atmos. Sci.*, **36**, 1308–1324, [https://doi.org/10.1175/1520-0469\(1979\)036<1308:MSCPIH>2.0.CO;2](https://doi.org/10.1175/1520-0469(1979)036<1308:MSCPIH>2.0.CO;2).
- Scott, R. B., and Y. Xu, 2009: An update on the wind power input to the surface geostrophic flow of the World Ocean. *Deep-Sea Res. I*, **56**, 295–304, <https://doi.org/10.1016/j.dsr.2008.09.010>.
- Seager, R., and I. R. Simpson, 2016: Western boundary currents and climate change. *J. Geophys. Res. Oceans*, **121**, 7212–7214, <https://doi.org/10.7916/D8KH0WWW>.
- , Y. Kushnir, N. H. Naik, M. A. Cane, and J. Miller, 2001: Wind-driven shifts in the latitude of the Kuroshio–Oyashio Extension and generation of SST anomalies on decadal time-scales. *J. Climate*, **14**, 4249–4265, [https://doi.org/10.1175/1520-0442\(2001\)014<4249:WDSITL>2.0.CO;2](https://doi.org/10.1175/1520-0442(2001)014<4249:WDSITL>2.0.CO;2).
- Sen Gupta, A., and Coauthors, 2021: Future changes to the upper ocean western boundary currents across two generations of climate models. *Sci. Rep.*, **11**, 9538, <https://doi.org/10.1038/s41598-021-88934-w>.
- Seo, H., 2017: Distinct influence of air–sea interactions mediated by mesoscale sea surface temperature and surface current in the Arabian Sea. *J. Climate*, **30**, 8061–8080, <https://doi.org/10.1175/JCLI-D-16-0834.1>.
- , M. Jochum, R. Murtugudde, A. J. Miller, and J. O. Roads, 2007: Feedback of tropical instability wave-induced atmospheric variability onto the ocean. *J. Climate*, **20**, 5842–5855, <https://doi.org/10.1175/JCLI4330.1>.
- , Y.-O. Kwon, and J.-J. Park, 2014: On the effect of the East/Japan Sea SST variability on the North Pacific atmospheric circulation in a regional climate model. *J. Geophys. Res. Atmos.*, **119**, 418–444, <https://doi.org/10.1002/2013JD020523>.
- , A. J. Miller, and J. R. Norris, 2016: Eddy–wind interaction in the California current system: Dynamics and impacts. *J. Phys. Oceanogr.*, **46**, 439–459, <https://doi.org/10.1175/JPO-D-15-0086.1>.
- , Y.-O. Kwon, T. M. Joyce, and C. C. Ummerhofer, 2017: On the predominant nonlinear response of the extratropical atmosphere to meridional shift of the Gulf Stream. *J. Climate*, **30**, 9679–9702, <https://doi.org/10.1175/JCLI-D-16-0707.1>.
- , A. C. Subramanian, H. Song, and J. S. Chowdary, 2019: Coupled effects of ocean current on wind stress in the Bay of Bengal: Eddy energetics and upper ocean stratification. *Deep-Sea Res. II*, **168**, 104617, <https://doi.org/10.1016/j.dsr2.2019.07.005>.
- , H. Song, L. W. O'Neill, M. R. Mazloff, and B. D. Cornuelle, 2021: Impacts of ocean currents on the south Indian Ocean extratropical storm track through the relative wind effect. *J. Climate*, **34**, 9093–9113, <https://doi.org/10.1175/JCLI-D-21-0142.1>.
- Sheldon, L., A. Czaja, B. Vannière, C. Morcrette, B. Sohet, M. Casado, and D. Smith, 2017: A warm path to Gulf Stream–

- troposphere interactions. *Tellus*, **69**, 1299397, <http://doi.org/10.1080/16000870.2017.1299397>.
- Shi, Q., and M. A. Bourassa, 2019: Coupling ocean currents and waves with wind stress over the Gulf Stream. *Remote Sens.*, **11**, 1476, <https://doi.org/10.3390/rs11121476>.
- Shinoda, T., S. Pei, W. Wang, J. X. Fu, R.-C. Lien, H. Seo, and A. Soloviev, 2021: Climate process team: Improvement of ocean component of NOAA climate forecast system relevant to Madden-Julian oscillation simulations. *J. Adv. Model. Earth Syst.*, **13**, e2021MS002658, <https://doi.org/10.1029/2021MS002658>.
- Shroyer, E., and Coauthors, 2021: Bay of Bengal intraseasonal oscillation and the 2018 monsoon onset. *Bull. Amer. Meteor. Soc.*, **102**, E1936–E1951, <https://doi.org/10.1175/BAMS-D-20-0113.1>.
- Singleton, A. T., and C. J. C. Reason, 2006: Numerical simulations of a severe rainfall event over the Eastern Cape coast of South Africa: Sensitivity to sea surface temperature and topography. *Tellus*, **58A**, 335–367, <https://doi.org/10.1111/j.1600-0870.2006.00180.x>.
- Siqueira, L., and B. P. Kirtman, 2016: Atlantic near-term climate variability and the role of a resolved Gulf Stream. *Geophys. Res. Lett.*, **43**, 3964–3972, <https://doi.org/10.1002/2016GL068694>.
- , —, and L. C. Laurindo, 2021: Forecasting remote atmospheric responses to decadal Kuroshio stability transitions. *J. Climate*, **34**, 379–395, <https://doi.org/10.1175/JCLI-D-20-0139.1>.
- Skyllingstad, E. D., and J. B. Edson, 2009: Large-eddy simulation of moist convection during a cold-air outbreak over the Gulf Stream. *J. Atmos. Sci.*, **66**, 1274–1293, <https://doi.org/10.1175/2008JAS2755.1>.
- , D. Vickers, L. Mahrt, and R. Samelson, 2007: Effects of mesoscale sea-surface temperature fronts on the marine atmospheric boundary layer. *Bound.-Layer Meteor.*, **123**, 219–237, <https://doi.org/10.1007/s10546-006-9127-8>.
- , S. P. de Szoeke, and L. W. O'Neill, 2019: Modeling the transient response of tropical convection to mesoscale SST variations. *J. Atmos. Sci.*, **76**, 1227–1244, <https://doi.org/10.1175/JAS-D-18-0079.1>.
- Small, R. J., S.-P. Xie, Y. Wang, S. K. Esbensen, and D. Vickers, 2005a: Numerical simulation of boundary layer structure and cross-equatorial flow in the eastern Pacific. *J. Atmos. Sci.*, **62**, 1812–1830, <https://doi.org/10.1175/JAS3433.1>.
- , —, and J. Hafner, 2005b: Satellite observations of mesoscale ocean features and copropagating atmospheric surface fields in the tropical belt. *J. Geophys. Res.*, **110**, C02021, <https://doi.org/10.1029/2004JC002598>.
- , and Coauthors, 2008: Air–sea interaction over ocean fronts and eddies. *Dyn. Atmos. Oceans*, **45**, 274–319, <https://doi.org/10.1016/j.dynatmoce.2008.01.001>.
- , R. Msadek, Y.-O. Kwon, J. F. Booth, and C. Zarzycki, 2019: Atmosphere surface storm track response to resolved ocean mesoscale in two sets of global climate model experiments. *Climate Dyn.*, **52**, 2067–2089, <https://doi.org/10.1007/s00382-018-4237-9>.
- Smirnov, D., M. Newman, M. A. Alexander, Y.-O. Kwon, and C. Frankignoul, 2015: Investigating the local atmospheric response to a realistic shift in the Oyashio sea surface temperature front. *J. Climate*, **28**, 1126–1147, <https://doi.org/10.1175/JCLI-D-14-00285.1>.
- Song, H., J. Marshall, P. Gaube, and D. J. McGillicuddy Jr., 2015: Anomalous chlorofluorocarbon uptake by mesoscale eddies in the Drake Passage region. *J. Geophys. Res. Oceans*, **120**, 1065–1078, <https://doi.org/10.1002/2014JC010292>.
- , —, M. J. Follows, S. Dutkiewicz, and G. Forget, 2016: Source waters for the highly productive Patagonian shelf in the southwestern Atlantic. *J. Mar. Syst.*, **158**, 120–128, <https://doi.org/10.1016/j.jmarsys.2016.02.009>.
- , —, D. J. McGillicuddy Jr., and H. Seo, 2020: The impact of the current–wind interaction on the vertical processes in the Southern Ocean. *J. Geophys. Res. Oceans*, **125**, e2020JC016046, <https://doi.org/10.1029/2020JC016046>.
- Song, Q., P. Cornillon, and T. Hara, 2006: Surface wind response to oceanic fronts. *J. Geophys. Res.*, **111**, C12006, <https://doi.org/10.1029/2006JC003680>.
- , D. B. Chelton, S. K. Esbensen, N. Thum, and L. W. O'Neill, 2009: Coupling between sea surface temperature and low-level winds in mesoscale numerical models. *J. Climate*, **22**, 146–164, <https://doi.org/10.1175/2008JCLI2488.1>.
- , —, —, and A. R. Brown, 2017: An investigation of the stability dependence of SST-induced vertical mixing over the ocean in the operational Met Office model. *J. Climate*, **30**, 91–107, <https://doi.org/10.1175/JCLI-D-16-0086.1>.
- Souza, R., L. Pezzi, S. Swart, F. Oliveira, and M. Santini, 2021: Air–sea interactions over eddies in the Brazil–Malvinas confluence. *Remote Sens.*, **13**, 1335, <https://doi.org/10.3390/rs13071335>.
- Spall, M. A., 2007a: Midlatitude wind stress–sea surface temperature coupling in the vicinity of oceanic fronts. *J. Climate*, **20**, 3785–3801, <https://doi.org/10.1175/JCLI4234.1>.
- , 2007b: Effect of sea surface temperature–wind stress coupling on baroclinic instability in the ocean. *J. Phys. Oceanogr.*, **37**, 1092–1097, <https://doi.org/10.1175/JPO3045.1>.
- Sprattall, J., V. J. Coles, K. A. Reed, A. H. Butler, G. R. Foltz, S. G. Penny, and H. Seo, 2020: Best practice strategies for process studies designed to improve climate modeling. *Bull. Amer. Meteor. Soc.*, **101**, E1842–E1850, <https://doi.org/10.1175/BAMS-D-19-0263.1>.
- Stevens, B., and Coauthors, 2003: Dynamics and chemistry of marine stratocumulus—DYCOMS-II. *Bull. Amer. Meteor. Soc.*, **84**, 579–594, <https://doi.org/10.1175/BAMS-84-5-579>.
- , and Coauthors, 2019: DYAMOND: The dynamics of the atmospheric general circulation modeled on non-hydrostatic domains. *Prog. Earth Planet. Sci.*, **6**, 61, <https://doi.org/10.1186/s40645-019-0304-z>.
- , and Coauthors, 2021: EUREC<sup>4</sup>A. *Earth Syst. Sci. Data*, **13**, 4067–4119, <https://doi.org/10.5194/essd-13-4067-2021>.
- Stoffelen, A., R. Kumar, J. Zou, V. Karaev, P. S. Chang, and E. Rodriguez, 2019: Ocean surface vector wind observations. *Remote Sensing of the Asian Seas*, V. Barale and M. Gade, Eds., Springer, 429–447, [https://doi.org/10.1007/978-3-319-94067-0\\_24](https://doi.org/10.1007/978-3-319-94067-0_24).
- Su, Z., J. Wang, P. Klein, A. F. Thompson, and D. Menemenlis, 2018: Ocean submesoscales as a key component of the global heat budget. *Nat. Commun.*, **9**, 775, <https://doi.org/10.1038/s41467-018-02983-w>.
- Subramanian, A. C., and Coauthors, 2019: Ocean observations to improve our understanding, modeling, and forecasting of sub-seasonal-to-seasonal variability. *Front. Mar. Sci.*, **6**, 427, <https://doi.org/10.3389/fmars.2019.00427>.
- Sugimoto, S., B. Qiu, and N. Schneider, 2021: Local atmospheric response to the Kuroshio large meander path in summer and its remote influence on the climate of Japan. *J. Climate*, **34**, 3571–3589, <https://doi.org/10.1175/JCLI-D-20-0387.1>.
- Sullivan, P. P., and J. C. McWilliams, 2010: Dynamics of winds and currents coupled to surface waves. *Annu. Rev. Fluid Mech.*, **42**, 19–42, <https://doi.org/10.1146/annurev-fluid-121108-145541>.



- , and —, 2019: Langmuir turbulence and filament frontogenesis in the oceanic surface boundary layer. *J. Fluid Mech.*, **879**, 512–553, <https://doi.org/10.1017/jfm.2019.655>.
- , —, J. C. Weil, E. G. Patton, and H. J. S. Fernando, 2020: Marine boundary layers above heterogeneous SST: Across-front winds. *J. Atmos. Sci.*, **77**, 4251–4275, <https://doi.org/10.1175/JAS-D-20-0062.1>.
- , —, —, —, and —, 2021: Marine boundary layers above heterogeneous SST: Alongfront winds. *J. Atmos. Sci.*, **78**, 3297–3315, <https://doi.org/10.1175/JAS-D-21-0072.1>.
- Sun, X., and R. Wu, 2022: Spatial scale dependence of the relationship between turbulent surface heat flux and SST. *Climate Dyn.*, **58**, 1127–1145, <https://doi.org/10.1007/s00382-021-05957-9>.
- Sutton, R., and P. P. Mathieu, 2002: Response of the atmosphere–ocean mixed-layer system to anomalous ocean heat-flux convergence. *Quart. J. Roy. Meteor. Soc.*, **128**, 1259–1275, <https://doi.org/10.1256/003590002320373283>.
- Suzuki, N., B. Fox-Kemper, P. E. Hamlington, and L. P. Van Roekel, 2016: Surface waves affect frontogenesis. *J. Geophys. Res. Oceans*, **121**, 3597–3624, <https://doi.org/10.1002/2015JC011563>.
- Swart, S., and Coauthors, 2019: Constraining Southern Ocean air–sea–ice fluxes through enhanced observations. *Front. Mar. Sci.*, **6**, 421, <https://doi.org/10.3389/fmars.2019.00421>.
- Sweet, W., R. Fett, J. Kerling, and P. La Violette, 1981: Air–sea interaction effects in the lower troposphere across the north wall of the Gulf Stream. *Mon. Wea. Rev.*, **109**, 1042–1052, [https://doi.org/10.1175/1520-0493\(1981\)109<1042:ASIEIT>2.0.CO;2](https://doi.org/10.1175/1520-0493(1981)109<1042:ASIEIT>2.0.CO;2).
- Taguchi, B., S.-P. Xie, N. Schneider, M. Nonaka, H. Sasaki, and Y. Sasai, 2007: Decadal variability of the Kuroshio Extension: Observations and an eddy-resolving model hindcast. *J. Climate*, **20**, 2357–2377, <https://doi.org/10.1175/JCLI4142.1>.
- , H. Nakamura, M. Nonaka, and S.-P. Xie, 2009: Influences of the Kuroshio/Oyashio Extensions on air–sea heat exchanges and storm-track activity as revealed in regional atmospheric model simulations for the 2003/04 cold season. *J. Climate*, **22**, 6536–6560, <https://doi.org/10.1175/2009JCLI2910.1>.
- , —, —, K. Komori, A. Kuwano-Yoshida, K. Takaya, and A. Goto, 2012: Seasonal evolutions of atmospheric response to decadal SST anomalies in the North Pacific subarctic frontal zone: Observations and a coupled model simulation. *J. Climate*, **25**, 111–139, <https://doi.org/10.1175/JCLI-D-11-00046.1>.
- Takahashi, N., T. Hayasaka, A. Manda, and N. Schneider, 2020: Impact of the Oyashio Extension SST front on synoptic variability of oceanic low-level cloud in summertime based on WRF numerical simulation. *J. Geophys. Res. Atmos.*, **125**, e2020JD032518, <https://doi.org/10.1029/2020JD032518>.
- , —, B. Qiu, and R. Yamaguchi, 2021: Observed response of marine boundary layer cloud to the interannual variations of summertime Oyashio Extension SST front. *Climate Dyn.*, **56**, 3511–3526, <https://doi.org/10.1007/s00382-021-05649-4>.
- Takatama, K., and N. Schneider, 2017: The role of back pressure in the atmospheric response to surface stress induced by the Kuroshio. *J. Atmos. Sci.*, **74**, 597–615, <https://doi.org/10.1175/JAS-D-16-0149.1>.
- Thompson, D. W. J., and J. M. Wallace, 2000: Annular modes in the extratropical circulation. Part I: Month-to-month variability. *J. Climate*, **13**, 1000–1016, [https://doi.org/10.1175/1520-0442\(2000\)013<1000:AMITEC>2.0.CO;2](https://doi.org/10.1175/1520-0442(2000)013<1000:AMITEC>2.0.CO;2).
- Thomson, J., 2012: Wave breaking dissipation observed with “SWIFT” drifters. *J. Atmos. Oceanic Technol.*, **29**, 1866–1882, <https://doi.org/10.1175/JTECH-D-12-00018.1>.
- , and J. Garton, 2017: Sustained measurements of Southern Ocean air–sea coupling from a Wave Glider autonomous surface vehicle. *Oceanography*, **30**, 104–109, <https://doi.org/10.5670/oceanog.2017.228>.
- Thum, N., S. K. Esbensen, D. B. Chelton, and M. J. McPhaden, 2002: Air–sea heat exchange along the northern sea surface temperature front in the eastern tropical Pacific. *J. Climate*, **15**, 3361–3378, [https://doi.org/10.1175/1520-0442\(2002\)015<3361:ASHEAT>2.0.CO;2](https://doi.org/10.1175/1520-0442(2002)015<3361:ASHEAT>2.0.CO;2).
- Tokinaga, H., Y. Tanimoto, S.-P. Xie, T. Sampe, H. Tomita, and H. Ichikawa, 2009: Ocean frontal effects on the vertical development of clouds over the western North Pacific: In situ and satellite observations. *J. Climate*, **22**, 4241–4260, <https://doi.org/10.1175/2009JCLI2763.1>.
- Tozuka, T., M. F. Cronin, and H. Tomita, 2017: Surface frontogenesis by surface heat fluxes in the upstream Kuroshio Extension region. *Sci. Rep.*, **7**, 10258, <https://doi.org/10.1038/s41598-017-10268-3>.
- , S. Ohishi, and M. F. Cronin, 2018: A metric for surface heat flux effect on horizontal sea surface temperature gradients. *Climate Dyn.*, **51**, 547–561, <https://doi.org/10.1007/s00382-017-3940-2>.
- Trindade, A., M. Portabella, A. Stoffelen, W. Lin, and A. Verhoef, 2020: ERAstar: A high-resolution ocean forcing product. *IEEE Trans. Geosci. Remote Sens.*, **58**, 1337–1347, <https://doi.org/10.1109/TGRS.2019.2946019>.
- Trowbridge, J., R. Weller, D. Kelley, E. Dever, A. Plueddemann, J. A. Barth, and O. Kawka, 2019: The Ocean Observatories Initiative. *Front. Mar. Sci.*, **6**, 74, <https://doi.org/10.3389/fmars.2019.00074>.
- Tsopouridis, L., C. Spensberger, and T. Spengler, 2021: Cyclone intensification in the Kuroshio region and its relation to the sea surface temperature front and upper-level forcing. *Quart. J. Roy. Meteor. Soc.*, **147**, 485–500, <https://doi.org/10.1002/qj.3929>.
- Vannière, B., A. Czaja, H. Dacre, and T. Woollings, 2017: A “cold path” for the Gulf Stream–troposphere connection. *J. Climate*, **30**, 1363–1379, <https://doi.org/10.1175/JCLI-D-15-0749.1>.
- Vecchi, G. A., S.-P. Xie, and A. S. Fischer, 2004: Ocean–atmosphere covariability in the western Arabian Sea. *J. Climate*, **17**, 1213–1224, [https://doi.org/10.1175/1520-0442\(2004\)017<1213:OCITWA>2.0.CO;2](https://doi.org/10.1175/1520-0442(2004)017<1213:OCITWA>2.0.CO;2).
- Verdy, A., and M. R. Mazloff, 2017: A data assimilating model for estimating Southern Ocean biogeochemistry. *J. Geophys. Res. Oceans*, **122**, 6968–6988, <https://doi.org/10.1002/2016JC012650>.
- Villas Bôas, A. B., and W. R. Young, 2020: Directional diffusion of surface gravity wave action by ocean macroturbulence. *J. Fluid Mech.*, **890**, R3, <https://doi.org/10.1017/jfm.2020.116>.
- , and N. Pizzo, 2021: The geometry, kinematics, and dynamics of the two-way coupling between wind, waves, and currents. *U.S. CLIVAR Variations*, No. 19, U.S. CLIVAR Project Office, Washington, DC, 18–26, <https://usclivar.org/newsletters>.
- , O. T. Sato, A. Chaigneau, and G. P. Castelão, 2015: The signature of mesoscale eddies on the air–sea turbulent heat fluxes in the South Atlantic Ocean. *Geophys. Res. Lett.*, **42**, 1856–1862, <https://doi.org/10.1002/2015GL063105>.
- , and Coauthors, 2019: Integrated observations of global surface winds, currents, and waves: Requirements and challenges for the next decade. *Front. Mar. Sci.*, **6**, 425, <https://doi.org/10.3389/fmars.2019.00425>.

- , B. D. Cornuelle, M. R. Mazloff, S. T. Gille, and F. Ardhuin, 2020: Wave–current interactions at meso- and submesoscales: Insights from idealized numerical simulations. *J. Phys. Oceanogr.*, **50**, 3483–3500, <https://doi.org/10.1175/JPO-D-20-0151.1>.
- Wai, M. M., and S. A. Stage, 1989: Dynamical analyses of marine atmospheric boundary layer structure near the Gulf Stream oceanic front. *Quart. J. Roy. Meteor. Soc.*, **115**, 29–44, <https://doi.org/10.1002/qj.49711548503>.
- Wallace, J. M., T. P. Mitchell, and C. Deser, 1989: The influence of sea surface temperature on sea surface wind in the eastern equatorial Pacific: Seasonal and interannual variability. *J. Climate*, **2**, 1492–1499, [https://doi.org/10.1175/1520-0442\(1989\)002<1492:TIOSSST>2.0.CO;2](https://doi.org/10.1175/1520-0442(1989)002<1492:TIOSSST>2.0.CO;2).
- Wang, Q., and Coauthors, 2018: CASPER: Coupled air–sea processes and electromagnetic (EM) ducting research. *Bull. Amer. Meteor. Soc.*, **99**, 1449–1471, <https://doi.org/10.1175/BAMS-D-16-0046.1>.
- Wanninkhof, R., 1992: Relationship between wind speed and gas exchange over the ocean. *J. Geophys. Res.*, **97**, 7373–7382, <https://doi.org/10.1029/92JC00188>.
- , W. E. Asher, D. T. Ho, C. Sweeney, and W. R. McGillis, 2009: Advances in quantifying air–sea gas exchange and environmental forcing. *Annu. Rev. Mar. Sci.*, **1**, 213–244, <https://doi.org/10.1146/annurev.marine.010908.163742>.
- , G.-H. Park, D. B. Chelton, and C. M. Risien, 2011: Impact of small-scale variability on air–sea CO<sub>2</sub> fluxes. *Gas Transfer at Water Surfaces 2010*, S. Komori, W. McGillis, and R. Kurose, Eds., Kyoto University Press, 431–444.
- , and Coauthors, 2019: A surface ocean CO<sub>2</sub> reference network, SOCONET and associated marine boundary layer CO<sub>2</sub> measurements. *Front. Mar. Sci.*, **6**, 400, <https://doi.org/10.3389/fmars.2019.00400>.
- Warner, T. T., M. N. Lakhtakia, J. D. Doyle, and R. A. Pearson, 1990: Marine atmospheric boundary layer circulations forced by Gulf Stream sea surface temperature gradients. *Mon. Wea. Rev.*, **118**, 309–323, [https://doi.org/10.1175/1520-0493\(1990\)118<0309:MABLCF>2.0.CO;2](https://doi.org/10.1175/1520-0493(1990)118<0309:MABLCF>2.0.CO;2).
- Weaver, A. J., and Coauthors, 2012: Stability of the Atlantic meridional overturning circulation: A model intercomparison. *Geophys. Res. Lett.*, **39**, L20709, <https://doi.org/10.1029/2012GL053763>.
- Wenegrat, J. O., and R. S. Arthur, 2018: Response of the atmospheric boundary layer to submesoscale sea surface temperature fronts. *Geophys. Res. Lett.*, **45**, 13 505–13 512, <https://doi.org/10.1029/2018GL081034>.
- Wengel, C., S.-S. Lee, M. F. Stuecker, A. Timmermann, J.-E. Chu, and F. Schloesser, 2021: Future high-resolution El Niño/southern oscillation dynamics. *Nat. Climate Change*, **11**, 758–765, <https://doi.org/10.1038/s41558-021-01132-4>.
- Willison, J., W. A. Robinson, and G. M. Lackmann, 2013: The importance of resolving mesoscale latent heating in the North Atlantic storm track. *J. Atmos. Sci.*, **70**, 2234–2250, <https://doi.org/10.1175/JAS-D-12-0226.1>.
- Wills, S. M., and D. W. J. Thompson, 2018: On the observed relationships between wintertime variability in Kuroshio–Oyashio Extension sea surface temperatures and the atmospheric circulation over the North Pacific. *J. Climate*, **31**, 4669–4681, <https://doi.org/10.1175/JCLI-D-17-0343.1>.
- , —, and L. M. Ciasto, 2016: On the observed relationships between variability in Gulf Stream sea surface temperatures and the atmospheric circulation over the North Atlantic. *J. Climate*, **29**, 3719–3730, <https://doi.org/10.1175/JCLI-D-15-0820.1>.
- Wineteer, A., H. S. Torres, and E. Rodriguez, 2020: On the surface current measurement capabilities of spaceborne Doppler scatterometry. *Geophys. Res. Lett.*, **47**, e2020GL090116, <https://doi.org/10.1029/2020GL090116>.
- Winton, M., S. M. Griffies, B. L. Samuels, J. L. Sarmiento, and T. L. Frölicher, 2013: Connecting changing ocean circulation with changing climate. *J. Climate*, **26**, 2268–2278, <https://doi.org/10.1175/JCLI-D-12-00296.1>.
- Woolf, D. K., 1993: Bubbles and the air–sea transfer velocity of gases. *Atmos.–Ocean*, **31**, 517–540, <https://doi.org/10.1080/07055900.1993.9649484>.
- Woollings, T., J. M. Gregory, J. G. Pinto, M. Meyers, and D. J. Brayshaw, 2012: Response of the North Atlantic storm track to climate change shaped by ocean–atmosphere coupling. *Nat. Geosci.*, **5**, 313–317, <https://doi.org/10.1038/ngeo1438>.
- Wu, L., and Coauthors, 2012: Enhanced warming over the global subtropical western boundary currents. *Nat. Climate Change*, **2**, 161–166, <https://doi.org/10.1038/nclimate1353>.
- Wu, R., B. P. Kirtman, and K. Pegion, 2006: Local air–sea relationship in observations and model simulations. *J. Climate*, **19**, 4914–4932, <https://doi.org/10.1175/JCLI3904.1>.
- Xie, S.-P., 2004: Satellite observations of cool ocean–atmosphere interaction. *Bull. Amer. Meteor. Soc.*, **85**, 195–209, <https://doi.org/10.1175/BAMS-85-2-195>.
- Xie, T., W. Perrie, and W. Chen, 2010: Gulf Stream thermal fronts detected by synthetic aperture radar. *Geophys. Res. Lett.*, **37**, L06601, <https://doi.org/10.1029/2009GL041972>.
- Yang, H., G. Lohmann, W. Wei, M. Dima, M. Ionita, and J. Liu, 2016: Intensification and poleward shift of subtropical western boundary currents in a warming climate. *J. Geophys. Res. Oceans*, **121**, 4928–4945, <https://doi.org/10.1002/2015JC011513>.
- Yoda, K., K. Shiomi, and K. Sato, 2014: Foraging spots of streaked shearwaters in relation to ocean surface currents as identified using their drift movements. *Prog. Oceanogr.*, **122**, 54–64, <https://doi.org/10.1016/j.pocean.2013.12.002>.
- Yu, L., 2019: Global air–sea fluxes of heat, fresh water, and momentum: Energy budget closure and unanswered questions. *Annu. Rev. Mar. Sci.*, **11**, 227–248, <https://doi.org/10.1146/annurev-marine-010816-060704>.
- Zanna, L., P. G. Porta Mana, J. Anstey, T. David, and T. Bolton, 2017: Scale-aware deterministic and stochastic parametrizations of eddy–mean flow interaction. *Ocean Modell.*, **111**, 66–80, <https://doi.org/10.1016/j.ocemod.2017.01.004>.